T.C.

EGE ÜNİVERSİTESİ

Fen Bilimleri Enstitüsü

# DESIGN AND CHARACTERIZATION OF SELF-HEALING GEOPOLYMER MORTAR CONTAINING MAGNETIC NANOPARTICLES

**Master's Thesis**


**Kerem ŞENÇAMLAR**

**Deparment of Civil Engineering**


**İzmir**

**2023**

T.C.

EGE ÜNİVERSİTESİ

Fen Bilimleri Enstitüsü

# DESIGN AND CHARACTERIZATION OF SELF-HEALING GEOPOLYMER MORTAR CONTAINING MAGNETIC NANOPARTICLES

**Kerem ŞENÇAMLAR**

**Supervisor: Prof. Dr. Özge ANDİÇ ÇAKIR**

**Department of Civil Engineering**

**Civil Engineering Master Programme**

**İzmir**

**2023**

# KABUL ve ONAY SAYFASI

Kerem ŞENÇAMLAR tarafından Yüksek Lisans Bitirme Tezi olarak sunulan "Design and characterization of self-healing geopolymer mortar containing magnetic nanoparticles" başlıklı bu çalışma EÜ Lisansüstü Eğitim ve Öğretim Yönetmeliği ile EÜ Fen Bilimleri Enstitüsü Eğitim ve Öğretim Yönergesi'nin ilgili hükümleri uyarınca tarafımızdan değerlendirilerek savunmaya değer bulunmuş ve 03.05.2023 tarihinde yapılan tez savunma sınavında aday oybirliği/oyçokluğu ile başarılı bulunmuştur.

| **Jüri Üyeleri:** | | **İmza** |
|---|---|---|
| **Jüri Başkanı** | **: Prof. Dr. Özge ANDİÇ ÇAKIR** | **...............................** |
| **Raportör Üye** | **: Doç. Dr. Aylin ŞENDEMİR** | **...............................** |
| **Üye** | **: Prof. Dr. Halit YAZICI** | **…………………….** |

# EGE ÜNİVERSİTESİ FEN BİLİMLERİ ENSTİTÜSÜ

## ETİK KURALLARA UYGUNLUK BEYANI

EÜ Lisansüstü Eğitim ve Öğretim Yönetmeliğinin ilgili hükümleri uyarınca Yüksek Lisans Tezi olarak sunduğum “Design and characterization of self-healing geopolymer mortar containing magnetic nanoparticles” başlıklı bu tezin kendi çalışmam olduğunu, sunduğum tüm sonuç, doküman, bilgi ve belgeleri bizzat ve bu tez çalışması kapsamında elde ettiğimi, bu tez çalışmasıyla elde edilmeyen bütün bilgi ve yorumlara atıf yaptığımı ve bunları kaynaklar listesinde usulüne uygun olarak verdiğimi, tez çalışması ve yazımı sırasında patent ve telif haklarını ihlal edici bir davranışımın olmadığını, bu tezin herhangi bir bölümünü bu üniversite veya diğer bir üniversitede başka bir tez çalışması içinde sunmadığımı, bu tezin planlanmasından yazımına kadar bütün safhalarda bilimsel etik kurallarına uygun olarak davrandığımı ve aksinin ortaya çıkması durumunda her türlü yasal sonucu kabul edeceğimi beyan ederim.

03/05/2023

Kerem ŞENÇAMLAR

# PROLOGUE

I am sharing the analysis and results of my experimental studies that I conducted at the laboratory of the Department of Civil Engineering of Ege University, the laboratory of the Department of Bioengineering of Ege University and the Application and Research Center of the Central Research Test and Analysis Laboratory (Ege MATAL). Within the scope of this thesis, the determination of the self-healing efficiency of geopolymer mortar caused by biocalcification was carried out with the design and characterization of geopolymer mortar and different immobilization techniques.

The objective and scope of the study are explained in Chapter 1. In Chapter 2 and in Chapter 3, geopolymer binder system and related studies of geopolymer binders are mentioned. In Chapter 4, self-healing concrete are given. In Chapter 5, The materials and methods used in the experimental study carried out within the scope of the thesis are given. The results obtained in the experiments are given in Chapter 6. The results of the study are summarized in Chapter 7.

# ABSTRACT


## DESIGN AND CHARACTERIZATION OF SELF-HEALING GEOPOLYMER MORTAR CONTAINING MAGNETIC NANOPARTICLES

**ŞENÇAMLAR, Kerem**

**M.Sc Thesis in Civil Engineering**

**Supervisor: Prof.Dr. Özge ANDİÇ ÇAKIR**
**May 2023, 126 pages**

In this study, the self-healing geopolymer mortar containing *Sporosarcina pasteurii* bacteria encapsulated by nanoparticles are investigated. For the purpose of geopolymer mortar design and characterization, 19 different geopolymer mortar mixtures containing class F fly ash (FA), granulated blast furnace slag (GBFS) and brick powder (PB) in different proportions were prepared. The geopolymer mortar that contains 65% fly ash, %20 granulated blast furnace slag and 15% brick powder as binder material was optimum ratio of binder materials according to its flexural and compressive strength. Sixteen different geopolymer mortar mixtures were prepared with three different modulus of silica (Ms) ratio, four different water/binder (w/b) ratio and nine different cure regime using optimum binder system. The energy consumption was calculated during the curing regime. It was determined that the best performance given by geopolymer mortar that cured for 3 days at 50°C with a water-binder ratio of 0.42 and Ms ratio of 1.3 with a compressive strength of 54.3 MPa and a flexural strength of 8.23 MPa.

Three different mortar mixtures were prepared to study the effect of different concentrations of non-encapsulated bacterial addition on the strength properties. It was observed that the addition of non-encapsulated bacteria has a negative effect on the flexural strength of the geopolymer mortar. Four geopolymer mortar mixtures were prepared and cured in water for different time periods to study the effect of water curing on the strength properties. It

was determined that water curing does not have a significant effect on the strength of geopolymer mortar.

In order to investigate the self-healing effectiveness of geopolymer mortar, a total of thirteen different geopolymer mortars were prepared. In addition to control mortars without bacteria, three series of mortars with encapsulated bacteria in three different concentrations, three series of non-encapsulated bacteria in three different concentrations, three series encapsulated bacteria with nanoparticles which obtained green synthesis method in three different amounts and three series encapsulated bacteria with magnetic nanoparticles in three different amounts were prepared. The ultrasonic pulse velocity (UPV) measurements were recorded before and immediately after cracking the samples and 1, 2, 4, 6 hours and 1, 2, 4, 7, 14, 21 and 28 days after cracking and the healing is determined as a percentage of the UPV value in the measurement day to the UPV value time after cracking. Effective self-healing was determined by taking the substracting the amount of the healing of control samples from the amount of the healing in the bacteria-containing samples to define the measured healing is due to self-healing or due to continuing geopolymerization (autogenous healing). No healing was maesured in bacteria-free sample. Among the geopolymer mortars containing non-encapsulated bacteria, the sample containing bacteria at a concentration of $10^{10}$ cfu/ml showed the highest effective healing with 4.77% at the end of 28 days. Among the geopolymer mortars containing encapsulated bacteria, the sample containing encapsulated bacteria at a concentration of $10^{9}$ cfu/ml showed the highest effective healing with 4.09% at the end of 28 days. While the effective healing level of the mixture with a magnetic nanoparticles at 1% of amount of bacteria ($10^{9}$ cfu/ml) was %4.86 healing, the mixture with a nanoparticles obtained by green synthesis method at 0.5% of amount of bacteria ($10^{9}$ cfu/ml) showed %2.45 effective healing.

**Keywords:** Self-healing, Geopolymer, Nanoparticle, *S.Pasteurii*, Encapsulation

# TABLE OF CONTENTS

**Page**

## LIST OF FIGURES

**Page**

# LIST OF TABLES

**Page**

# 1 INTRODUCTION

Sustainability, increasing demands for, service duration, reduction of resources and energy consumption, $CO_2$ emissions and current focus on the gradual improvement of the efficiency of the construction sector to adopt a more innovative approach is emerging as a propelling force (Justnes and Martius-Hammer, 2016). The increase in the consumption of natural resources over time creates environmental, economic and social problems. This issue attracts the attention of researchers and alternative ways to reduce the consumption of natural resources are being sought through research. When the concept of “sustainability”, which aims to protect the artificial and natural environment by ensuring the continuity of resources, is adapted to building materials, the concept of “sustainable construction material” emerges. Sustainable building materials are materials that consume minimal energy throughout their life cycles and do not harm the environment and human health during the acquisition, processing, use, maintenance-repair and waste generation of their raw materials.

In addition to being the most frequently used construction material, concrete is also the most widely used man-made material in the world, coming in second only to water in terms of consumption (Mehta and Monteiro, 2014). Considering its widespread use, the importance of making it sustainable by increasing the service life of traditional concrete and/or creating environmental friendly alternatives to this material is even better understood. With appropriate approaches to the nature of concrete, it is possible to reduce the $CO_2$ emission in the construction and use process of the structure and to make this indispensable material even more environmentally friendly. Worldwide production of cement-based materials exceeds 10 billion tons. In recent years, about 4.4 billion tons of cement, 17.5 billion tons of aggregate and 1.6 billion tons of water have been consumed annually worldwide for concrete production (Garside, 2020; Miller et al., 2016; Ebead, et al., 2022)**.** During cement production, a significant amount of fuel and raw materials are needed due to excavation operations, the need for high-temperature production and grinding operations. As a result of consuming 2.5 tons of raw materials and fuel per 1 ton of portland cement production, almost one ton of $CO_2$ emissions are emitted to the atmosphere and it is estimated that there are about 1.35 billion tons of $CO_2$ emissions per year (Xie and Ozbakkaloglu, 2015).

It is estimated that it accounts for about 8% of the total greenhouse gas released into the environment (Andrew, 2019). The production of portland cement is almost impossible without significant amount of $CO_2$ emission (Gartner, 2004). According to the United Nations Environment Programme Report, the demand for cement is increasing by 6% every year (Amrina and Vilsi, 2015). In 2050, it is expected that the total cement demand in the World will increase by about 200% compared to 2010 (Pacheco-Torgal, et al., 2011). Therefore, $CO_2$ emissions and raw material consumption are prompting researchers to think about alternative sustainable binder materials. Alternative binder systems that provide low $CO_2$ emissions include cements containing high amounts of natural or artificial pozzolan, calcium aluminate-based cements and calcium sulfate-based systems. The use of cement as a binder in building materials is indispensable today. However, the biggest technical disadvantage of cement-based construction materials is that they are not show sufficient resistance to some chemical effects. The studies carried out so far reveal the positive effects of some natural and waste materials on the mechanical properties of concrete.

Alternative binders include geopolymer binder systems, which are significant. Alkalis are used to activate powder materials based on aluminosilicate to create amorphous geopolymer binders. The powder material for the production of connector geopolimer can be made from natural pozzolans that are amorphous in nature (volcanic tuff, volcanic glass, and shaved), calcined aluminosilicates (metakaolin, calcined clay), as the resulting aluminosilicate materials, and industrial wastes (Tuyan, 2017). These powder materials, in combination with alkaline activators, water and aggregates, form materials with mechanical properties similar to conventional concrete, more resistant to fire and relatively high acid resistance (Duxton, et al., 2007). Geopolymers have 11% less embedded energy and 55% fewer comparable $CO_2$ emission (Kan, et al., 2019). Alongside these advantages, difficulties in quality control of binder materials, the lack of international standards related to geopolymer binders, and problems in workability and setting time from a technical point of view constitute the disadvantages of geopolymer binders (Tuyan, 2017).

Concrete is designed to provide a specification that predicts inevitable deterioration over time. Cracks occur in concrete due to reasons such as placement of the structure, thermal expansion, thermal shrinkage, drying shrinkage, heavy load, incorrect or insufficient compactment, insufficient depth of concrete cover and corrosion (Warscheid & Braams, 2000; Achal et al., 2011). In order to reduce these distortions, expensive maintenance, repair or renovation costs are required. A significant budget is allocated worldwide for the repair of structures. In Europe, maintenance and reinforcement work is thought to account for 50% of the annual building budget (Cailleux and Pollet, 2009). These expensive costs lead to the search for new alternatives.

Self-healing concrete is a good alternative for sustainability by reducing resource consumption and expensive repair costs. Recently, there has been a focus on the biotechnology and civil engineering aspect of the development of self-healing concrete technology. In line with the researches, the self-healing properties of concrete is gained with addition of chemicals, bacteria, enzymes, fungal spores, shape memory alloys, nanomaterials by various methods such as encapsulation and vascular system (Zhang et al., 2020).

Considering the negative effects of the consumption of natural resources and the increase in maintenance and repair costs on sustainability, geopolymer binding systems capable of self-healing are an innovative approach in terms of reducing these effects. Although there are studies on the effect of self-healing properties on geopolymer systems using methods such as microcapsules, vacuum impregnation of light aggregates with healing agents (Garces, et al., 2021; Zhang, et al., 2022), there are not studies on the properties of self-healing on geopolymer mortar containing immobilized bacterial spores with nanoparticles. With this experimental thesis study, it is aimed to contribute to the properties of self-healing geopolymer mortars in which industrial waste products are used as binders.

## 1.1 Objectives and Scope

The aim of this study is to investigate the design and characterization of geopolymer mortar using industrial waste powder materials and the effectiveness of self-healing due to biocalcification.

Within the scope of geopolymer mortar design, 19 different geopolymer mortar mixtures with a ternary binder system consisting a combination of class F fly ash, blast furnace slag and brick powder were prepared. After a preliminary study for mix design, the three mixtures that give the best compressive and flexural strength have been prepared with class F fly ash with different properties for considering the sustainability related to fly ash supply. The mixture with the highest flexural strength has been selected for the optimization process of Ms ratio, water-binder ratio and curing conditions. Seven different mortar designs with optimized binder system have been prepared for different Ms ratios (1.2, 1.3 and 1.4) and different water-binder ratios (0.42, 0.44, 0.46 and 0.48). Then, nine mortar mixtures were prepared to be subjected to curing conditions at different temperatures (40, 50 and 60°C) and for different periods (1, 3 and 7 days). The amounts of energy expended during the curing period were determined. As a result of the curing time, the mortar mixture, which shows the optimum energy expended-strength ratio, was selected to determine the effectiveness of self-healing. Four mortar mixtures with optimum values were prepared and kept in water for different periods (7, 14, 21 and 28 days) after the curing period, and the effect on compressive and flexural strength was studied.

At the stage of self-healing determination, mortar mixtures were prepared by adding three different concentrations ($10^8$, $10^9$ and $10^{10}$ cfu/ml) of bacterial culture as a substitute in the mixing water to examine the effect on compressive and flexural strength. In order to determine the effectiveness of self-healing, seven different mortar mixtures were prepared by using a control mixture without a healing agent, substituting bacterial culture of three different concentrations from the mixing water as agents, and encapsulating these bacterial culture liquids with sodium alginate and adding them to the binder. Cracks were formed with width of 0.3 mm on the samples with controlled loading and at different time intervals (before the crack, 1, 2, 4, 6 hours, 1, 2, 4, 7, 14, 21, 28 days) and ultrasonic pulse velocity (UPV) readings were recorded. Effective self-healing was determined by taking the substracting the amount of the healing of control samples from the amount of the healing in the bacteria-containing samples. In the immobilization process with nanoparticles, the concentration of bacteria determined to show the best healing was used. Bacteria cultures were immobilized with magnetic nanoparticles and nanoparticles obtained by green synthesis method in three different amounts of nanoparticles and encapsulated with sodium alginate. These mixture were prepared by adding the bacterial culture-nanoparticle structure as a healing agent to the geopolymer mortar and the UPV test was carried out to determined the self-healing characteristics. As a result of the self-healing tests, four methods were compared and the most effective method was determined.

# 2 GEOPOLYMER BINDERS

## 2.1 Binder Raw Materials

Silica and alumina-rich materials of amorphous structure can be used as binder materials for geopolymers. Fly ash, slag and metakaolin are the three powder ingredients that are most frequently utilized for geopolymer binders. Along with these materials, natural pozzolans, bottom ash, calcined clays, stilbite, red mud, brick powder and all the materials mentioned above are used in binary and ternary binder systems and laboratory research is done on them (Chindaprasirt et al., 2007; Kutti et al., 1982; Kovalchuk et al., 2007; Pacheco-Torgal et al., 2008; Hardjito et al., 2004; Bondar et al., 2011**;** Fernandez-Jimenez and Palomo, 2003).

## 2.2 Alkali Activators

The type and properties of alkali activator is significant for the geopolymerization process. As in powder materials, the properties of alkali activators affect the properties of geopolymer. Alkali activators are soluble alkali metals that usually based on sodium or potassium. Sodium hydroxide (NaOH), potassium hydroxide (KOH), sodium silicate ($Na_2SiO_3$) and potassium silicate ($K_2O_3Si$) is the most preffered alkali activator. The geopolymerization reaction is slower when only alkali hydroxides are used than when used together with soluble silicate (Palomo et al., 1999). More minerals dissolve when NaOH is used in place of KOH (Xu and Van Deventer, 2000).

The substance created when $SiO_2$ and $Na_2CO_3$ fuse together is known as water glass, and it is melted at temperatures above 1100°C to create sodium silicate (McDonald and Thompson, 2006). It is noted to pay attention to the negative effect of sodium silicate in the solid state on strength compared to its liquid state (Xiang et al., 2018). Soluble silicates decrease alkali saturation in the pores and increase the adhesion between paste and aggregate at the interface (Lee and Van Deventer, 2004). The single use of sodium silicate as an activator is rare. It is often used with NaOH to obtain sufficient activation potential.

Sodium hydroxide is the most commonly used alkaline activator. It is produced by electrolysis of seawater (Du et al., 2018). Heat is released with its dissolution. The addition of NaOH accelerates the chemical dissolution and prevents the formation of ettringite and CH during the formation of the binder (Wang et al., 2004). In addition, higher NaOH concentrations provide higher strength in the early ages of the reaction, while negatively affecting the strength at an lately age due to excess OH in solution (Wang et al., 2004). It has been discovered that sodium hydroxide as an activator which increases their stability in hostile environments of sulfates and acids, as they develop greater crystallinity (Garcia et al., 2007).

## 2.3 History of Geopolymer Binders

Kühl published experiments on the setting time behavior of combinations of crushed slag and alkalis in the early 1900s, alkali was first used to make a binder (Kühl, 1908). Chassevent used caustic potassium and soda solutions to assess the reactivity of slags in 1937, although the goal of this research was to analyze slags rather than create binders from them (Chassevent, 1937). Although Feret's work in 1939 is acceptable regarding alkali-activated binders, the work is considered to be related to the use of blast furnace slag with portland cement (Feret, 1939).

The first thorough experimental study on cements made from calcareous and non-calcareous slag and caustic soda was carried out by Purdon in 1940. (Purdon, 1940). Glukhovsky started looking into the binders used in ancient structures in the context of the demand for portland cement substitutes in the mid-1950s and the former Soviet Union. He later found that it might be possible to produce binders using solutions containing low-calcium or calcium-free aluminosilicates and alkali metals (Glukhovsky, 1959). To describe the binders, Glukhovsky used the terms "soil cements" and "soil silicates" for the matching concretes (Glukhovsky, 1965). In the late 1970s, Davidovits named the term “geopolymer” to describe alkali-activated methacaoline-based binders (Davidovits, 1979). Forss focused specifically on a system of superplasticizing alkali-activated blast furnace slag known as F-concrete in 1983 (Forss, 1983). In 1985, a hybrid ordinary portland cement /alkali activated material concrete named

“Pyrament” was marketed through the Geopolymer Institute (Davidovits ans Sawyer, 1985).

RILEM created the initial technical committee for the creation of binders with alkaline activations. A thorough study on alkali-activated materials was released in 2013 by the RILEM Technical Committee on Alkali-Activated Materials, which had finished its research in 2012 (Provis and van Deventer, 2013). In this report, the importance of developing new standards at the international level for the commercialization of this material was emphasized. Important pioneering studies on the development of alkali-activated materials and alkaline cements summarizes in Table 2.1 (Roy, 1999).

**Table 2.1** Pioneering studies on geopolymer summarized chronologically (Roy, 1999).

| Author | Year | Signifiance |
|---|---|---|
| **Feret** | 1393 | Slags used for cement |
| **Purdon** | 1940 | Alkali-slag combinations |
| **Glukhovsky** | 1959 | Theoretical basis and development of alkaline cements |
| **Glukhovsky** | 1965 | First called “alkaline cements” |
| **Davidovits** | 1979 | “Geopolymer” term |
| **Malinowski** | 1979 | Ancient aqueducts characterized |
| **Forss** | 1983 | F-cement (slag-alkali-superplasticizer) |
| **Langton and Roy** | 1984 | Ancient building materials characterized |
| **Davidovits and Sawyer** | 1985 | Patent of “Pyrament” cement |
| **Krivenko** | 1986 | DSc thesis, $R_2O$-RO-$SiO_2$-$H_2O$ |
| **Malolepsy and Petri** | 1986 | Activation of synthetic melilite slags |
| **Malek et al.** | 1986 | Slag cement-low level radioactive wastes forms |
| **Davidovits** | 1987 | Ancient and modern concretes compared |
| **Deja and Malolepsy** | 1989 | Resistance to chlorides shown |
| **Kaushal et al.** | 1989 | Adiabatic cured nuclear waste forms from alkaline mixture |
| **Roy and Langton** | 1989 | Ancient concretes analogs |
| **Majundar et al.** | 1989 | C12A7 - slag activation |
| **Talling and Brandstetr** | 1989 | Alkali-activated slag |
| **Wu et al.** | 1990 | Activation of slag cement |
| **Roy et al.** | 1991 | Rapid setting alkali-activated cements |
| **Roy and Silsbee** | 1992 | Alkali-activated cements: an overview |
| **Palomo and Glasser** | 1992 | CBC with metakaolin |
| **Roy and Malek** | 1993 | Slag cement |
| **Glukhovsky** | 1994 | Ancient, modern and future concretes |
| **Krivenko** | 1994 | Alkaline cements |
| **Wang and Scrivener** | 1995 | Slag and alkali-activated microstructure |

## 2.4 Definition and Mechanism of Geopolymerization

Polymers are chemical products with a long molecular chain compound structure formed by various physical and chemical interactions of molecules and elements called monomers. Polymers are also used to create composite materials (Zeybek, 2009). Polymers in which C; N; O; H elements commonly found in living chemistry form monomers are called organic polymers, while polymers in which other halogen, metal, metalloid and mineral elements form the main component of monomers are called inorganic polymers (Yaşar, 1992). The polymer bond structure is usually covalent bond structure. The covalent bond structure is formed by the sharing of electrons at the final energy levels between various molecules and elements (Diercks and Yaghi, 2017).

Geopolymer binders are an instance of the inorganic polymer type and have an Al and Si ion-based chain structure (Tuyan, 2017). The preliminary name “Geo” has also received due to the fact that it consists of oxygen, silicon and aluminum, which are the most abundant elements in the earth’s crust. Geopolymer binders are amorphous, in contrast to natural zeolitic materials, which are identical in chemical composition (Palomo vd., 1999; Xu and Van Deventer, 2000).

When materials such as fly ash, blast furnace slag are activated with alkali activators, they can be able to form binder. Inorganic polymers with an amorphous structure known as "geopolymers" are produced when aluminosilicate fly ash reacts with activators, while the reaction of blast furnace slag produces hydrated calcium silicate, which is comparable to the C-S-H gel in cement-based binders (Aydın, 2010).

Geopolymerization is an exothermic chemical process involving the dissolution, transport, orientation and polycondensation movements of molecules in a highly alkaline environment (Davidovits, 1999).

Geopolymerization is based on the synthesis of aluminates and silicates found in aluminosilicate materials to form covalently bonded compounds by sharing oxygen atom electrons. The formation of poly(siloxane) Si-O-Si-O, poly(sialate) Si-O-Al-O and poly(sialate-disiloxo) Si-O-Al-O-Si-O polymeric covalent bonds by multiple condensation of dimers, trimers and higher molecules from monomers. Although silicate ($SiO_2$) minerals are extremely stable compounds, geopolymerization progresses by weakening the three-dimensional network structure in an alkaline environment and formed sialates, which are the main compound of geopolymers (Davidovits, 2008).

Sialate (Si-O-Al-O-), polysialate siloxo or polysialate di-siloxo are formed according to the frequency level of the oxygenated sequence of the polymer bond structure and the elements. The structure of sialate is formed by all oxygen atoms between $SiO_4$ and $AlO_4$ molecules, forming tetrahedral bonds (Davidovits, 1999). The Si/Al molar ratio of sialate and aluminate in the raw material and alkaline solution in the geopolymer reaction affects the material properties (Davidovits, 2008). Polysialates have a slightly more crystalline structure, while polysialate siloxo has a more amorphous structure. The general formula giving the polysialate structure is as follows;

$Mn\ [-(SiO_2)z - AlO_2]n\ .\ wH_2O$

M: monovalent cation (such as Na, K),

n: number of polycondensations (degree of polymerization),

z: three-dimensional polycondensation is the number of repetitions of the network structure (1, 2, 3 or higher).

The groups of molecules formed in the geopolymer reaction described by Joseph Davidovits are as follows (Davidovits, 1999):

- Si-O-Si-O-siloxo, poly(siloxo)

- Si-O-Al-O- sialate, poly(sialate)

- Si-O-Al-O-Si-O- sialate-siloxo, poly(sialate-siloxo)

- Si-O-Al-O-Si-O-Si-O- sialate-disiloxo, poly(sialate-disiloxo)

- P-O-P-O- phosphate, poly(phosphate)

- P-O-Si-O-Al-O-P-O- phospho-sialate, poly(phospho-sialate)

- (R)-Si-O-Si-O-(R) organo-siloxo, poly-silicone

Glukhovsky (1994) proposed a geopolymerization mechanism that takes place in three stages: destruction-solidification (aggregation), solidification-condensation and condensation-crystallization.

The destruction-solidification stage begins with the reaction of OH-ions in the alkali activator  by weakening and breaking the covalent bonds in the Si-O-Si structure. Silanol (-Si-OH) and Siloxo (-Si-O) are formed. The formation of $Si-O^{-}-Na^{+}$ bonds between siloxo (-Si-O) and the alkaline cation (siloxsonate) prevents conversion back to siloxane (-Si-O-Si).

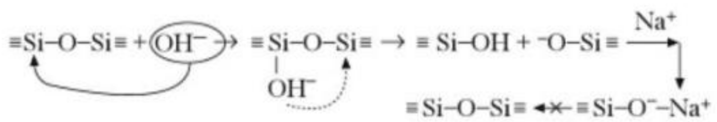

**Figure 2.1** Formation of silanol and siloxo (Glukhovsky, 1994)

The Si-O-Al bonds (sialate bonds) are impacted by the OH- group. Aluminum atoms in solution combine to create the anion complex Al(OH)-4.

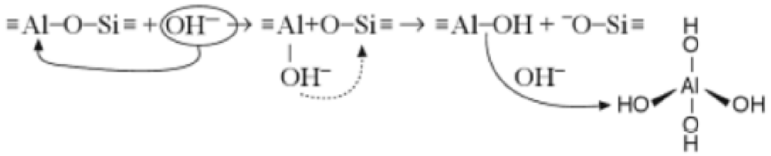

**Figure 2.2** Dissolution of $Al(OH)^{-}_{4}$ (Glukhovsky, 1994)

In the second stage, silica monomers and dimers react with each other. OH- ions act as the catalyst in this phase. The silicic acid heaps that come from the polymerization process start to spread out in all directions. In polymerization, aluminates take the place of silica.

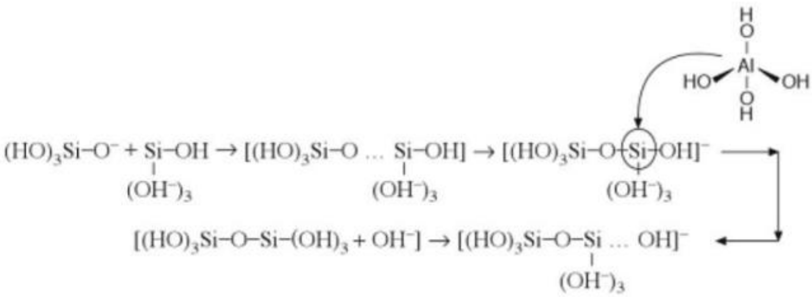

**Figure 2.3** Reaction of silica monomers and silica dimers (Glukhovsky, 1994)

At the stage of solidification-crystallization, the reaction products precipitate. The activator employed, the curing circumstances, the mineralogical and chemical makeup of the binder powder material, etc. all affect how the products are composed.

For the alkali activation of fly ash, Palomo et al. (2005) suggested a two-stage model that included nucleation and growth. The nucleation stage is explained by the dissolution of aluminates contained in fly ash and the polymerization process, which produces complicated ion molecules. When the ion molecules in the growth phase grow to a critical size, the crystal structure also starts to grow. Fly ash is subjected to an alkaline activation process that results in aluminosilicate gel matrix with a binding property, the primary constituent of which is referred to as N-A-S-H gel.

A number of researchers have since revised this concept (Shi et al., 2011; Palomo et al., 2005; Duxson et al., 2007a; Fernández-Jiménez et al., 2005). The new model predicts that the aluminosilicates primarily separate into silica and aluminate monomers when the powdered material interacts with the alkaline solution. The interaction between these monomers creates dimers. In addition, Additionally, these monomers interact with other monomers to create structures like trimer, tetramer, and others. The N-A-S-H gel starts to precipitate when the solution is saturated. This gel initially contains a lot of Al. It is recognized as the semi-stable intermediate reaction product and goes by the name "gel 1". (Fernández-Jimenez et al., 2006). This gel forms because the reactive aluminates dissolve more quickly due to the weaker Al-O bonds than the Si-O bonds, which leads to the early reaction's high concentration of $Al^{3+}$ ions in the alkaline medium. As the reaction goes on, more Si-O groups from the aluminosilicate source dissolve, increasing the silica concentration in the N-A-S-H gel (Gel 2) and in the medium.

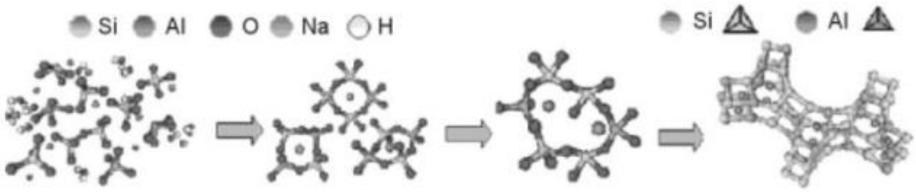


**Figure 2.4** Formation N-A-S-H gel (Shi et al., 2011; Fernandez-Jimenez et al., 2005a**)**

Alkaline aluminosilicate hydrate of amorphous structure, also known as N-A-S-H, is the major reaction product produced by the alkaline activation of silica and aluminate-rich materials (Palomo et al., 2005). In these types of systems, zeolite structures such as hydroxysodalite, Na-cabasite, zeolite P, zeolite Y and fojacite are formed as the second reaction product (Palomo et al., 1999; Fernández-Jiménez et al., 2003, Fernández-Jiménez et al., 2006; Duxson et al., 2007b).

## 2.5 Advantages and Disadvantages of Geopolymer Binders

Geopolymer binder systems have many advantages in economic, environmental and technical terms. Geopolymer binder systems lessen the requirement for the pricey clinker generation required in Portland cements, as well as the high energy consumption brought on by the requisite high temperatures (1400–1500°C) during cement manufacture (Fernandez-Jimenez and Palomo, 2006). Pozzolanic materials, industrial waste materials are less costly. According to Fernandez-Jimenez, 20–30% of the fly ash that was accessible was utilised worldwide. (Fernandez-Jimenez et al., 2005b). The widespread use of geopolymer binders will have a positive impact on the environment as well as the economy by increasing the using of fly ash substituted instead of cement.

Due to the consumption of 2.5 tons of raw materials and fuel, the manufacture of one ton of portland cement results in the release of around one ton of $CO_2$ into the environment. It is estimated that there are about 1.35 billion tons of $CO_2$ emissions per year (Xie and Ozbakkaloglu, 2015). Shinde and Kadam estimate that switching to geopolymer concrete from portland cement concrete will result in savings of 0.25 million tons of coal, 80 million electricity production units, and 1.5 million tons of $CO_2$ from entering the atmosphere (Shinde and Kadam, 2015). In the research of Dixon et al., presented a $CO_2$ emissions from various alkali-activated binders. In the chlor-alkali process, $CO_2$ was created while producing $Na_2O$, and $SiO_2$ was employed as the main input as aqueous sodium silicate. When compared to portland cement, it has demonstrated $CO_2$ savings of around 80%. (Duxson et al., 2007c). In addition, the use of unwanted pozzolanic by-products of power plants will stop these materials from being disposed of in their hazardous form into the environment.

Sulfates and other acids are very resistant to geopolymer binders. The significant development of gypsum and etringite, which results in cracking and flaking in the concrete, is blamed for the degrading effects of sulfate attack on portland cement. The decreased calcium concentration of the parent material is thought to be responsible for geopolymeric materials' greater performance in acidic conditions. Heat-treated, low-calcium fly ash-based geopolymers do not create gypsum or etringite, hence the sulfate attack mechanism is not present in these materials (Rangan, 2008). After being submerged in solutions of sodium chloride (NaCl) and MgSO4 salts for 1.5 years, cured samples revealed no visible corrosion products, and two years later, x-ray diffraction examination was unable to detect the presence of substantial hydration products (Skvara et al., 2006). Khale and Chaudhary indicate that over the course of a 24-week exposure period, the sample length changed by less than 0.02 percent, whereas a geometric expansion of 0.5% caused by the sulfate attack is regarded as a failure. In addition, after being submerged in solutions of saltwater, sodium sulfate, and sulfuric acid, metakaolin based geopolymer mortars showed barely any degradation in microstructure and strength (Khale and Chaudhary, 2007). Rangan's sulfuric acid test revealed only a 3% mass loss in the geopolymer sample, whereas Khale's portland cement test samples were completely destroyed (Rangan, 2008; Khale and Chaudhary, 2007).

Geopolymers are inorganic, hard, stable up to a temperature of 1250°C and non-flammable (Davidovits, 1991). After 150 freeze/thaw cycles, geopolymer samples still had 70% of their initial compressive strength (Skvara et al., 2006). In different study, it was reported that samples exposed to temperatures as high as 1100°C only lost a maximum of 60% of their residual strength in the range of 500–600°C, yet after firing, geopolymer samples were still stronger than portland cement (Sumajouw et al., 2004). Fernandez-Jimenez et al., indicated that while geopolymer flexural strength only decreased by 33% when exposed to temperatures of 1000°C, they found that the strength of samples containing portland cement decreased to almost zero above 600°C. For fly ash-based samples, the compressive strength values recorded from the same series of studies were higher than portland cement samples. The compressive strength values reported from the same series of experiments were much higher than those of portland cement for fly ash-based samples (Fernandez-Jimenez et al., 2008). While the compressive strength of the alkali-activated ash material remained constant between 800 and 1000°C, regardless of the curing, the compressive strength for the control of portland cement concrete approached zero at temperatures above 800°C. (Fernandez-Jimenez et al., 2008). A two times increase in compressive strength and a six times increase in flexural strength were noted after exposure to temperatures of 1200°C. The fundamental reason for this high temperature resistance, according to a material characterisation examination employing microscopic technologies, is the crystallization of the mineral akermanite ($Ca_2MgSi_2O_7$) (Zuda et al.,2008).

A "good" alkali-activated binder can offer more benefits than a standard performance portland cement when it comes to the performance of the binder, but using a new binder can have disadvantages (Provis and van Deventer, 2013).

One of the most important disadvantages of geopolymer binder systems is that the chemical and physical properties of the powdered aluminosilicate materials used are not always constant, which causes great problems in terms of quality control. In particular, the properties of waste powder materials obtained as an industrial by-product may change over time as a result of a small change made during the production of the main product. The characteristics of the binder system are greatly impacted by changes in the powder material's properties (Pacheco-Torgal vd., 2014). Calcium's quantity and physical characteristics in the raw state has a important impact the reaction and the final product's physical characteristics (Duxson et al., 2007b). It was discovered that in fly ash, silica typically makes up 40–60% of the ash material, alumina makes up 20–30%, and the amount of iron varies significantly (Khale and Chaudhary, 2007). The fineness of the ash is also important for the development of mechanical strength, however pastes made from ashes with particle sizes less than 45 m have shown values of 70 MPa. Since fly ash particles are naturally not homogeneous, care must be taken to create an ideal mixture and a consistent final product (Duxson et al., 2007b). These variables should be thoroughly examined before the combination design is finished since they are extremely important to the entire development of geopolymer cements. In addition, the high temperature requirement in the curing process of geopolymer concretes can be seen as a disadvantage. These disadvantages will increase the control and research/development of costs.

In contrast to Portland cement concretes, geopolymer binders have different rheological characteristics. Pozzolan-based geopolymer binders may need vibrational efforts to reduce entrained air in the fresh paste since they have higher static and dynamic viscosities than portland cement products. (Skvara et., 2006). Superplasticizers are another option for a hard combination, however proper considerations for mixture design should be addressed to avoid ratio distortions. The workability of fresh geopolymer is increased by naphthalene sulfonate-based superplasticizer addition up to 4% of fly ash by mass; however, doses larger than 2% may induce a minor loss in compressive strength in the hardened product (Rangan, 2008).

## 2.6 Application Areas of Geopolymers

Sialates and aluminates contained in the raw material and alkaline solution during geopolymerization affect the material properties in Accord with Si/Al ratio. As the Si/Al ratio decreases, it is possible to obtain more crystalline structures. When the ratio increases more amorphous structures and more fluid geopolymers are obtained (Şinik, 2019). These changes in material properties allow geopolymers to have a wider range of uses.

In systems where the Si/Al ratio is 1, brick ceramics and fire protective products similar to zeolite crystal can be obtained. When this ratio is 2, geopolymer cement and concrete can be synthesized in a ceramic amorphous structure, as well as structures necessary for stocking radioactive waste can be produced with a slightly more advanced technology. In cases where the Si/Al ratio is 3, the fluid polymeric character increases slightly and furnace coatings, fiber glass, fire protective coatings, and materials that can withstand 1000 ºC can be produced. When the Si/Al ratio rises above 3, foams can be produced as a filling materials. When this ratio is above 15, a geopolymer paste is formed in a 2-dimensional molecular network structure, and this structure can be used in the production of nano-composite materials with high fire and heat resistance that can be used in combat aircraft (Davidovits, 2008). Davidovits suggested possible application areas for geopolymer binder materials according to Si/Al molar ratios (Davidovits, 1999).

**Table 2.2** Application area for geopolymers in terms of Si:Al (Davidovits, 1999)

| Si:Al | Applications |
|---|---|
| 1 | Bricks, ceramics and fire protection |
| 2 | Low $CO_2$ cement and concrete or radioactive waste encapsulation |
| 3 | Heat resistance composites, fiber glass composites or foundry equipments |
| >3 | Sealants for industry |
| 20<Si:Al<35 | Heat and fire resistant fibre composites |

In addition, the potential application areas identified by the Geopolymer Institute are listed below (Davidovits, 2002):

- Prefabricated bearing element

- Prefabricated non-bearing element

- Places where exposed to chemical and toxic effects

- Thermal insulation material in places exposed to high temperature

- Insulating material in the production of refractory material.

# 3 GEOPOLYMER MORTAR AND CONCRETE

## 3.1 Effect of Binder Raw Materials in Geopolymer Properties

Allahverdi and Kani (2009) investigated alkali activation of different construction waste based on $Na_2SiO_3$ and NaOH combinations. Geopolymer mortar mixtures with various water-binder ratio, modulus of silica and sodium oxide concentration were prepared. The binder system was designed by uses of waste concrete and waste brick. When the concentration of sodium oxide increases, it was observed that while increasing the compressive strength, it reduces the setting time. Among the mortar mixtures cured at room temperature for 28 days, the mixture containing %60 waste concrete and %40 waste brick showed 16.5 MPa compressive strength, while the compressive strength of the mortar mixture using only waste brick reached 40 MPa. It was stated that the results showed that waste brick is a more suitable binder alternative for geopolymer systems compared to waste concrete (Allahverdi and Kani, 2009).

According to Gourley, class F fly ash is favored above class C fly ash. Class C fly ash has a high calcium content that alters the binder's microstructure and limits geopolymerization (Gourley, 2003).

Kaya et al. (2020) examined the effect of class F fly ash and class C fly ash on the workability and the strength of geopolymer mortar. The combination of sodium silicate and sodium hydroxide was used as an alkaline activator. It was determined that class C fly ash reduces the workability compared to class F fly ash. When all curing times and curing temperatures were evaluated, the flexural strength of class C fly ash based-geopolymer mortars were in the range of 1.13 and 3.02 MPa. The sample cured at 60°C for 2 days and kept at room temperature for 360 days has a flexural strength of 1.13 MPa, while the sample cured at 60°C for 2 days and kept at room temperature for 90 days showed a flexural strength of 3.02 MPa. The lowest flexural strength was determined as 2.23 MPa while the highest flexural strength was determined as 12.42 MPa in class F based geopolymer mortars. The sample with the lowest flexural strength was cured at 50°C for 3 days and kept at room temperature for 360 days, while the sample with the highest flexural strength was cured at 90°C for 3 days and kept at room temperature for 360 days. The lowest compressive strength was 10.22 MPa and the highest compressive strength was 15.83 MPa among the samples produced with C class fly ash for 2 days at different temperatures. On the other hand, the compressive strength of the class F fly ash-based samples cured for 3 days at different temperatures was stated in the range of 3.21-48.96 MPa. While geopolymer mortars produced with class C fly ash did not have a significant increase in strength at later ages, an increase has been observed in samples produced with class F fly ash cured at low temperatures over time (Kaya et al., 2020).

Kumar et al. (2009) studied the effect of blast furnace slag on properties of fly ash-based geopolymer. By substituting 5-50% of the fly ash with blast furnace slag, mortar mixtures were prepared. While the setting time decreased significantly when blast furnace slag was added to the mixture from 5% to 25%, there was no decrease in setting time as the amount of addition increases. It was noted that the reaction in the samples cured at 27°C for 2 days was dominated by the dissolution and precipitation of C–S–H gel due to the alkaline activation of the slag. While the compressive strength of the fly ash based geopolymer mortar was below 5 MPa, the compressive strength of the mortar with the addition of 50% blast furnace slag was 30 MPa. Among the samples cured at 60°C for 4 days, the compressive strength of the geopolymer mortar produced only from fly ash was 10 MPa, while the compressive strength of the mixture with the addition of 50% blast furnace slag was 45 MPa. It was noted that the combined interaction of fly ash and slag is confirmed by the coexistence of the calcium silicate hydrate and alumina silicate hydrate gel in the reaction products (Kumar et al., 2009).

Rovnanik et al. (2016) investigated the alkaline activation of fly ash and waste brick powder. Sodium silicate and sodium hydroxide were used as alkaline activator ($SiO_2/Na_2O$:1.6). Four different geopolymer mortar mixtures were prepared by substituting 0%, 25%, 50% and 100% by weight of fly ash into the binder with brick powder. It was noted that an increase in strength was observed in all samples at later ages. As the amount of brick powder increased, the flexural and compressive strength of gopolymer mortars reduced (Rovnanik et al., 2016).

Zawrah et al. (2016) investigated the alkali activation potential of granulated blast furnace slag and waste brick powder. Geopolymer mortar mixtures were prepared by using 20%, 40%, 60% and 80% granulated blast furnace slag instead of waste bricks and cured at room temperature for 3, 7, 14, 28 and 90 days. The compressive strength of the geopolymer mortar containing only brick powder reached 15 MPa at the end of 90 days. The geopolymer mortar mixture containing 40% brick dust and 60% granulated blast furnace slag showed the highest compressive strength with 83 MPa. The compressive strength increased as the amount of granulated blast furnace slag in the mixture increased but there was a decrease in strength of the mixture containing 80% granulated blast furnace slag due to formation of cracks (Zawrah et al., 2016).

## 3.2 Effect of the Modulus of Silica in Geopolymer Properties

Reig et al. (2013) examined the effect of silica modulus on the workability and strength of brick powder-based geopolymer mortar. The combination of sodium hydroxide and sodium silicate was used as an alkaline activator. The compressive strength of the samples with a Ms ratio of 0 remained below 15 MPa among the mortar mixtures cured at 65°C for 7 days. It was noted that the 7-day compressive strengths of mortar mixtures with a ratio of 1.60 Ms, water-binder ratios of 0.45 and 0.30 reached approximately 30 MPa and 50 MPa, respectively. It was stated that the compressive strength increases as the amount of sodium silicate increases. However, it was found that a higher amount of silica reduces the workability, and the optimal $SiO_2/Na_2O$ value was determined as 1.6 (Reig et al., 2013).

Cho et al. (2017) studied the compressive strength of fly ash-based geopolymer by considering variables including sodium oxide content, $SiO_2/Na_2O$ ratios. For geopolymer mortar with the constant Ms ratio and curing condition, it was stated that when the $Na_2O$ ratio increased from 4% to 6%, there was a 348% increase in the 28-day compressive strength, and when the $Na_2O$ ratio increased from 6% to 8% and from 8% to 10%, there was a 181% and 115% increase in compressive strength, respectively. On the other hand, for geopolymer mortar mixtures with a constant $Na_2O$ ratio and curing condition, when the Ms ratio increased from 0.8 to 1.4, the compressive strength increased from 30 MPa to 45 MPa, while the geopolymer mortar with a 2.0 Ms ratio decreased to 28-day compressive strength to 25 MPa (Cho et al., 2017).

Tuyan et al. (2018) investigated that the effect of alkaline activator concentration on the consistency and strength of waste brick based geopolymer mortar. It was stated that the compressive strength increases with the increase of sodium oxide content. However, this increase was more pronounced in mixtures with lower Ms ratios. The sample with a ratio of 10% $Na_2O$ and 1.8 Ms showed the highest compressive strength with 17 MPa, while the geopolymer mortar with a ratio of 4% $Na_2O$ and 1.6 Ms showed the lowest compressive strength with about 4 MPa. It was shown that as the Ms ratio rose from 1.2 to 1.6, the compressive strength of mixes containing a 10% sodium oxide component increased from 7.1 MPa to 16.7 MPa. However, with a rise in the Ms ratio from 1.6 to 2.2, the compressive strength fell from 16.7 MPa to 13.1 MPa. As the $Na_2O$ or Ms ratio rises, the geopolymer mortar's flow diameter grows (Tuyan et al., 2018).

Deb et al. (2014) evaluated the impact of various slag and activator content ratios on the workability and strength characteristics of fly ash-based geopolymer concrete. Slag was added with varying sodium silicate/sodium hydroxide ratios (1.5-2.5) as 0%, 10%, and 20% of the total binder. With an increase in the slag concentration or a drop in the Ms ratio, the workability of geopolymer concrete compositions decreased. It was stated that the 20% slag mixture showed a slump value of 195 mm compared to the 250 mm shown by the 10% slag mixture. The mixture with Ms ratio of 1.5 showed a slump value of 180 mm, while the mixture with Ms ratio of 2.5 had a slump value of 195 mm. An increase in the slag content from 10% to 20%, the 28-day compressive strength increased by 17%. For a specimen containing 20% slag, when the Ms ratio was reduced from 2.5 to 1.5, it achieved a 15% higher 28-day compressive strength (Deb et al., 2014).

## 3.3 Effect of the Water-Binder Ratio in Geopolymer Properties

Patankar et al. (2013) examined the effect of the water-binder ratio on the workability and compressive strength of fly ash-based geopolymer concrete, which was cured at 900°C for 8 hours. It was stated that the flow increases with the increase of the water-geopolymer binder ratio by keeping the other values constant and the suitable water-binder ratio range for geopolymer concrete is between 0.25 and 0.35. While decomposition was observed in a higher ratio, a lower proportion gave a dry mixture. It was noted that at a water-binder ratio of 0.40, the samples had a wet surface even after curing at 900°C for 8 hours. At a water-binder ratio of 0.20, the mixture is dry and unworkable. The compressive strength of geopolymer concrete decreased with an increase in the water-binder ratio. The mixture with a water-binder ratio of 0.25 showed the highest compressive strength with 61.33 MPa (Patankar et al., 2013).

The impact of the water-binder ratio on the compressive strength of waste brick-based geopolymer mortars was examined by Tuyan et al. (2018). Different w/b ratios (0.46, 0.44, 0.42, and 0.40) of mixtures were prepared. The mixture with 10% $Na_2O$ content and Ms ratio of 1.6 was cured at 70°C for 7 days. When the water-binder ratio increased from 0.40 to 0.46, the compressive strength of the mixtures decreased from 20.7 MPa to 16.7 MPa, while the flow diameter increased from 124 mm to 152 mm. It stated that when the water-binder ratio is used at values lower than 0.40, an unworkable geopolymer mortar was obtained (Tuyan et al., 2018).

## 3.4 Effect of the Curing Regime in Geopolymer Properties

Cho et al. (2017) examined the relationship between the compressive strength of the fly ash-based geopolymer mortar and curing regimes. Mortar mixture with 8% $Na_2O$ content and 1.4 Ms ratio cured at different temperatures (40°C, 70°C, 80°C, 90°C and 100°C) and durations (6, 12, 24, 48, 72 and 168 hours). Compared to the sample cured at 40°C, the 28-day compressive strengths of the geopolymer samples increased to 197% (70°C), 204.1% (80°C), 226.2% (90°C) and 245.1% (100°C). While early age strength increased with increasing curing time, this period increased for more than 72 hours because compressive strength of specimens decreased due to the formation of pore structure with Al-rich gel (Cho and et al., 2017).

Verma and Dev (2011) examined the effect of curing conditions on geopolymer concrete containing ground granulated blast furnace slag and fly ash. Geopolymer mixtures were prepared as 100/0, 75/25, 50/50 and 25/75 according to the percentage of fly ash/slag weight. Sodium hydroxide and sodium silicate were used as alkaline activators. All samples were cured at ambient temperature and/or 80°C for 24 hours after being removed from the mold. The strength of samples cured at ambient temperature was lower than that of samples cured at 80°C. It was stated that the mixture with the highest flexural and compressive strength in both types of cured samples was the mixture with a fly ash/slag ratio of 75/25. The addition of slag instead of fly ash increased the early age flexural and compressive strength of the mixture, while the addition of slag beyond 25% had a negative effect on the compressive strength of specimens. For samples cured at room temperature, the sample with a fly ash/slag ratio of 75/25 showed the highest flexural and compressive strenght with 3.6 $N/mm^2$ and 24.3 $N/mm^2$, respectively. For the 75/25 mixture cured at 80°C, the flexural strength was 5.3 $N/mm^2$, while the compressive strength was 32.9 $N/mm^2$ (Verma and Dev, 2011).

Tuyan et al. (2018) examined the effect of different curing conditions on the compressive strength of waste brick based geopolymer mortar. Geopolymer mortar samples were cured at different temperatures (50°C, 60°C, 70°C, 80°C, 90°C and 100°C) and durations (1, 3, 5 and 7 days). It was stated that when the curing temperature increases from 50°C to 70°C, the compressive strength increases at a certain level. The effect of temperature increases above 70°C on compressive strength is less compared to lower temperatures. Geopolymer mortar samples cured at 80°C had almost the same compressive strengths obtained at the end of 5 to 7 days of curing, and a decrease in strength was observed after 5 days in samples cured at 90°C, and after 3 days in samples cured at 100°C. The highest compressive strength was showed by the sample cured at 80°C for 5 days with 36.2 MPa. In samples cured at room temperature,there was no gain in compressive strength for 7 days, the compressive strength reached 18.7 MPa at the end of 90 days (Tuyan et al.,).

# 4 SELF-HEALING CONCRETE

Self-healing concrete is described as concrete that has ability to repair and treats its cracks spontaneously. Like all other scientific approaches, it is inspired by natural organisms, such as animals or trees (Souradeep and Kua, 2016).

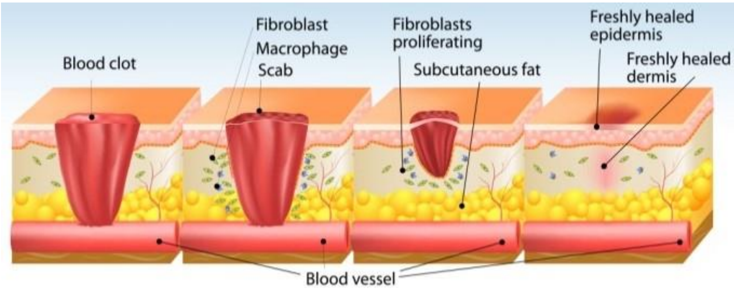


**Figure 4.1** Stages of wound healing (Orsted et al., 2018)

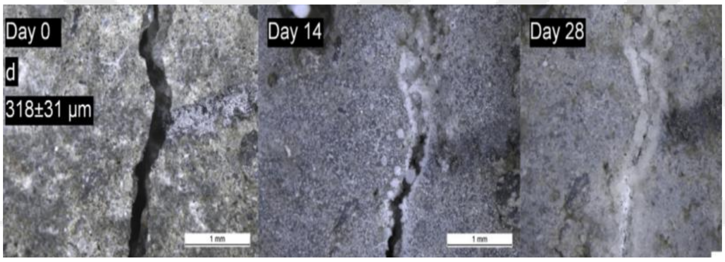


**Figure 4.2** Stages of crack closure (Erşan et al., 2016)

Self-healing concrete increases impermeability by healing cracks. In this way, the entry of harmful substances such as water and acid that can enter the concrete is prevented. It increases the freeze-thawing and acid resistance of concrete and reduces corrosion. It strengthens the microstructure of concrete by filling gaps in the microstructure of concrete with the expansion of healing agents such as bacteria that precipitate calcite. The strength of the concrete is improved by this. The healing of cracks that will occur over time, the maintenance cost decreases and the service life is extended (Vijay et al., 2017; Ghodke and Mote, 2018).

Besides all these advantages, the use of porous aggregate for immobilization of the healing agent negatively affects the strength of concrete, while the use of glass capsules can lead to an alkali-silica reaction. The fact that its use in the sector is not well known, there is no standard for the addition of bacteria and the high cost of production are other disadvantages of self-healing concrete (Ghodke and Mote, 2018).

## 4.1 History of Self-Healing Concrete

The mechanism of self-healing has been known for a long time. In 1836, autogenous healing of cracks in concrete was identified by the French Academy of Sciences in structures exposed to water during their service life (van Breugel, 2007). According to Hearn, self-healing effect in concrete was studied by Hyde at the end of the 1980s (Hearn, 1998; Hyde and Smith, 1889). A more thorough analysis of the self-healing system was conducted by Glanville in 1931 (Glanville, 1931). Jacobsen and Sellevold observed self-healing of concrete samples subjected to freeze-thaw cycles (Jacobsen et al., 1996). Recently, there has been a focus on the biotechnology and civil engineering aspect of the development of self-healing concrete technology (Ponraj et al., 2015). Although there were only a few articles in the 1980s, studies in this area began to rise in the late 1990s (Talaiekhozani et al., 2014).

Bacteria based self-healing concrete was first introduced to seal Mount Rushmore by Sookie Bang. On Mount Rushmore, which is subject to climatic factors, there is a suggestion to use it as a sealer. A bacterial *Bacillus pasteurii*/glass capsule structure has been developed, which he believes increases the strength of concrete by 24 percent. Due to a lack of interest from the commercial engineering industry, the implementation of the theory has not advanced (Zolfagharifad, 2011).

The idea of bacteria-based self-healing concrete was first introduced by Sookie Bang (Bang et al., 2001). Then, microbiologist Hendrik Jonkers was developed bacteria-based concrete (Jonkers, 2007).

## 4.2 Self-Healing Process

Self-healing concrete comes in two different varieties. These self-healing processes are autogenous and autonomous healing (Khattap et al., 2019).

### 4.2.1 Autogenous self-healing

Cracks in concrete can be partially healed with some extent by natural treatment. Cracks can be healed by the following four processes (Wu et al., 2012).

- Recrystallization of calcium hydroxide in the form of calcium carbonate ($CaCO_3$)

- Mechanical filling of cracks by impureness in water

- Additional hydration of cement -based materials

- Swelling and formation of calcium silicate hydrate gels inside the crack

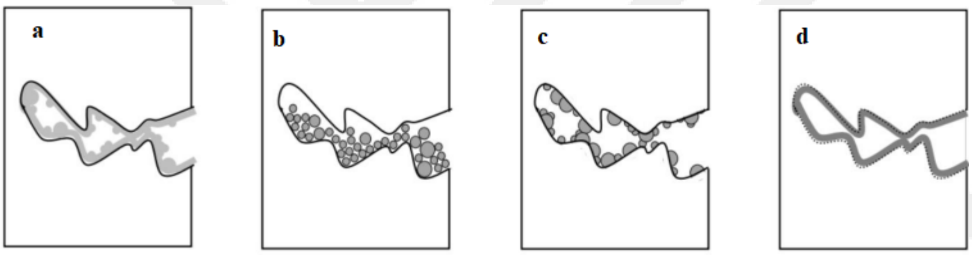


**Figure 4.3** Mechanism of natural self-healing (a) Formation of $CaCO_3$; (b) sealing by impurities; (c) Advanced hydration; (d) Hydrated cement expansion (Wu et al., 2012)

While the most of these techniques can partially fill the crack, which can not completely heal all cracks. The development of calcium carbonate is the best way to heal cracks in concrete.

Water dissolves atmospheric carbon dioxide, and calcium ions are produced from concrete. Calcium carbonate crystals are formed by the reaction of $CO^2$ and $Ca^{2+}$. The reaction is shown in equation (1). Calcium carbonate crystals are attached to the crack surface. Thus, the crack width is reduced (Edvardsen, 1999).

$$H_2O + CO_2 \leftrightarrow H_2CO_3 \leftrightarrow H^+ + HCO_3^- \leftrightarrow 2H^+ + CO_3^{2-} \quad (1)$$

Self-healing is a natural process for repairing cracks and occurs in the presence of moisture in concrete. It is noted that the deposition of calcium carbonate is produced according to the following reactions. The reaction shown in equations (2) and (3) can only come at pH values somewhere above 8, or 7.5 – 8 (Edvardsen, 1999).

$$Ca^{2}+ + CO_3^{2-} \leftrightarrow CaCO_3 \qquad pH_{water} > 8 \qquad (2)$$

$$Ca^{2} + HCO_3^{-} \leftrightarrow CaCO_3 + H^{+} \qquad 8 > pH_{water} > 7.5 \qquad (3)$$

Neville indicated that the additional hydration of unhydrated cement grains is due to the natural self-healing properties of concrete. This process applies only to concretes of an early age. The formation of calcium carbonate can be the cause of self-healing after the age of concrete increases (Neville, 2002). Natural self-healing can be sufficient for cracks with a width of 0.1– 0.2 mm (Li and Yang, 2007).

### 4.2.2 Autonomous self-healing

#### 4.2.2.1 Chemical self-healing

Through the addition of chemical agents into cracks, this procedure is another way to heal concrete. In addition to mixing the healing agent with other ingredients, liquid healing agents need to be mixed with concrete in small holders to design chemical self-healing concrete. The two main techniques used for the improvement of concrete with adhesive substances are the vascular system and the encapsulation technique (Talaiekhozani et al., 2014).

There are two modes for the vascular system. The first mode is the active mode. This mode uses a vascular flow network connected to external sources of adhesive substances for their distribution into the concrete. In passive mode, capsules, fragile thin tubes and a flow network are used for adhesive material distribution and are not connected to an external source (Khattap et al., 2019).

The adhesive substance which is used as polyethylene, ethly cyanocrylate, epoxy resin, acrylic and methyl methacrylate mixed with other components such as water, chemicals such as curative substances (Homma et al., 2009; Joseph et al., 2007; Mihashi et al., 2000; Nishiwaki, 1997; Dry, 2000). These chemical materials are preferred when there is no access to moisture in the concrete. The healing agent contained in the fragile pipes goes to the crack and heals them, tearing it as the crack spreads. Basically the idea was inspired by the structure of human bone or human vascular system (Seifan et al., 2016).

Apart from thin pipes filled with adhesive, a fixed vascular network in concrete connected to an external source at one end into a concrete sample was used for adhesive distribution (Talaiekhozani, 2014).

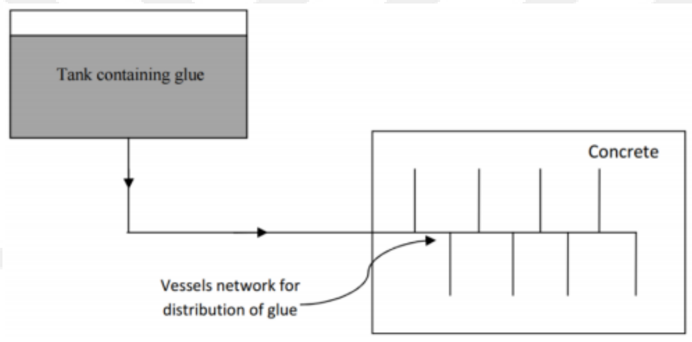


**Figure 4.4** Vascular system in passive mode (Talaiekhozani, 2014)

The encapsulation process is inspired by a cell and an egg (Hemsley et al., 2000). There are capsules of different sizes, from micro capsules to nano capsules, to hold the adhesive substance (Carolyn, 1990). Cracks allow the agent to infiltrate and fill the crack surfaces by exploding the micro capsules in the concrete. Since the volume of microcapsules is limited, it is expected that the healing agent has a higher healing capacity. The compressive and flexural strength may decrease if the amount or size of the micro capsule is increased in order to increase the amount of the healing agent. In addition to capsules' properties, the bond between the capsule shell and the cement-based matrix is also important (Talaeikhozani, 2014).

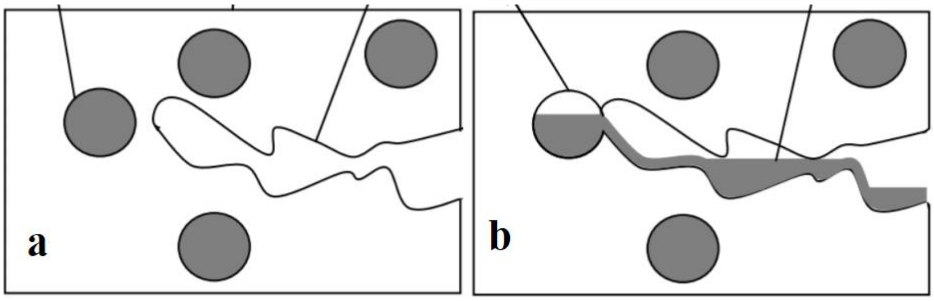


**Figure 4.5** Encapsulated healing agent (a) Formation crack in concrete; (b) The crack ruptures the microcapsules and the agent released (Khattap et al., 2019)

#### 4.2.2.2 Biological self-healing

Bacteria must be added in some special standards and be able to withstand different natural concrete situations. The choice of additives in concrete is also related to the pH value. The pH level of fresh concrete is between 12 and 13. The formation of calcium carbonate from the reaction of calcium hydroxide with atmospheric carbon dioxide lowers the pH of the concrete surface. Most bacteria cannot survive naturally, but are able to control the pH value when it is less than 10 (Bashir et al., 2016).

Anaerobic and aerobic bacteria can be used in concrete. It was reported that anaerobic bacteria related to *Shewanella* species increase the compressive strength by 25-30% when mixed into concrete (Bashir et al., 2016). Aerobic bacteria are different species to be used in concrete (Soundharya and Nirmal, 2014).

Biocalcification is based on a natural process in which bacterial cells produce calcite as part of their basic metabolic activity. This method is also known as microbiologically induced calcite precipitation (MCIP) (Sarda et al., 2009). Under the right conditions, the majority of bacteria can cause calcium carbonate to precipitate (Boquet et al., 1973). Because it can produce more ureases in harsh settings than other bacteria, *Bacillus pasteurii* is commonly used (Wong, 2015), it is more active (Siddique and Chahal, 2011) and it is non-pathogenic (Pan et al., 2015).

In the bacterial biocalcification mechanisms caused by urea hydrolysis bacteria, it is first catalyzed to produce urease by the metabolism of its bacteria (Eq.(1)), then to hydrolysis of urea by urease to carbonic acid and ammonia (Eq.(2)). Then, carbonic acid and ammonia undergo hydrolysis to carbonate and ammonium ion, respectively (Eq.(3) and Eq.(4)). The reaction shown in Eq. (4) results in an elevation in pH, which might alter the bicarbonate balance and cause carbonate ions to form Eq.(5). Bacterial cell walls, which are nucleation sites, are negatively charged (Garcia-Gonzales et al., 2017), therefore calcium cations are attached to the surfaces of the cell walls and $CaCO_3$ precipitation occurs (Eq.(6)). In this way, the reaction is irreversible and the enzyme continues to rapidly form $CaCO_3$ until the reaction products are exhausted (Eq.(7)) (Siddique and Chahal, 2011).

$CO(NH_2)_2 + H_2O \rightarrow NH_2COOH + NH_3$ (1)

$NH_2COOH + H_2O \rightarrow NH_3 + H_2CO_3$ (2)

$H_2CO_3 \leftrightarrow HCO_3^- + H^+$ (3)

$2NH_3 + 2H_2O \leftrightarrow 2NH_4^+ + 2OH^-$ (ph increase) (4)

$HCO_3^- + H^+ + 2OH^- \leftrightarrow CO_3^{2-} + 2H_2O$ (5)

$CO_3^{2-} + Ca^{2+} \rightarrow CaCO_3$ (6)

CO(NH2)2 + 2H2O + Ca2+ $\rightarrow$ 2NH4+ + $CaCO_3\downarrow$ (7) (overall reaction)

Jonkers et al. (2008) investigated the potential of bacteria to be used as a self-healing agent. *Bacillus* bacteria group was selected for its high alkali resistance spores. In order to examine the vitality of bacteria, the pore size distribution of aging samples, the influence of agent additions on strength, and the self-healing characteristics of cement mortar, samples of cement mortar with and without bacteria were created at a water-cement ratio of 0.40 and 0.50. Samples containing bacteria were prepared by substituting spores instead of mixing water at a concentration of 1-10x$10^8$ spores/$cm^3$ and cured at room temperature. It has been stated that bacterial spores added directly to the cement mortar mixture remain alive for 4 months. As a result of mercury intrusion porosimetry analysis, two main cement mortar matrix pore diameter size classes were observed as 0.01-

0.1 and 0.1-1 μm. The pore sizes of the samples cured for 3 and 7 days at room temperature are larger compared to the samples cured for 28 days. At later ages, samples show a rapid decrease in pores with a size of 0.8–1 μm, which is the typical size class of bacterial spores. The gap size decreasing below the typical size of bacteria limits the lifespan of microorganisms. Specimens containing bacterial spores at a concentration of $6x10^8$ spores/$cm^3$ showed a decrease of less than 10% in compressive strength for 3, 7 and 28 days. Since it was discovered that bacterial cement mortar samples produce significantly more crack-clogging minerals than control samples, the potential use of bacterial spores as a self-healing agent appears promising in the context of the results (Jonkers et al., 2008).

Ramachandran et al. (2001) examined the healing effect of *Pseudomonas aeruginosa* and *Sporosarcina pasteurii* bacteria on cracks in concrete. In this context, two different methods tested, namely mixing microorganisms with other components and placing microorganism to the simulated crack. For the first method, microorganisms were added in live or killed form at concentrations of $7.6x10^3$, $7.6x10^5$ and $7.6x10^7$ cell/$cm^3$. Two types of cement mortar containing *S.pasteurii* culture and a mixture of *Pseudomonas aeruginosa* and *Sporosarcina pasteurii* in equal concentration were prepared and cured at room temperature. It was stated that the 28-day compressive strength of the control sample without bacteria was 55 MPa, while the compressive strengths of all samples containing microorganisms were in the range of 55-65 MPa. The specimen containing *S.pasteurii* at a concentration of $7.6x10^3$ cell/$cm^3$ with 65 MPa showed the highest compressive strength in 28 days. Live *bacillus* cells increased the compressive strength of cement mortar at lower concentrations and with a longer incubation period. It was stated that the increase in strength of matrix of specimens containing a mixture of *S.pasteurii* and *Pseudomonas* depends on the concentration of *Bacillus pasteurii*. The extracellular material produced by pseudomonas does not have a significant effect on strengthening the matrix. For the simulated crack method, 50.8x50.8x50.8mm microorganism-free mortar samples were prepared. The samples were cut to a thickness of 3.175 mm and a depth of 25.4 mm and cracks were created. The control samples' fissures were left open and they were exposed to air. The initial batch of samples had their cracks filled with a sand and water mixture, then they were cured in water. The fissures were filled with sand and water in the second batch, and they were then cured in urea-calcium chloride ($CaCl_2$) medium. For microbial clogging of cracks in concrete, mixture of *S.pasteurii* with three different concentrations ($2.6x10^7$, $5.2x10^7$ and $2.6x10^8$ cell/$cm^3$) and sand was placed in simulated crack and left to Urea-$CaCl_2$ medium. The 28th day compressive strength of the samples with bacteria showed higher compressive strength compared to the control sample. It was stated that the concentration of $5.2x10^7$ cell/$cm^3$ shows the highest compressive strength with 46 MPa. Among the bacteria-free control samples, the compressive strength of the specimen cured in urea-$CaCl_2$ medium is 42 MPa, while the compressive strength of the samples cured in water and left in air is 34 and 36 MPa, respectively (Santhosh et al.,2001).

Chalal et al. (2012) studied the effect of *Sporosarcina pasteurii* bacteria on the compressive strength and water absorption capacity of concrete with the addition of fly ash. The cement was substituted with fly ash at the levels of 10%, 20% and 30% by weight. Bacteria with three different cell concentrations ($10^3$, $10^5$, $10^7$ cells/ml) were used in concrete mixtures. It was noted that the 28-day compressive strength of concrete specimen increased when the bacterial cell concentration increased to $10^5$ cells/ml, and then there was a decrease in strength at $10^7$ cfu/ml. The bacteria-free control concrete (0% fly ash) showed a compressive strength of 24 MPa, while the compressive strength of the control concrete with $10^5$ cells/ml of bacteria cells was showed at 28 MPa with an improvement of 22%. Similarly, with the addition of $10^5$ cells/ml of bacterial cells, there was a 20%, 15% and 11% improvement in the compressive strengths of concretes containing 10%, 20% and 30% fly ash, respectively. It was observed that the water absorption of fly ash concretes decreased when the bacterial concentration increased to $10^5$ cells/ml and then increased slightly when it increased to $10^7$ cells/ml (Siddique et al., 2012).

Bacteria used as a healing agent need a special coating to prevent them from falling apart during mixing and to ensure that they remain dormant until triggered. Some researchers use different coating methods such as using porous aggregates, capsules, sodium alginate (Barrasa et al., 2014; Cui et al., 2019).

Wang et al. (2014) investigated that the viability of encapsulated spores produced for self-healing concrete and the effect of microcapsules on cement mortar samples. The bacterial spores were encapsulated by the melamine-based microcapsulation process. Capsules with a size of about 5 μm were obtained. The concentration of spores in microcapsules was $10^9$ cells/g. Different amounts of bacteria-free microcapsules (%1, %2, %3, %4 and %5 by weight of cement) were added to the samples by mixing with water to investigate to the effect of microcapsules on strength of specimens. The samples were prepared using ordinary portland cement, standard sand and tap water with a cement-sand ratio of 1:3 and a water-cement ratio of 0.5. While the addition of microcapsules did not significantly affect the volume density, it had a negative effect on the mechanical properties of the samples. It is noted that the tensile strength is significantly reduced for a dose of microcapsules higher than 3%. With the addition of 1% to 5% microcapsules, the compressive strength of the samples decreased by 15% to 34%, respectively. Within the scope of self-healing detection, 4 types of bacteria-free samples were prepared, including control, containing all the nutrients necessary for bio-precipitation, containing 3% of empty microcapsules, containing nutrients and 3% of empty microcapsules. In addition, two types of samples containing nutrients and microcapsules with 3% and 5% bacteria were prepared. It was noted that in samples without bacteria, 18% to 50% of the crack area healed, while in samples with bacteria, the crack area showed 48% to 80% healing. While the maximum healing crack width is 250 μm in non-bacterial serial samples, this value is approximately 4 times higher with 970 μm in samples containing bacteria. It was observed that the water permeability of samples containing bacteria was lower compared to samples without bacteria (Wang et al., 2014).

Pungrasmi et al. (2019) examined three different encapsulation techniques for encapsulating *Bacillus sphaericus* bacterial spores with sodium alginate, namely extrusion, spray drying and freeze drying. The diameter of the extruded capsules was the range of 600-800 μm and had a spherical shape with a rough surface, while the diameter of the spray-dried capsules was the range of 1-10 μm and had a smooth spherical shape. The shape and morphology of the freeze-dried capsules were irregular. While freeze-drying method gives the highest bacterial viability rate with 100%, extrusion and spray drying methods show viability rates of 93.8% and 79.9% respectively. Mortar samples with bacterial spores encapsulated by freeze drying, which was selected as the most efficient technique, were prepared in the ratio of 1:3 cement/sand and 0.5 water/cement ratio. Microcapsules were added at the level of 2% by weight of cement. The progress of the crack healing process was examined and it was stated that the crack in the specimen containing non-encapsulated bacterial spores showed 72.7% reducing of crack area while this value reached 95.4% in the sample containing encapsulated bacterial spores (Pungrasmi et al., 2019).

Shahid et al. (2020) investigated the effect of the use of various *Bacillus* strains encapsulated with sodium alginate on the compressive strength of concrete and its ability to heal on its own crack. It was stated that encapsulation with sodium alginate protects the bacterial mass by preventing the infiltration of bacterial spores during the mixing stage. As a result of SEM images, $CaCO_3$ precipitation of bacteria was observed. The amount of calcium carbonate deposited in microcracks increased with the increase of bacterial content in the samples and decreased the water absorption capacity. The best results in terms of calcium carbonate precipitation are obtained by the bacterium *Bacillus subtilis*. *Bacillus Subtilis* and *Bacillus Anthracis* bacteria increased the compressive strength of concrete by 16% and 6%, respectively, while there was no increase in the use of *Bacillus pasteurii* bacteria. As the capsule structures in the concrete samples increased, the strength of the concrete samples decreased. While the 28-day average compressive strength of the reference concrete without capsules was 37.31 MPa, the compressive strength of the concrete with the addition of capsule structures at the level of 2% decreased to 35 MPa. Increasing the percentage of capsules in concrete from 5% to 15% levels reduced the compressive strength of concrete by 19% to 40%, respectively. It was stated that the healing of microcracks and cracks with widths of 2.7-1.5 mm formed on the samples were detected by the naked eye at the end of 30 days and confirmed by SEM analysis, in which $CaCO_3$ precipitates were found in the crack areas. The addition of capsules at the level of 2-3% was chosen as the optimal value considering that the increase in the amount of capsules increases the healing capacity and reduces the strength (Shahid et al., 2020)

Wang et al. (2015) examined the potential of alginate encapsulated carbonate-producing bacteria to be applied within the scope of self-healing of concrete. *Bacillus sphaericus* spores are encapsulated in a sodium alginate-based hydrogel. Encapsulated bacterial spores continued to show vitality after exposure to UV irradiation, freeze-drying and mixing processes and were able to precipitate $CaCO_3$ at the level of 70% of its weight. Two types of mortar mixture were prepared by adding encapsulated bacterial spores and free bacterial spores and artificial cracks were formed on the samples. Encapsulated bacterial spores showed bacterial activity on the crack surface, while free bacterial spores did not show oxygen consumption. The addition of capsule structures reduces the workability of the fresh mortar mixture. While the average flow diameter of the reference mixtures was 200 mm, this value decreased to 190 mm with the addition of the cement weight of the capsules at the level of 0.5% and to 185 mm at the level of 1%. It was stated that with the addition of capsules by 0.5% and 1%, the compressive strengths decreased to 16.2% and 23.4%, respectively (Wang et al., 2015).

Some researchers focus on other microorganisms, such as fungi. Luo et al. (2018) designed a fungus-based self-healing concrete. This concrete is based on the spores of the filamentous *Trichoderma reesei* fungus. Spores remain dormant until the cracks form, after which they begin to fill the cracks.

## 4.3 Nanoparticles on Self-Healing Concrete Technology

Nanoparticles can disperse throughout a material, penetrate cracks and help initiate the process of self-healing. The commonly used nanomaterials are nano alumina, nano-silica, polycarboxylates, carbon nanotubes, titanium oxides, nanokaolin, nanoiron, nanoclay and nanosilver. The effectiveness of the self-healing process depends on the type, size and shape of the nanoparticles. Most applications of nanomaterials in self-healing have been used to control corrosion (Huseien et al., 2019). Considering to their effective interaction with microbial membranes, iron oxide nanoparticles can be used for the immobilization of bacteria (Seifan et al., 2019). The fact that nanoscale metallic particles, such as iron oxide nanoparticles, have a large interaction with bacterial cell walls. It was showed that a high potential for application as an immobilizer material (Seifan et al., 2018).

In general, physical adsorption or covalent binding between the cell membrane and the immobilizer is used to immobilize bacteria cells with nanoparticles (Kourkoutas et al., 2004). Carboxyl or phosphate groups in teichoic acids attached to peptidoglycan or the underlying plasma membrane causes the cell surface of the gram-positive bacterium to have a negative charge (Scott and Barnett 2006). The immobilization of bacillus species by magnetic nanoparticles is shown schematically in Figure 4.6.

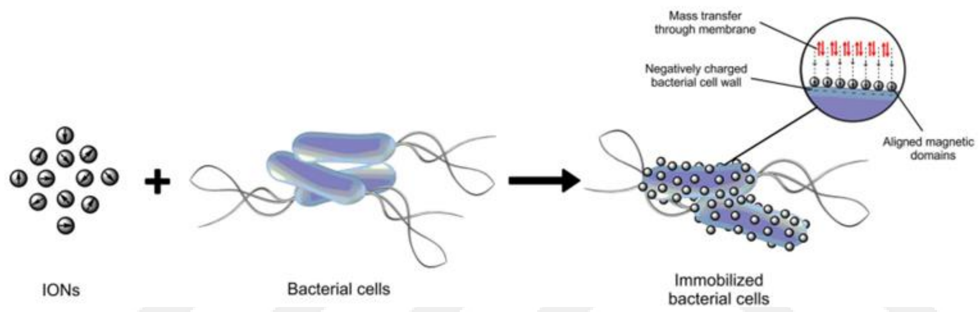


**Figure 4.6** Bacterial cells are immobilized in a schematic manner by magnetic iron oxide nanoparticles (IONs) (Seifan et al., 2018)

When the magnetic iron oxide nanoparticles interact with the bacterial cell walls, they begin to align, and adsorption is carried out accordingly. In contrast, when bacteria are immobilized, mass transfer restrictions through diffusion, changes in membrane permeability, impacts of osmotic pressure and surface tension, decreased water activity, disturbances in growth pattern, hindered cell-to-cell communication, and changes in cell morphology may take place. In order to maintain cell permeability and CaCO3 production without inhibiting growth, it is essential to decorate the cells with the proper number of nanoparticles (Seifan et al., 2018). Khushnood et al. (2019), were related the healing effectiveness of iron oxide nanoparticles with their homogeneous distribution in the mixture with the help of nano size and better protection of bacteria. The homogeneous distribution feature ensures uniform and even distribution of the bacterium. Thus, in addition, nanoparticles behave as a filling material thanks to their size (Bederina et al., 2011; Wiktor and Jonkers, 2011).

Shaheen et al. (2019) studied the effects of directly and immobilized addition of '*Bacillus subtilis*' bacteria for self-healing concrete on the compressive strength and healing potential of concrete. Iron oxide nanoparticles and bentonite nanoparticles were used for the immobilization process. While the 28-day compressive strength of reference mixture was 32 MPa, the addition of bacteria directly with the mixture water increased the compressive strength by 8%, and the addition of bacteria that immobilized by iron nanoparticle increased it by 21%. It was stated that samples containing bacteria immobilized with bentonite nanoparticle had the lowest compressive strength in 28-day compressive strength results, while the compressive strength at an early age was high compared to the reference mixture. 1.2 mm wide cracks in samples containing bacteria immobilized with iron nanoparticles were closed and the pre-crack compressive strength was regained at the level of 85%. On the other hand, in samples containing bacteria immobilized with bentonite nanoparticle and directly added bacteria, cracks with a width of 0.20 mm and 0.44 mm were closed, respectively, and the recovery in compressive strengths were 45% and 65%, respectively (Shaheen et al.,2019).

Khushnood et al. (2019) investigated that the applicability of *Bacillus subtilis* microorganisms with various immobilization techniques in the effective healing of cracks formed in concrete. In the immobilization processes, iron oxide nanoparticles, limestone microparticles and siliceous sand were used. The samples were loaded at the level of 80% of their maximum compressive strengths after at the end of the 3, 7, 14 and 24-day curing periods for crack formation then the cracked samples were cured in water for 28 days to examine the regain levels of the compressive strength. It was indicated that for all immobilization techniques, microorganisms contributed to the compressive strength and healing capacity of the cement mortar. Specimen containing iron oxide nanoparticles showed a 23% increase in compressive strength compared to the reference specimen. While there was a negligible increase in the sample containing limestone microparticles, the increase in the samples containing sand was observed at the level of 14%. Sample containing iron oxide nanoparticles showed the highest compressive strength recovery during all curing times in pre-cracked samples. While approaching the final compressive strength in the sample with a curing time of 3 days, it was observed that it recovered 91.32% in 7 days, 79.9% in 14 days and about 70% in the sample cured for 28 days. The compressive strength recovery levels of the samples containing limestone microparticles cured for 3, 7, 14 and 28 days were stated as 90%, 77.6%, 57.8% and approximately 50%, respectively. On the other hand, in samples containing sand as a bacterial immobilizer, these values were approximately 85%, 72.9%, 69.1% and 60%, respectively. The increase in the curing time before crack formation reduces the strength recoveries for all immobilization types. It was indicated that a lower levels of compressive strength recovery were observed in samples without microorganisms with autogenous healing (Khushnood et al., 2019).

Seifan et al. (2018) studied the effects of magnetic iron oxide nanoparticles on self-healing concrete for bacterial immobilization for the first time in the literature. As a result of SEM images, magnetic iron oxide nanoparticles were successfully absorbed into the cell surface of *Bacillus* bacteria. It was stated that the water absorption rate of concrete containing bacteria immobilized with nanoparticles increased by 26% compared to the control samples. The bacteria based concrete has a higher crack healing ability compared to the control sample, as well as pore and gap repair efficiency. The control samples showed a limited healing in cracks due to the additional hydration of dry cement grains after being re-immersed in water (Seifan et al., 2018).

Metal and metal oxides are produced through both physical and chemical processes. The synthesis of nanoparticles necessitates the employment of poisonous and reactive reducing chemicals, which can be fatal and have harmful impacts on the environment and living things (Gurunathan et al., 2009). The major reaction that takes place during the biosynthesis of nanoparticles is reduction/oxidation (Naik et al., 2002). Plant extracts' antioxidant or reducing qualities are typically what cause metal compounds to be reduced into the corresponding nanoparticles. Green synthesis is an improvement over chemical and physical methods because it is less expensive, more environmentally friendly, and easier to scale up for large-scale synthesis. It also eliminates the need for harmful chemicals, high pressure, energy, and temperature (Ahmad and Sastry, 2004).

Hoag et al. (2009) synthesized iron nanoparticles using green tea leaf extract containing polyphenols without adding surfactants or polymers. Green tea extract is prepared at a rate of 20 g/L. Then, 0.1 M $FeCl_3$ solution was prepared and added to green tea extract in a ratio of 2:1 by volume. All these processes were carried out at room temperature, and the polyphenols in green tea acted reductively, resulting in spherical iron particles with a diameter of 5-10 nm (Hoag et al.,2009).

Shahwan et al. (2011) added 0.10 M ferric chloride solution to green tea extract in 2:3 volume ratios to synthesize iron nanoparticles. 1.0 M NaOH solution was added until the pH value of the mixture reached 6.0. Iron nanoparticles with diameters of 40-60 nm were obtained by evaporating the water in the solution (Shahwan et al., 2011).

Huang et al. (2014) 60.0 g/L green tea extract was heated and kept at 80 C for 1 hour. Then, 0.1 mol / L $FeSO_4$ solution was added to the vacuum filtered tea extracts in a 1:2 ratio by volume. The diameter of the nanoparticles obtained as a result of the characterization process was in the range of 40-50 nm (Huang et al., 2014).

## 4.4 Self-Healing Geopolymer Mortar

Jadhav et al. (2018) investigated the effectiveness of bacterial-based self healing metakaolin-based geopolymer. Sodium silicate was used as an activator and S.pasteurii spores were freely added to the geopolymer mixture without undergoing the immobilization process. The average crack width of pre-cracked geopolymer samples that do not contain bacteria is 39±5 μm. No reduction in the crack area was observed before and after exposure to urea-CaCl2 medium. Pre-cracked samples containing bacteria were exposed to two different media containing only urea and containing urea and CaCl2. It was noted that cracks with a crack width of 25±6 μm and a width of 89±3 μm healed in samples exposed to an environment containing urea and CaCl2, while healing was not observed in samples exposed only to a urea environment (Jadhav et al.,2018).

Polat and Uysal (2021) examined the effect of the use of *S.pasteurii* bacterial spore as a healing agent on the self-healing property of metakaolin-based geopolymer mortar. The combination of sodium silicate and sodium hydroxide was used as an alkaline activator. The bacterial culture was absorbed into metakaolin (at least $10^5$ cells per 1 g mortar), dried for 24 hours at 40°C, and then added to the mortar in the first way. The bacteria on the surface of the solid agar were collected in distilled water for the second technique, which was then put to the mortar. The prepared samples were loaded at the level of 70% of the maximum flexural strength, and cracks with a width in the range of 50-400 μm were formed. A smaller amount of voids was observed in all samples containing bacteria compared to samples without bacteria. It was stated that the UPV value of the sample containing bacterial culture was 3.03% lower than the value of the control sample. While crack healing was observed in all samples containing bacteria, healing was delayed as the amount of NaOH in the activator increased. While the water absorption rates of the samples showing improvement decreased, there was no increase in compressive strength. Polat and Uysal related this relationship by confirming with SEM images that the cracks were filled with weaker structures than the stable calcite structure (Polat and Uysal, 2021).

Ekinci et al. (2021) investigated the effect of the addition of *Bacillus subtilis* on the compressive strength and water absorption rate of ground blast furnace slag based geopolymer mortar. In the mortar design, 0.55 water/binder ratio, 1:2 binder aggregate ratio and sodium silicate were used as alkaline activator. Bacterial cultures prepared at concentrations of $10^7$ and $10^9$ cfu/ml were added to sodium silicate at 1%, 2% and 3% by weight of the binder. The samples were subjected to urea-$CaCl_2$ medium, water and ambient conditions for 7 and 28 days. It was stated that sample containing 1% bacteria at a concentration of $10^7$ cfu/mL showed the highest compressive strength with 33 MPa at the end of a 7-day ambient cure, while other samples containing bacteria had lower compressive strengths compared to the control sample. Specimen containing 2% bacteria at a concentration of $10^9$ cfu/ml showed the lowest compressive strength with 26.4 MPa at the end of a 7-day ambient cure. An increase in the amount of bacteria in the mixture negatively affected the 7-day compressive strength for all samples. An increasing the amount of bacteria from %1 to %3 in samples cured in urea-$CaCl_2$ medium and containing bacteria at a concentration of $10^9$ and $10^7$ cfu/ml, increased the 28-day compressive strength 13% and 9%, respectively, compared to 7-day compressive strength. It was stated that this increase was at the level of 25% and 30%, respectively, compared to the control sample. In the samples cured under water and ambient conditions, the increase in the amount of bacteria reduced the compressive strength. It was observed that the compressive strengths of the samples cured in Urea-$CaCl_2$ medium were higher in the range of 17.5%-188% compared to the samples cured in water and ambient conditions with the same ingredients. When the amount of bacteria increased in samples cured in urea-$CaCl_2$ medium and containing bacteria at $10^9$ cfu/ml and 107 cfu/ml concentrations, the water absorption rates decreased by 8.6% and 7.25%, respectively. On the other hand, in water-cured samples, the water absorption rate increased by 3.2% and 11%, respectively, and in samples cured under ambient conditions, there was an increase in the levels of 3.5% and 4%. While the lowest water absorption rate was %4.3 showed by a sample containing bacteria at a concentration of $10^7$ cfu/ml at a dosage of 3%, cured in urea-$CaCl_2$ medium, the highest water absorption rate was %6.24 showed by a water-cured sample containing bacteria in a 3% dosage at a concentration of $10^9$ cf/ml (Ekinci et al., 2021).

# 5 MATERIALS AND METHODS

## 5.1 Materials

Within the scope of the experimental study, the materials are used described in this section.

### 5.1.1 Binder materials

The chemical and physical properties of a class F fly ash obtained from Izdemir Enerji Elektrik Üretim A.Ş. and its compliance with with TS EN 450-1 standard and the properties of a granulated blast furnace slag obtained from Karcimsa Çimento San. Ve Tic. A.Ş. and its compliance with EN 15167-1 standard are given in Table 5.1.

Waste bricks supplied from Yuksel Toprak Sanayi ve Ticaret A.Ş. were used in geopolymer mortar mixtures. Since the waste brick was not in powder form when they were supplied. They are pulverized with the help of a ball grinder. The chemical and physical properties of waste brick powder obtained from the TUBITAK project called “Doğal ve Atık Malzemelerle Geopolimer Harç ve Beton Geliştirilmesi” are presented in the Table 5.1.

**Table 5.1** Physical and chemical properties of binder materials

| Oxide composition, % | (İzdemir) Fly ash (%) | TS EN 450-1: 2013 Limits | Granulated blast furnace slag (%) | EN 15167-1 Limits | Waste brick powder (%) |
|---|---|---|---|---|---|
| **$SiO_2$** | 57.17 | - | 33.87 | - | 66.15 |
| **$Al_2O_3$** | 23.81 | - | 12.23 | - | 15.36 |
| **$Fe_2O_3$** | 6.94 | - | 1.41 | - | 5.98 |
| **$SiO_2$+ $Al_2O_3$+ $Fe_2O_3$** | 87.92 | Min, %70 | 47.51 | - | 87.49 |
| **CaO** | 4.09 | - | 30.21 | - | 2.95 |
| **MgO** | 2.14 | Max. % 4.0 | 9.35 | Max. %18 | 2.13 |
| **(CaO+MgO)/$SiO_2$** | 0.10 | - | 1.17 | Min. %1.0 | 0.07 |
| **CaO+MgO+$SiO_2$** | 63.40 | - | 73.43 | Min. %66.67 | 71.23 |
| **$Na_2O$** | 1.44 | - | 0.49 | | 0.89 |
| **$K_2O$** | 1.96 | - | 0.78 | | 2.77 |
| **($Na_2O$+0.658*$K_2O$)** | 2.74 | Max. %5.0 | 1.00 | | 2.71 |
| **$SO_3$** | 0.15 | Max. %3.0 | 0.61 | Max. %2.5 | 0.11 |
| **$TiO_2$** | 0.87 | - | 1.35 | | - |
| **$Cl^-$** | 0.10 | Max. %0.1 | 0.013 | | - |
| **S-2** | - | - | 0.24 | Max. %2.0 | - |
| **$Mn_2O_3$** | - | - | 4.11 | - | - |
| **Physical Properties** | | | | | |
| **Specific gravity (g/cm$^3$)** | 2,27 | - | 2,90 | - | 2.70 |
| **Blaine Fineness (cm$^2$/g)** | - | - | 4465 | - | - |
| **Soundness (mm)** | 1 | - | 0 | - | - |
| **Activity Index–7d (%)** | - | - | 52.40 | Min. %45 | - |
| **Activity Index–28d (%)** | 80.8 | Min. %75 | 74.1 | Min. %70 | - |
| **Activity Index–90d (%)** | 91.0 | Min. %85 | - | | - |

SEM images and EDS analysis of fly ash obtained from İzdemir Elektrik Üretim A.Ş. is showed in Figure 5.1.

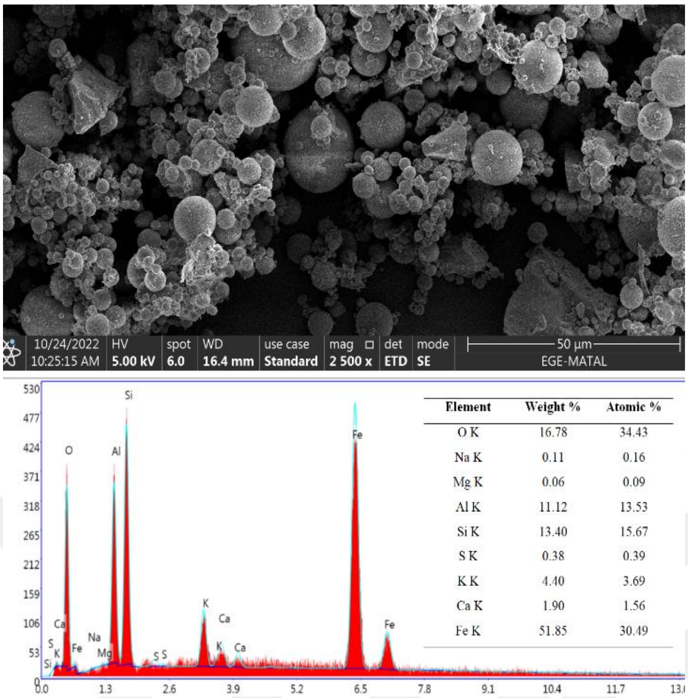


| Element | Weight % | Atomic % |
|---|---|---|
| O K | 16.78 | 34.43 |
| Na K | 0.11 | 0.16 |
| Mg K | 0.06 | 0.09 |
| Al K | 11.12 | 13.53 |
| Si K | 13.40 | 15.67 |
| S K | 0.38 | 0.39 |
| K K | 4.40 | 3.69 |
| Ca K | 1.90 | 1.56 |
| Fe K | 51.85 | 30.49 |

**Figure 5.1** SEM/EDS results of class F fly ash

SEM images and EDS analysis of granulated blast furnace slag is showed in Figure 5.2.

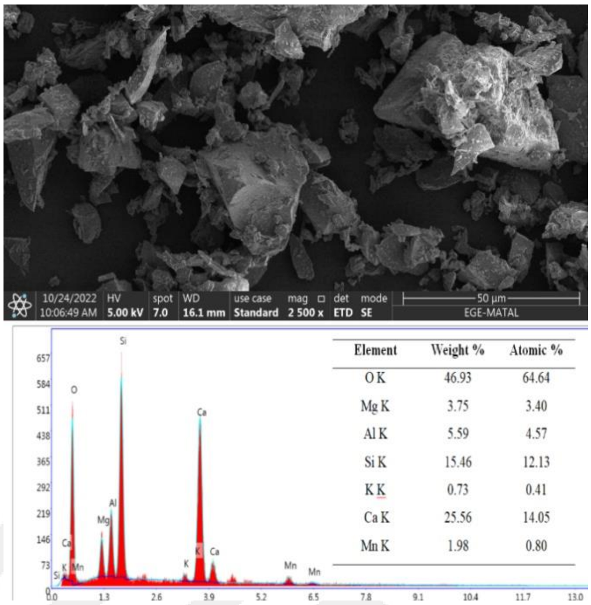


| Element | Weight % | Atomic % |
|---|---|---|
| O K | 46.93 | 64.64 |
| Mg K | 3.75 | 3.40 |
| Al K | 5.59 | 4.57 |
| Si K | 15.46 | 12.13 |
| K K | 0.73 | 0.41 |
| Ca K | 25.56 | 14.05 |
| Mn K | 1.98 | 0.80 |

**Figure 5.2** SEM/EDS results of granulated blast furnace slag

SEM images and EDS analysis of brick powder are showed in Figure 5.3.

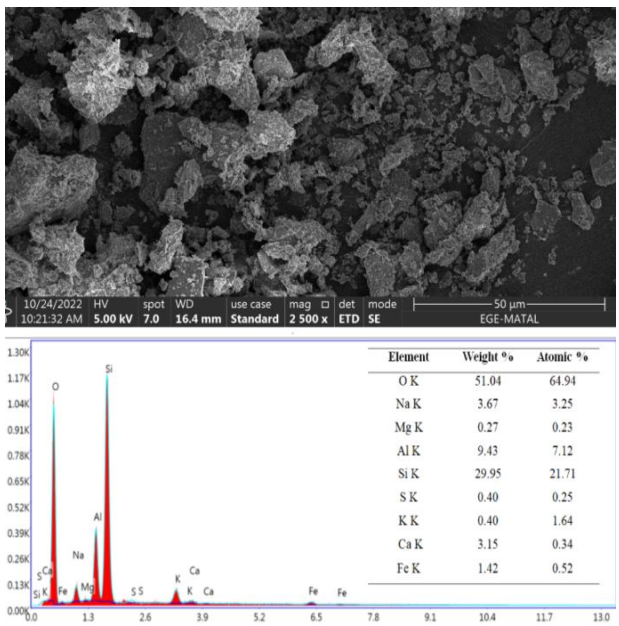


| Element | Weight % | Atomic % |
|---|---|---|
| O K | 51.04 | 64.94 |
| Na K | 3.67 | 3.25 |
| Mg K | 0.27 | 0.23 |
| Al K | 9.43 | 7.12 |
| Si K | 29.95 | 21.71 |
| S K | 0.40 | 0.25 |
| K K | 0.40 | 1.64 |
| Ca K | 3.15 | 0.34 |
| Fe K | 1.42 | 0.52 |

**Figure 5.3** SEM/EDS results of brick powder

The XRF results of the class F fly ash obtained from Muğla Yatağan thermal power plant, which was used in the optimization phase of binder materials, are given in Table 5.2.

**Table 5.2** XRF results of class F fly ash obtained from Muğla Yatağan thermal power plant

| Oxide composition % | Muğla Fly ash (%) | TS EN 450-1: 2013 Limits |
|---|---|---|
| $SiO_2$ | 58.90 | - |
| $Al_2O_3$ | 20.40 | - |
| $Fe_2O_3$ | 8.44 | - |
| $SiO_2+Al_2O_3+Fe_2O_3$ | 87.74 | Min. %70 |
| CaO | 3.86 | - |
| MgO | 1.70 | Max. %4.0 |
| $Na_2O$ | 1.44 | - |
| $K_2O$ | 2.11 | - |
| Na2O+0.658*$K_2O$ | 2.82 | Max. %5.0 |
| $SO_3$ | 0,86 | Max. %3.0 |
| $Cl^-$ | - | Max. %0.1 |
| **Physical Properties** | | |
| Specific gravity ($g/cm^3$) | 2.18 | - |

## 5.1.2 Sodium hydroxide and sodium silicate

Sodium hydroxide and sodium silicate chemicals were used to provide alkaline activation within the scope of the thesis. Sodium hydroxide, which is 97% pure and in granular form, was supplied by Merck company. 3 modules of sodium silicate produced by a company operating in Manisa province and consisting of a chemical composition of 10% $Na_2O$, 23.2% $SiO_2$ and 66.8% $H_2O$ were used.

## 5.1.3 Aggregate

In the experimental study, silica-based standard sand obtained from Limak Çimento San. Ve Tiç. A.Ş. with a maximum grain diameter of 2 mm was used as an aggregate in accordance with TS EN 196-1 standard.

### 5.1.4 Water

Bornova (Izmir) city mains water was used.

### 5.1.5 Spororascina pasteurii

*Spororascina pasteurii* (DSMZ 33) was produced and a biocalcification solution was prepared at the Department of Bioengineering of the Faculty of Engineering of Ege University for use in the bacterial biocalcification process.

## 5.2 Methods

Within the scope of the experimental study, methods are used described in this section.

### 5.2.1 Alkaline solution

Sodium hyroxide granules were dissolved in sodium silicate solution by mixing method and activator solution with three different Ms ratios (1.20, 1.30, 1.40) was produced. These solutions were obtained in such a way that the amount of $Na_2O$ to enter the mixture from the solution was 10% by weight of aluminosilicate. The solutions were used after resting for 24 hours under ambient conditions.

### 5.2.2 Geopolymer mortar mixture

Mixtures were prepared in Hobart mixer. All components are weighed on the 0.1g precision scale. In order to obtain a homogeneous dry mixture, firstly, the binder material and standard sand were mixed for 1 min. Then the alkaline activator solution prepared one day in advance was added to the mixture. After the addition of the solution, the mixture were prepared by mixing for a total of four minutes at low speed for 2 minutes and at high speed for 2 minutes. The prepared mixtures were filled in two layers into prismatic samples with a size of 40x40x160 mm in accordance with the applied experimental standard. Each layer was compressed with 25 mallet strokes and then dropped 25 times on the vibrating table. The prepared mixtures were subjected to curing process and kept until they reached the ambient temperature after the curing time was over. Samples that came to room temperature were removed from the mold and related experiments were carried out.

### 5.2.3 The activation of porosarcina pasteurii

In the study, the *S.Pasteurii* (DSMZ 33) strain registered in the DSMZ culture collection was used. Bacteria contained in glycerol and stored at -20°C were planted in petri dishes containing Nutrient Agar (NA) by the line planting method and incubated at 30°C for 48 hours and colonies were obtained.

### 5.2.4 The production of biomass

A full of inoculation loop of activated *S.pasteurii* cells were suspended with 10 ml of physiological saline and 200 ml of Nutrient broth containing 2% (w/v) urea prepared in 1L of Erlenmeyer flask were inoculated (3% v/v). After that, Erlenmeyer flask were incubated at 30°C at a shaking speed of 180 rpm for 48 hours.

### 5.2.5 Cell counting

In order to standardize the addition of cells to the biocalcification solution, it was determined how many living cells the fermentation liquid corresponds to with different absrobans values (0-1.0) at 600 nm on the spectrophotometer. Using petri dishes containing NA for live cell counting, the fermentation liquid diluted with physiological saline to $10^{-9}$ was inoculated into the media with the spreading plate method in 3 parallels before each dilution. The colonies formed in the media after incubation (48 hours 30°C) were counted and the number of living cells per millimeter of the fermentation liquid was determined by considering the dilution factor.

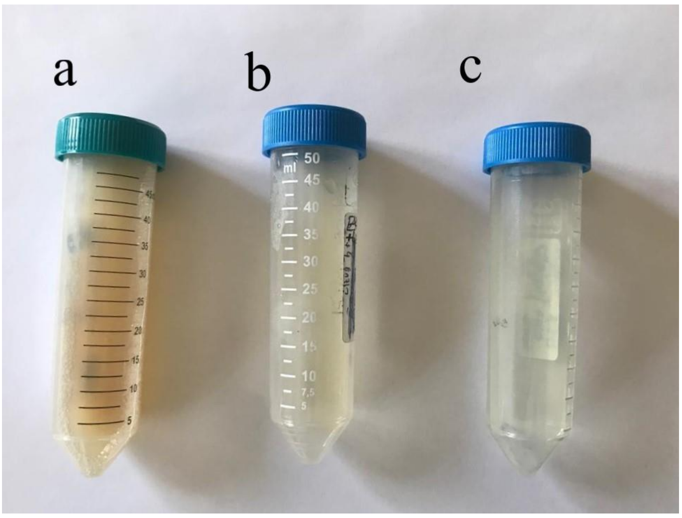


**Figure 5.4** (a) bacteria suspension at concentration of $10^{10}$ cfu/ml; (b) bacteria suspension at concentration of $10^9$ cfu/ml; (c) bacteria suspension at concentration of $10^8$ cfu/ml

### 5.2.6 Encapsulation of bacteria with sodium alginate

Sodium alginate and calcium chloride were used to encapsulate the bacteria. Sodium alginate solution prepared by dissolving in water at a concentration of 2% (w/v) as a coating material in encapsulation was mixed with the help of a magnetic mixer and sterilized by holding in an autoclave at 121°C for 15 minutes. After the sterilization process, the sodium alginate solution was mixed in a magnetic mixer for about 24 hours in order to maintain its homogeneity when it cooled down (Krasaekoopt et al., 2004). $CaCl_2$ solution dissolved in distilled water at a concentration of 2% (w/v) was used as a crosslinker in the encapsulation process. This solution was subjected to sterilization process in autoclave at 121°C for 15 minutes before being used in the study. For *S.Pasteurii*, $10^8$, $10^9$ and $10^{10}$ cfu/ml suspensions containing bacteria at a concentration of 2% (w/v) were used in the encapsulation process performed with sodium alginate solution (Pungrasmi et al., 2019).

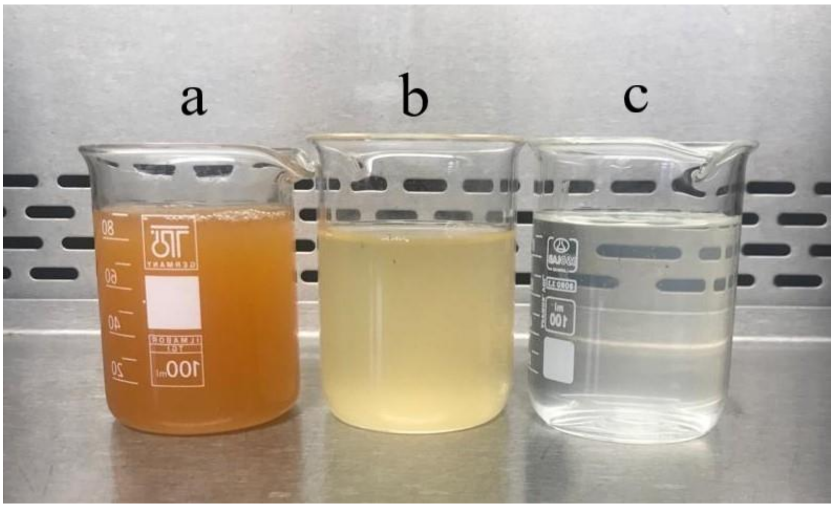


**Figure 5.5** Sodium alginate suspensions containing bacteria with different concentrations (a) Concentration of bacteria is $10^{10}$ cfu/ml; (b) Concentration of bacteria is $10^{9}$ cfu/ml; (c) Concentration of bacteria is $10^{8}$ cfu/ml

10 ml disposable sterile syringes and disposable sterile syringe needles (6mm) were used to create encapsulation by extrusion method. The suspension containing bacteria and sodium alginate solution was mixed in a magnetic mixer until it became homogeneous. Then it was extruded with the help of a sterile syringe and dripped from a height of 20 cm (the distance between the syringe tip and the surface of the liquid where the $CaCl_2$ solution is located) into the $CaCl_2$ solution at a concentration of 2% by free fall. When the suspension containing sodium alginate and bacteria was dripped into the $CaCl_2$ solution (after the extrusion process was completed), calcium alginate and sodium chloride (NaCl) compounds began to form and capsules were observed. After the encapsulation process was completed, the capsules formed were kept in $CaCl_2$ solution for 30 minutes in order to stabilize. The capsules taken from the $CaCl_2$ solution were filtered with Whatman filter paper and washed 3 times with distilled water. Capsules were placed in steel trays and left overnight in a 50°C to dry.

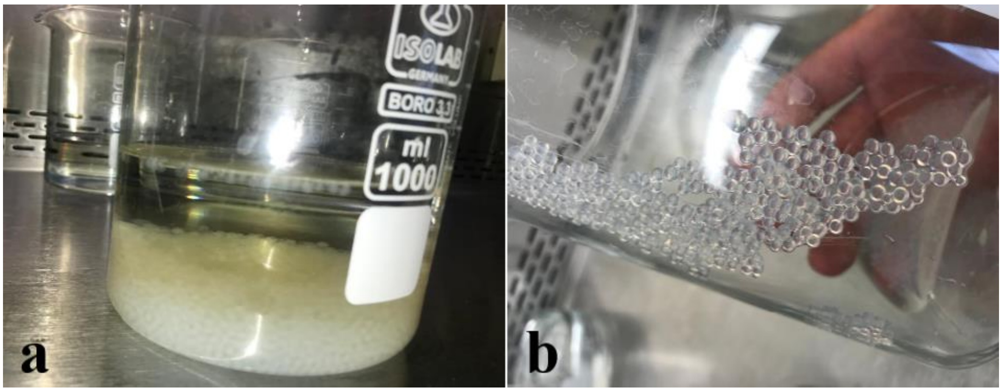


**Figure 5.6** Microcapsules (a) Microcapsules in $CaCl_2$ solution; (b) Microcapsules after filtration

**Figure 5.7** Dried microcapsules

### 5.2.7 Synthesis of iron magnetic nanoparticles

152 ml of ultrapure water (UPW) is added into the beaker. A magnetic mixer is put in it. 0.356g $FeSO_4$ and 0.692g $FeCl_3$ are added into beaker and mixed and heated. It is observed that the mixture, which is initially copper in color, reaches a darker color as the temperature rises (Magnetite $Fe_3O_4$). It is ensured that the mixture, which is constantly measured with a thermometer, reaches 80°C. When the mixture is measured at 80°C, 8 ml of ammonia is added drop by drop then mixture reaches a black color. After that, the heating process continues from 80°C to 90-100°C for 45 minutes. Since there will be high evaporation at this time, UPW is added frequently (6ml UPW for 2 min) to keep

the amount of 152 ml UPW constant. After the heating process is finished, the beaker is allowed to cool down for a while. Then it is carefully taken on the shaped magnet. After the particles attracted by the magnet adhere to the base of the beaker, the washing process is performed. Washing process is done in 3 repetitions by adding 40 ml of UPW each time, drizzling it in the mixture and then pouring it. After the particles are completely washed, 19 ml of UPW is added to the beaker again and carefully moved from the container to the 50-piece tube. about 20 ml of liquid+nanoparitcle mixture in a 50 ml tube is placed in the freezer at -20°C. After being left overnight, it is ready for lyophilization. After the lyophilization process is completed, the powders are ready for use (Shebl et al., 2017).

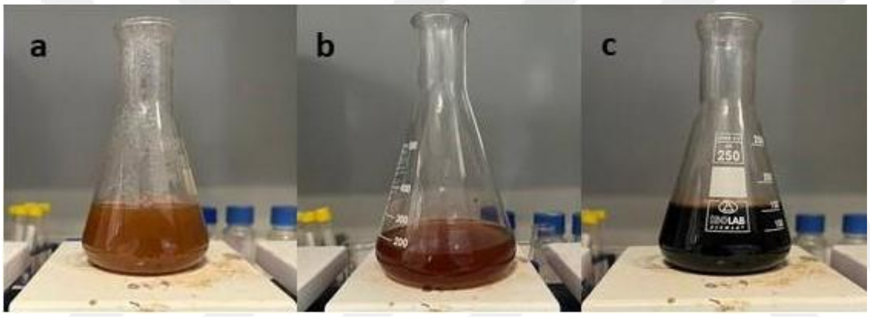


**Figure 5.8** $FeSO_4$ - $FeCl_3$ mixture (a) Before heating; (b) During heating; (c) Added ammonia


**Figure 5.9** Synthesized iron magnetic nanoparticles attracted by a shape magnet

### 5.2.8 Green synthesis of iron nanoparticles

60 g of green tea with 1000 ml of UPW is left in the heater to boil at 80-90°C. The green tea extract, which is boiled for 1.5 hours, is filtered into 3 pieces of erlen with filter paper. It is centrifugated at 2600 rpm for 15 minutes to thoroughly remove the residues from the filtered green tea extract. In the centrifugated green tea extract, those that fall to the bottom are discarded and the upper phase is collected. 0.1 M $FeCl_3$ solution is prepared to be half of the obtained extract volume. Erlens are coated so that they do not get light, and an equal amount of green tea extract is added. The $FeCl_3$ solution, which is prepared enough to be half the volume of tea in each erlen, is added to the erlen and placed in a shaker at 480 rpm for an hour. From this stage, the solution acquires a black color. Black solutions are centrifugated for 30 minutes at 2800 rpm. Top layer is poured a little and UPW water is added and centrifugated for another 10 minutes at 2800 rpm. Then, washing is done with a pastor straw and the particles remaining at the bottom are added to the petri dishes and left overnight in a 60°C to dry (Gottimukkala et al., 2017).

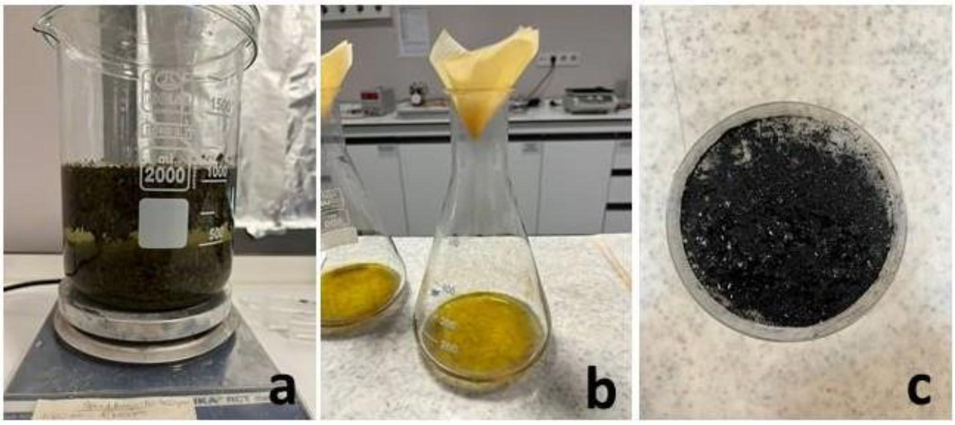


**Figure 5.10** (a) Boiling green tea process; (b) Filtered green tea extract; (c) Green synthesized iron nanoparticles

### 5.2.9 Encapsulation of bacteria immobilized by nanoparticles with sodium alginate

Sodium alginate and calcium chloride were used to encapsulate the bacteria with magnetic iron nanoparticles and iron nanoparticles obtained by green synthesis method. Sodium alginate solution prepared by dissolving in water at a concentration of 2% (w/v) as a coating material in encapsulation was mixed with the help of a magnetic mixer and sterilized by holding in an autoclave at 121°C for 15 minutes. After the sterilization process, the sodium alginate solution was mixed in a magnetic mixer for about 24 hours in order to maintain its homogeneity when it cooled down (Krasaekoopt et al., 2004). $CaCl_2$ solution dissolved in distilled water at a concentration of 2% (w/v) was used as a crosslinker in the encapsulation process. For *S.Pasteurii* $10^9$ cfu/ml suspensions containing *S.pasteurii* bacteria at a concentration of 2% (w/v) were used in the encapsulation process performed with sodium alginate solution (Pungrasmi et al., 2019). Three different series for two type of nanoparticles were formed by adding nanoparticles at the 0.5%, 1% and 1.5% levels of sodium alginate volume. 10 ml disposable sterile syringes and disposable sterile syringe needles (6mm) were used to create encapsulation by extrusion method. The suspension containing bacteria, nanoparticles and sodium alginate solution was mixed in a magnetic mixer until it became homogeneous. Then it was extruded with the help of a sterile syringe and dripped from a height of 20 cm (the distance between the syringe tip and the surface of the liquid where the $CaCl_2$ solution is located) into the $CaCl_2$ solution at a concentration of 2% by free fall. When the suspension containing sodium alginate, nanoparticles and bacteria was dripped into the $CaCl_2$ solution (after the extrusion process was completed), calcium alginate and sodium chloride (NaCl) compounds began to form and capsules were observed. After the encapsulation process was completed, the capsules taken from the $CaCl_2$ solution were filtered with Whatman filter paper and washed 3 times with distilled water. Capsules were placed in steel trays and left overnight in a 50°C to dry.

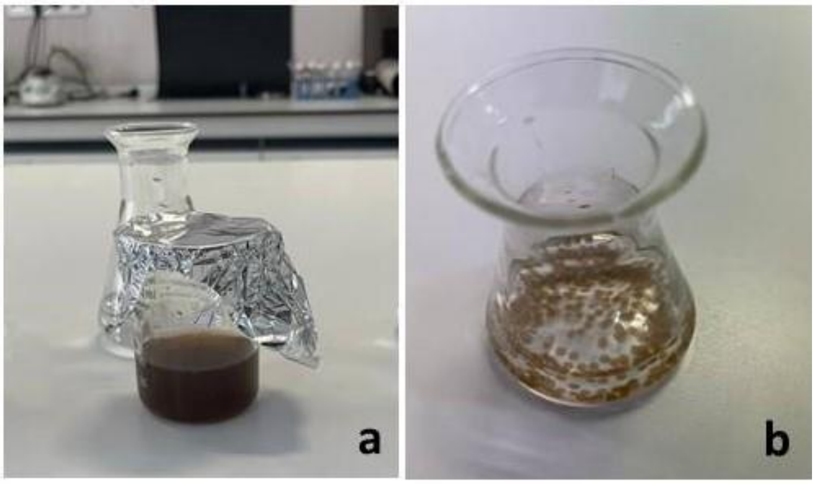

**Figure 5.11** (a) Mixture containing sodium alginate, bacteria and nanoparticles (front), $CaCl_2$ (back); (b) Microcapsules forms in $CaCl_2$

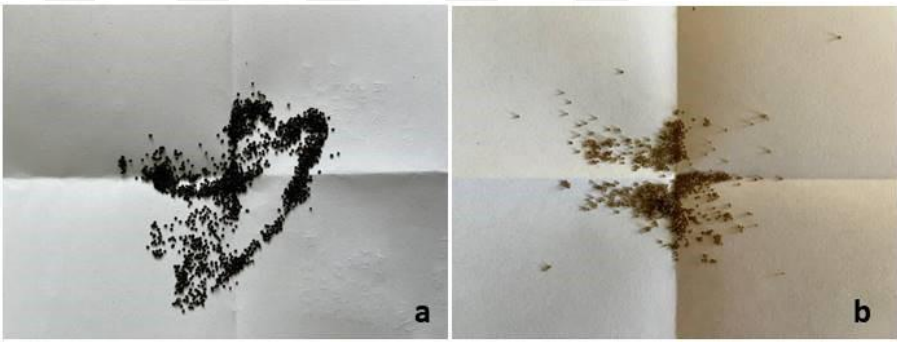

**Figure 5.12 (a)** Dried iron magnetic nanoparticles; (b) Dried iron nanopaticles obtained by green synthesis method

### 5.2.10 Preparation of geopolymer mortar mixture containing non-encapsulated bacteria

Mixtures were produced with the optimized proportions as a result of characterization processes. Binder powder materials and sand were added together to the mixer chamber and mixed at low speed (62 rpm) for 30 seconds. Bacterial culture liquid was used as mixture water. Alkali activator and bacterial culture liquid were added to the dry mixture and mixed at 62 rpm for 2 minutes and at 125 rpm for 2 minutes. The prepared mixtures were filled into prismatic molds with notches measuring 40x40x160 mm in two layers. Each layer was compressed with 25 mallet strokes and then dropped 25 times on the vibrating table. The prepared mixtures were subjected to curing process and kept until they reached the ambient temperature after the curing time was over. Samples that came to room temperature were removed from the mold and related experiments were carried out.

### 5.2.11 Preparation of geopolymer mortar mixtures containing encapsulated bacteria / and encapsulated bacteria with nanoparticles

Mixtures were produced with optimized proportions as a result of characterization processes. Binder powder materials and sand were added together to the mixer chamber and mixed at low speed (62 rpm) for 30 seconds. Then, capsules were added at a rate of 2 % by weight (capsule/binder) (Pungrasmi et al., 2019) and 30 seconds were mixed. Then water and alkaline activator were added and mixed at 62 rpm for 2 minutes and then mixed at 125 rpm for 2 minutes. The prepared mixtures were filled into prismatic molds with notches measuring 40x40x160 mm in two layers. Each layer was compressed with 25 mallet strokes and then dropped 25 times on the vibrating table. The prepared mixtures were subjected to curing process and kept until they reached the ambient temperature after the curing time was over. Samples that came to room temperature were removed from the mold and related experiments were carried out.

### 5.2.12 The controlled crack formation in geopolymer mortars by flexural loading

In order to determine the effective healing with flexural strength, controlled cracks were formed in the samples prepared using steel molds with a size of 40x40x160 mm. A material that can create notches with dimensions of 7x5x40 mm is placed in the middle of these molds.

**Figure 5.13** 40x40x160 mm steel molds with notches

The prepared mortar mixtures were placed in steel molds in two layers. After the first layer was placed, it was taken to the vibrating table and dropped 25 times. After the first layer placed, steel fibers were placed in the areas where cracks would be formed, which would ensure that the samples would stay together after the crack formation. After the second layer was poured into the molds, the shaking process was repeated and the surface was corrected with the help of gaging. Samples were left in the optimized curing regime.

**Figure 5.14** Placed steel fibers on the first layer of mortar

After the curing was completed, the universal tester was forced to bend so that the force was on the notch with the 3-point bending experiment device. In order to apply the Crack Mouth Opening Displacement Method (CMOD), the loading was stopped when the crack reached 0.3 mm with the help of an extensometer placed in the notch. After the crack was formed, it was expected that the healing process would be completed by continuing to cure under ambient conditions on metal stands without contacting water.


**Figure 5.15** CMOD method before loading

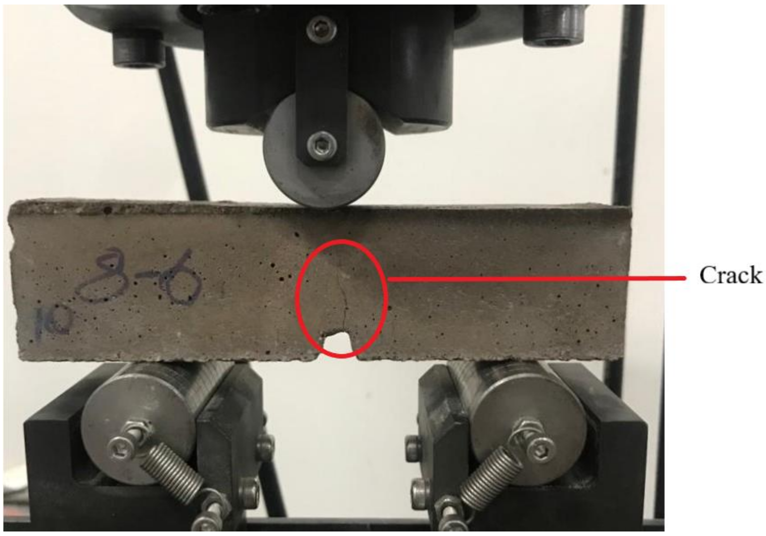


**Figure 5.16** CMOD method after loading

### 5.2.13 Determination of Geopolymer mortar consistency by flow table test

The flow diameter value of geopolymer mortars were determined according to ASTM C1437-20 standard. After the mixture was lowered 25 times in 15 seconds on the spreading table, two diameters perpendicular to each other were measured and the average of these two values was taken as the flow diameter value.

**Figure 5.17** Flow table test

### 5.2.14 Determination of setting time of geopolymer mortar by Gilmore test

Setting times of geopolymer mortars were determined based on ASTM C266 standard. Gillmore initial and final needles are used to mold and test a sample for setting time. The initial setting time is the interval between placing the sample in the oven and the point at which the paste cannot be completely circled by the Gillmore initial needle. The amount of time between placing the sample in the oven and the point at which the Gilmore final needle does not completely round the paste's surface is known as the final setting time.

### 5.2.15 Flexural strength test

Flexural strengths of geopolymer mortars were determined based on ASTM C348-21 standard. The capacity of the hydraulic press used in the experiment is 10 tons, the bearing opening is 100 mm and three-point loading was performed. The flexural strength of the samples was calculated with the help of Equation (1). and the average flexural strength of three samples was recorded as flexural strength.

$$\sigma = \frac{3FL}{2wd^2} \quad (1)$$

σ : flexural strength (MPa)

F: the maximum force applied (kN)

L: the length of span (mm)

w: the width of the sample (mm)

d: the depth of the sample (mm).

### 5.2.16 Compressive strength test

The compressive strength tests were carried out on a concrete press with a capacity of 2000 kN based on ASTM C349-18 standard. The remaining parts of the prism with the dimensions of 40x40x160 mm used in the flexural strength experiment were used as samples, and the average of six samples was recorded as a compressive strength value.

### 5.2.17 Determination of effective self-healing of Geopolymer mortar by Ultrasonic pulse velocity test

The ultrasonic pulse velocity (UPV) of the geopolymer mortars was determined on the prism samples by the Proceq brand Pundit device seen in the

Figure 5.13. The device was calibrated with a calibration rod before ultra sound transition velocity measurements were performed on the samples. UPV measurements were performed perpendicular to the casting direction of the sample and on flat surfaces of the sample. UPV measurements were recorded before cracks in the samples and the time after crack, after 1, 2, 4, 6 hours and 1, 2, 4, 7, 14, 21 and 28 days the crack.


**Figure 5.18** Ultrasonic pulse velocity test

Effective self-healing was determined by taking the substracting the amount of the healing of control samples from the amount of the healing in the Test (bacteria-containing) samples to define the measured healing is due to self-healing or due to continuing geopolymerization. Determination of effective healing is shown schematically in Figure 5.19.

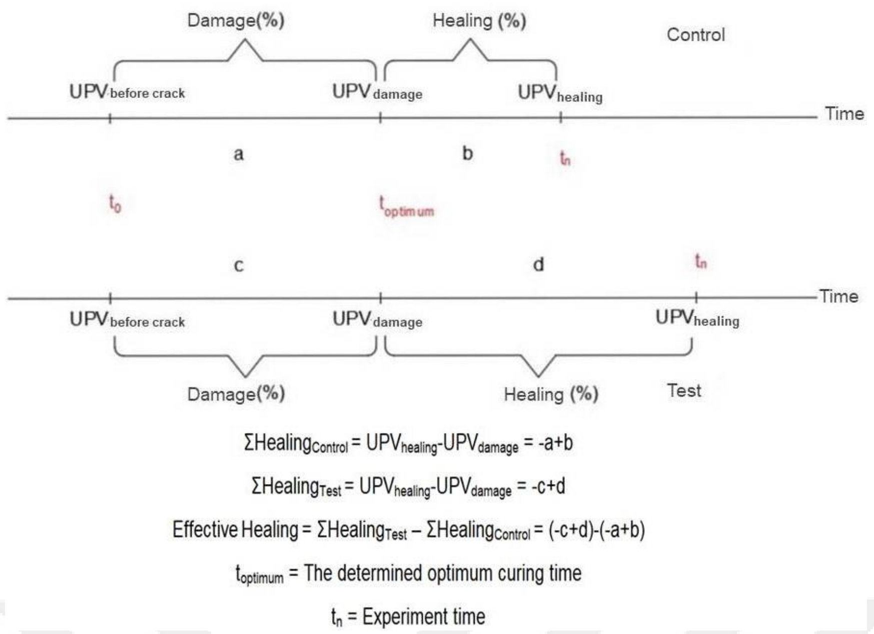


**Figure 5.19** Determination of effective healing of geopolymer mortars in a schematic manner

# 6 RESULTS AND DISCUSSION

## 6.1 Determination of Optimum Powder Materials

In order to examine the effect of powder material quantity changes in the binder system on the mortar, Ms ratio, $Na_2O$ concentration, water-binder ratio and curing conditions were kept constant. Water from sodium silicate was taken into account for the water-binder ratio of the mixture, which is 0.46. The aggregate/binder ratio of all mixtures was kept constant at 2.75 according to ASTM C109. The amounts of materials used within the scope of quantity optimization of binder materials of geopolymer mortars are given in Table 6.1.

**Table 6.1** Geopolymer mortar mixtures used in powder materials' optimization

| ID | Ms | $Na_2O$ (%) | Mugla-Fly Ash (g) | Granulated Blast Furnace Slag (g) | Brick Powder (g) | Sand (g) | Activator (g) | Water (g) | Cure Regime |
|---|---|---|---|---|---|---|---|---|---|
| 50FA+30BFS+20BP | 1.30 | 10 | 245.5 | 147.3 | 98.2 | 1350 | 309.2 | 42.1 | 3 days at 50°C |
| 50FA+35BFS+15BP | 1.30 | 10 | 245.5 | 171.85 | 73.65 | 1350 | 309.2 | 42.1 | 3 days at 50°C |
| 50FA+40BFS+10BP | 1.30 | 10 | 245.5 | 196.4 | 49.1 | 1350 | 309.2 | 42.1 | 3 days at 50°C |
| 55FA+25BFS+20BP | 1.30 | 10 | 270.05 | 122.75 | 98.2 | 1350 | 309.2 | 42.1 | 3 days at 50°C |
| 55FA+30BFS+15BP | 1.30 | 10 | 270.05 | 147.3 | 73.65 | 1350 | 309.2 | 42.1 | 3 days at 50°C |
| 55FA+35BFS+10BP | 1.30 | 10 | 270.05 | 171.85 | 49.1 | 1350 | 309.2 | 42.1 | 3 days at 50°C |
| 55FA+40BFS+5BP | 1.30 | 10 | 270.05 | 196.4 | 24.55 | 1350 | 309.2 | 42.1 | 3 days at 50°C |
| 60FA+20BFS+20BP | 1.30 | 10 | 294.6 | 98.2 | 98.2 | 1350 | 309.2 | 42.1 | 3 days at 50°C |
| 60FA+25BFS+15BP | 1.30 | 10 | 294.6 | 122.75 | 73.65 | 1350 | 309.2 | 42.1 | 3 days at 50°C |
| 60FA+30BFS+10BP | 1.30 | 10 | 294.6 | 147.3 | 49.1 | 1350 | 309.2 | 42.1 | 3 days at 50°C |
| 60FA+35BFS+5BP | 1.30 | 10 | 294.6 | 171.85 | 24.55 | 1350 | 309.2 | 42.1 | 3 days at 50°C |
| 65FA+20BFS+15BP* | 1.30 | 10 | 319.15 | 98.2 | 73.65 | 1350 | 309.2 | 42.1 | 3 days at 50°C |
| 65FA+25BFS+10BP | 1.30 | 10 | 319.15 | 122.75 | 49.1 | 1350 | 309.2 | 42.1 | 3 days at 50°C |
| 65FA+30BFS+5BP | 1.30 | 10 | 319.15 | 147.3 | 24.55 | 1350 | 309.2 | 42.1 | 3 days at 50°C |
| 70FA+15BFS+15BP | 1.30 | 10 | 343.7 | 73.65 | 73.65 | 1350 | 309.2 | 42.1 | 3 days at 50°C |
| 70FA+20BFS+10BP | 1.30 | 10 | 343.7 | 98.2 | 49.1 | 1350 | 309.2 | 42.1 | 3 days at 50°C |
| 70FA+25BFS+5BP | 1.30 | 10 | 343.7 | 122.75 | 24.55 | 1350 | 309.2 | 42.1 | 3 days at 50°C |
| 75FA+15BFS+10BP | 1.30 | 10 | 368.25 | 73.65 | 49.1 | 1350 | 309.2 | 42.1 | 3 days at 50°C |
| 75FA+20BFS+5BP | 1.30 | 10 | 368.25 | 98.2 | 24.55 | 1350 | 309.2 | 42.1 | 3 days at 50°C |

*65FA+20BFS+15BP: the contains %65 fly ash, %20 granulated blast furnace slag and %15 brick powder by weight percentage of the total binder.

### 6.1.1 The effect of powder materials on flow diameter

The flow diameter of the geopolymer mortar mixtures obtained as a result of the flow table test are shown in Figure 6.1. In terms of workability, the targeted flow diameter of mortar mixtures is 18±3 cm.

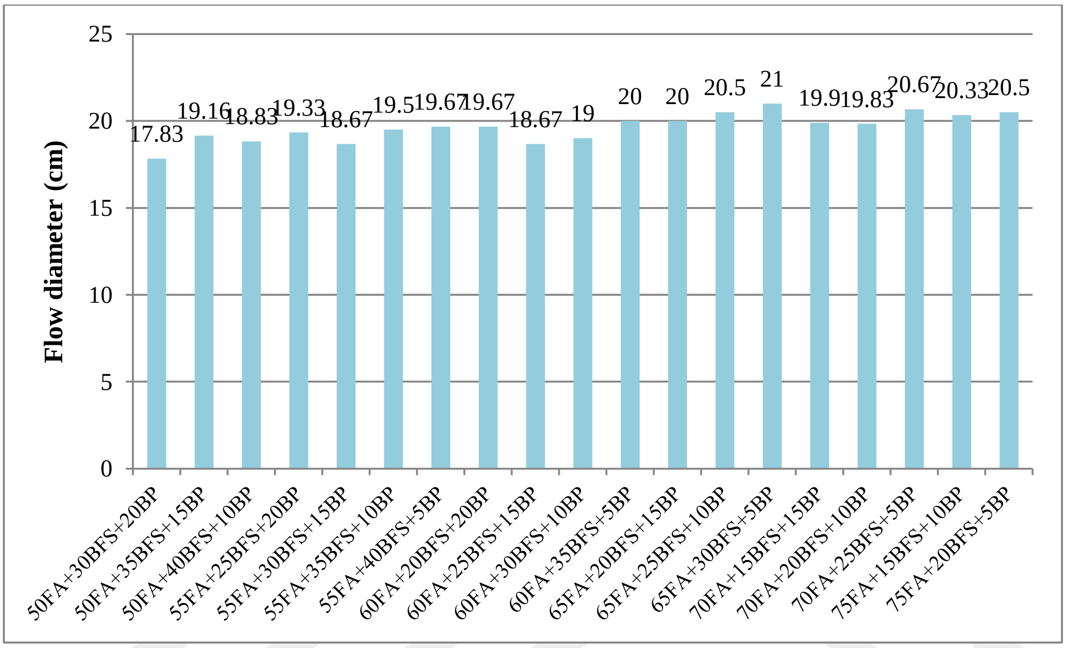


**Figure 6.1** Flow diameter of geopolymer mortars containing different binder system

As can be seen in Figure 6.1, the highest flow diameter was 65FA+30BFS+5BP with 21 cm. The lowest flow diameter was given by a mixture of 50FA+30BFS+20BP with 17.83 cm. Since the amount of fly ash in the binder increased from 50% to 65%, it was observed that it tended to increase in the flow diameter. When the amount of fly ash increased from 65% to 75%, there was a negligible decrease in the flow diameter. As the amount of brick dust in the mixtures increased, a decreased in the flow diameter. It was observed that all mortar mixtures are in the targeted range in terms of workability.

### 6.1.2 The effect of powder materials on flexural strength

The flexural strength of geopolymer mortars mixtures at the end of 3 days 50°C curing is given in Figure 6.2.

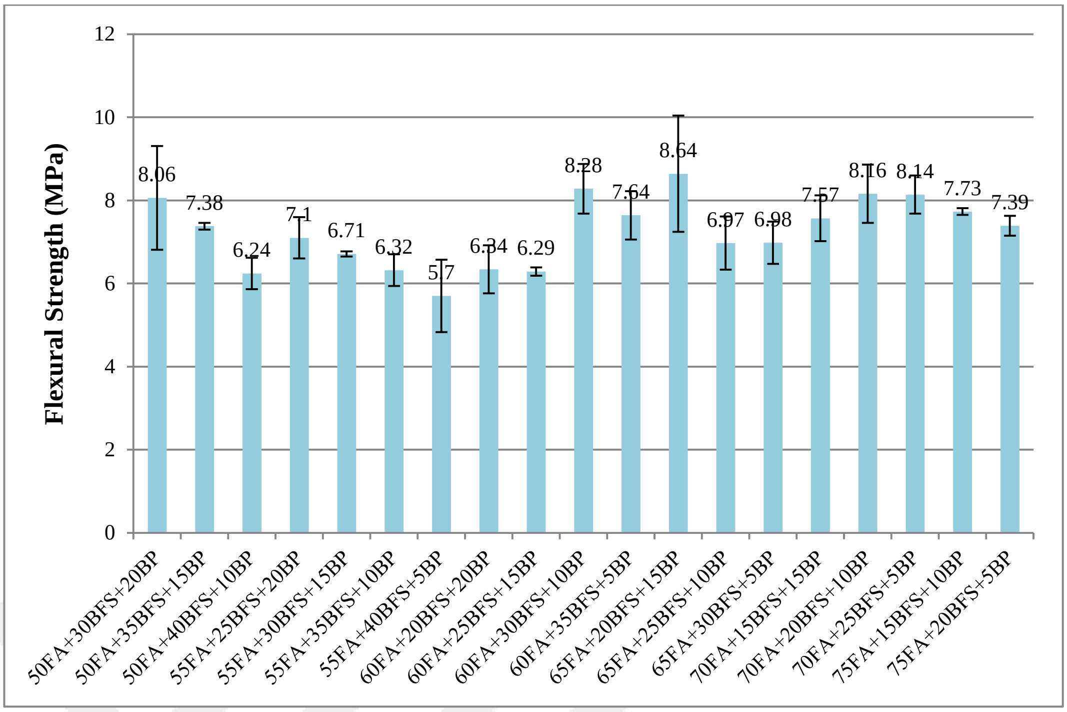


**Figure 6.2** Flexural strength of geopolymer mortars containing different binder system

The flexural strengths of the samples were in the range of 5.7-8.64 MPa. The highest flexural strength was given by a mixture of 65FA+20BFS+15BP with 8.64 MPa. Then, the second and third highest flexural strengths were shown by a mixture of 60FA+30BFS+10BP with 8.28 MPa and a mixture of 70FA+20BFS+10BP with 8.16 MPa, respectively. On the other hand, the mixture of 55FA+40BFS+5BP had the lowest flexural strength with 5.7 MPa. The most suitable ratios in terms of flexural strength were found to be in the range of 60-75% for fly ash, 20-30% for granulated blast furnace slag and 10-15% for brick dust. In mixtures where the amount of fly ash is constant, while an increase amount of granulated blast furnace slag and a decrease in the amount of brick dust, a decreased in flexural strength were observed except for mixtures of 60FA+30BFS+10BP, 60FA+35BFS+5BP, 70FA+20BFS+10BP and 70FA+25BFS+5PB.

### 6.1.3 The effect of powder materials on compressive strength

The compressive strength of geopolymer mortars mixtures at the end of 3 days 50°C curing is given in Figure 6.3.

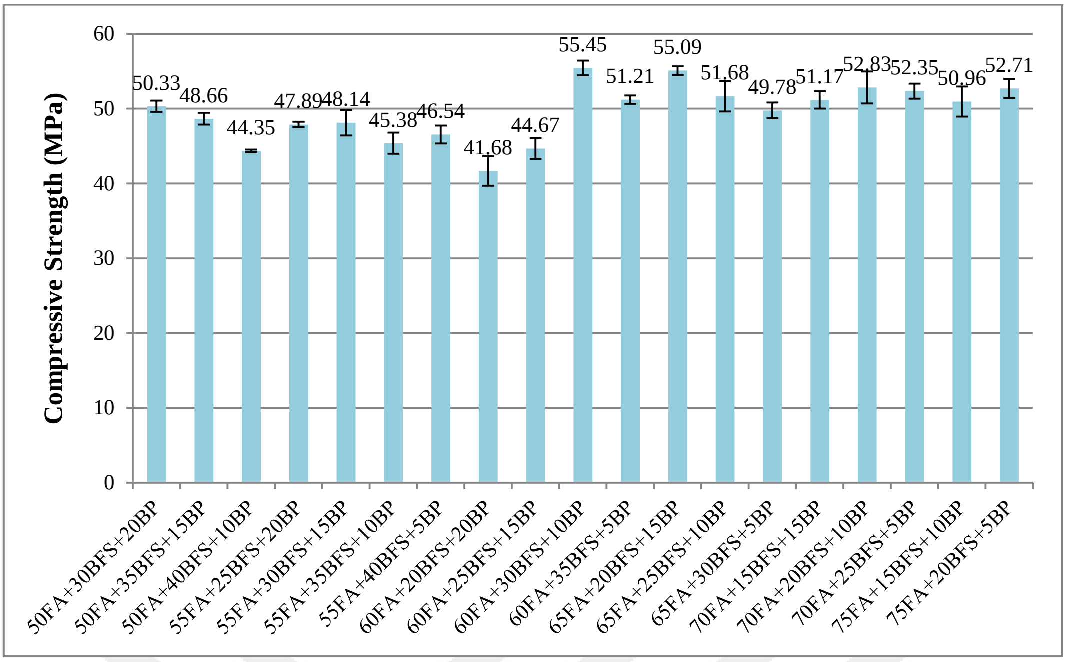


**Figure 6.3** Compressive strength of geopolymer mortars containing different binder system

As can be seen in Figure 6.3, the compressive strengths of the samples are in the range of 55.45-41.68 MPa. The mixture of 60FA+30BFS+10BP showed the highest compressive strength with 55.45 MPa. The same mixture showed the second highest flexural strength. Then, the highest compressive strengths were 55.09 MPa and 52.83 MPa with a mixture of 65FA+20BFS+15BP and a mixture of 70FA+20BFS+10BP, respectively. The mixtures showed the first and third highest flexural strengths, respectively. When the amount of fly ash in the binder increased from 50% to 60%, a decrease in compressive strength was observed, while an increase in compressive strength was detected in samples containing 60% or more fly ash. For the samples containing 60% or more amount of fly ash, increase in amount of granulated blast furnace slag increased the compressive strength.

There was a statistically significant difference between flexural strength of geopolymer mortars ($p<0.05$). There was also a statistically significant difference between compressive strength of geopolymer mortars ($p<0.05$). 60FA+30BFS+10BP, 65FA+20BFS+15BP and 70FA+20BFS+10BP mixtures, which have better performance in terms of strength performance, were found suitable for the continuation of experimental studies.

## 6.2 **Comparison of Class F Fly Ashes**

Experimental studies were continued with fly ash supplied from the Muğla Yatağan Thermal Power Plant, which is available in the Ege University Civil Engineering Laboratory due to the continuity problem in the supply of fly ash used in the binder material optimization phase. Fly ash obtained from İzmir Elektrik Üretim A.Ş. is named as “Izdemir-Fly Ash”, while the fly ash obtained from Muğla Yatağan thermal power plant is named as “Muğla-Fly Ash”. All specimens were cured at 50°C for 3 days. The amounts of materials belonging to the mortars used within the scope of comparison of class F fly ashes are given in Table 6.2.

**Table 6.2** Geopolymer mortar mixtures used in comparison of class F fly ashes

| ID | Ms | $Na_2O$ (%) | Muğla-Fly Ash (g) | İzdemir-Fly Ash (g) | Granulated Blast Furnace Slag (g) | Brick Powder (g) | Sand (g) | Activator (g) | Water (g) |
|---|---|---|---|---|---|---|---|---|---|
| 60FA+30BFS+10BP/I | 1.30 | 10 | - | 294.6 | 147.3 | 49.1 | 1350 | 309.2 | 42.1 |
| 60FA+30BFS+10BP/M | 1.30 | 10 | 294.6 | - | 147.3 | 49.1 | 1350 | 309.2 | 42.1 |
| 65FA+20BFS+15BP/I* | 1.30 | 10 | - | 319.15 | 98.2 | 73.65 | 1350 | 309.2 | 42.1 |
| 65FA+20BFS+15BP/M | 1.30 | 10 | 319.15 | - | 98.2 | 73.65 | 1350 | 309.2 | 42.1 |
| 70FA+20BFS+10BP/I | 1.30 | 10 | - | 343.7 | 98.2 | 49.1 | 1350 | 309.2 | 42.1 |
| 70FA+20BFS+10BP/M* | 1.30 | 10 | 343.7 | - | 98.2 | 49.1 | 1350 | 309.2 | 42.1 |

*65FA+20BFS+15BP/I: the binder of mixture contains %65 fly ash, %20 granulated blast furnace slag and %15 brick powder and used fly ash obtained from İzdemir.

**70FA+20BFS+10BP/M: the binder of mixture contains %70 fly ash, %20 granulated blast furnace slag and %10 brick powder and used fly ash obtained from Muğla province .

### **6.2.1 The effect of fly ashes on flow diameter**

The flow diameter of the geopolymer mortar mixtures obtained as a result of the flow table test are shown in Figure 6.4. In terms of workability, the targeted flow diameter of mortar mixtures is 18±3 cm.

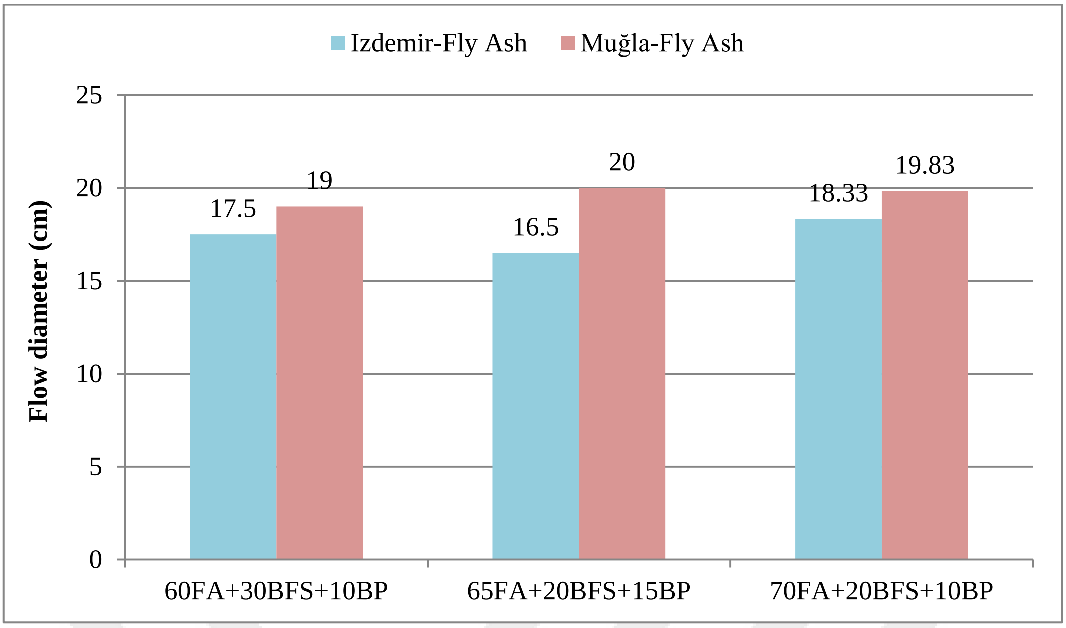


**Figure 6.4** Flow diameter of geopolymer mortars containing different class F fly ash

As shown in Figure 6.4, a decrease was observed in the flow diameter of geopolymer mortar samples containing Izdemir-Fly Ash compared to samples containing Mugla-Fly Ash. The highest flow diameter was given by a mixture of 18.33 cm and 70FA+20BFS+10PB/I, while the lowest flow diameter was shown by a mixture of 16.5 cm and 65FA+20BFS+15PB. It was observed that all mortar mixtures are in the targeted range in terms of workability

### 6.2.2 The effect of fly ashes on flexural strength

The flexural strength of geopolymer mortars mixtures at the end of 3 days 50°C curing is given in Figure 6.5.

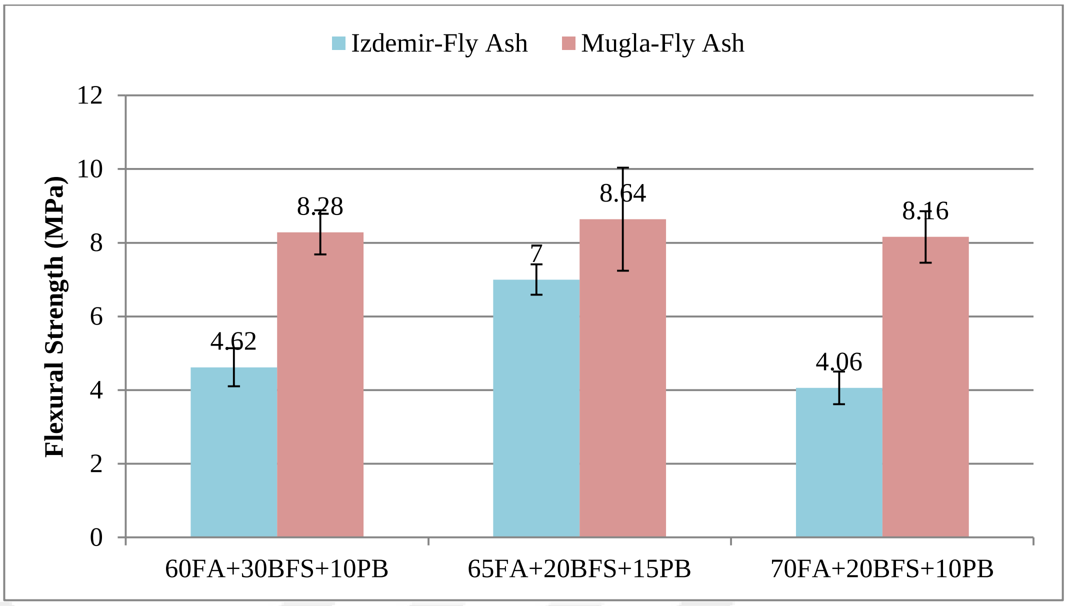


**Figure 6.5** Flexural strength of geopolymer mortars containing different class F fly ash

Flexural strengths of samples containing Izdemir-Fly Ash was in the range of 4.06-7 MPa. There was statistically significant difference between flexural strength of geopolymer mortars containing different class F fly ashes ($p<0.05$). The mixture of 65FA+20BFS+15BP/I with 7 MPa showed the highest flexural strength with 7 MPa. This mixture showed an 18.98% decrease in flexural strength compared to the mixture of 65FA+2BFS+15PB/M. The flexural strengths of 60FA+30BFS+10BP/I and 70FA+20BFS+10BP/I mixtures were determined as 4.62 and 4.06 MPa, respectively. On the other hand, a decrease of 44.02% and 50.24% were observed in the flexural strengths of these mixtures, respectively, compared to equivalent mixtures with the same binder ratios.

### 6.2.3 The effect of fly ashes on compressive strength

The compressive strength of geopolymer mortars mixtures at the end of 3 days 50°C curing is given in Figure 6.6.

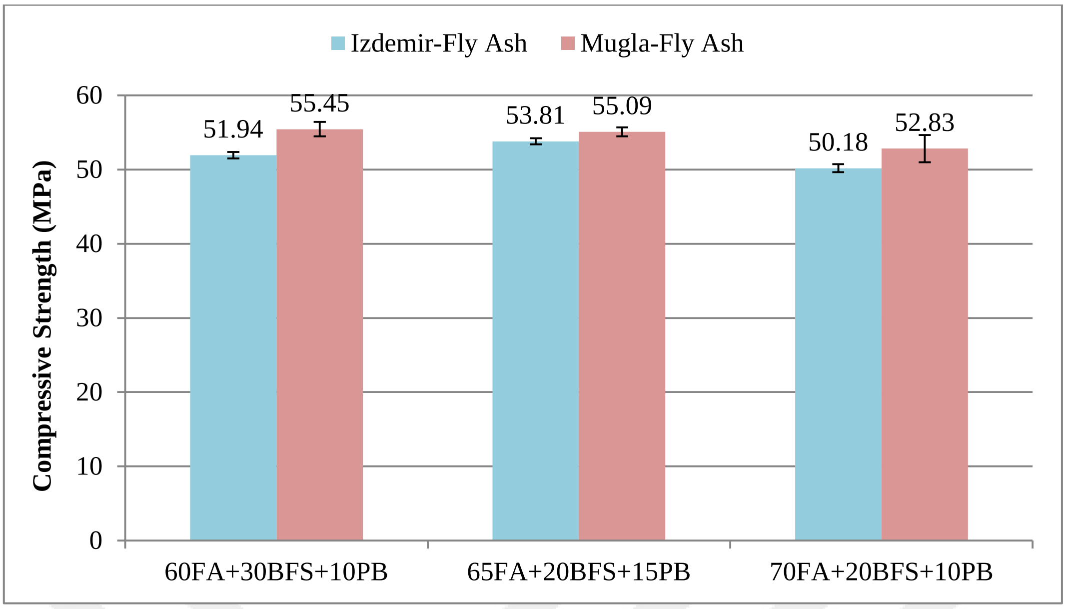


**Figure 6.6** Compressive strength of geopolymer mortars containing different class F fly ash

As shown in Figure 6.6, the compressive strengths of the samples are in the range of 53.81-50.18. There was no statistically significant difference between compressive strength of geopolymer mortars containing different class F fly ashes ($p>0.05$). The highest compressive strength was 53.81 MPa given by a mixture of 65FA+20BFS+15BP/I. This mixture showed a decrease in compressive strength at the level of 2.32% compared to the mixture of 65FA+2BFS+15PB/M. The compressive strengths of 60FA+30BFS+10BP/I and 70FA+20BFS+10BP/I mixtures are 51.94 MPa and 50.18 MPa, respectively. On the other hand, a decrease of 6.33% and 5.01% were observed in the compressive strengths of these mixtures, respectively, compared to the equivalent mixtures with the same binder ratios.

While there was statistically significant difference between flexural strength of geopolymer mortars containing different class F fly ashes ($p<0.05$), there was no statistically significant difference between compressive strength of geopolymer mortars containing different class F fly ashes ($p>0.05$). The mixture of 65FA+20BFS+15BP showed the most superior performance in terms of strength performances. The binder system consisting of 65% class F fly ash, 20% granulated blast furnace slag and 15% brick dust was selected as optimum for the continuation of the experimental studies.

## 6.3 Determination of Optimum of Modulus of Silica

The amounts of materials belonging to the mortars used within the scope of optimization of modulus of silica are given in Table 6.3. In order to examine the effect of modulus of silica on geopolymer mortar, $Na_2O$ concentration, water-binder ratio and curing conditions were kept constant. Water from sodium silicate was taken into account for the water-binder ratio of the mixture, which is 0.46.

**Table 6.3** Geopolymer mortar mixtures used in modulus of silica optimization

| ID | $Na_2O$ (%) | Fly Ash (g) | Granulated Blast Furnace Slag (g) | Brick Powder (g) | Sand (g) | Sodium Hydroxide (g) | Sodium Silicate (g) | Water (g) | Cure Regime |
|---|---|---|---|---|---|---|---|---|---|
| Ms-1.2 | 10 | 319.15 | 98.2 | 73.65 | 1350 | 3.58 | 253.96 | 56.3 | 3 days at 50°C |
| Ms-1.3* | 10 | 319.15 | 98.2 | 73.65 | 1350 | 27.85 | 275.13 | 42.1 | 3 days at 50°C |
| Ms-1.4 | 10 | 319.15 | 98.2 | 73.65 | 1350 | 25.12 | 296.30 | 28 | 3 days at 50°C |

*Ms-1.3: the mixture contains with Ms ratio of 1.3.

### 6.3.1 The effect of modulus of silica on flexural strength

The flexural strength of geopolymer mortars with different Ms ratios are presented in Figure 6.7.

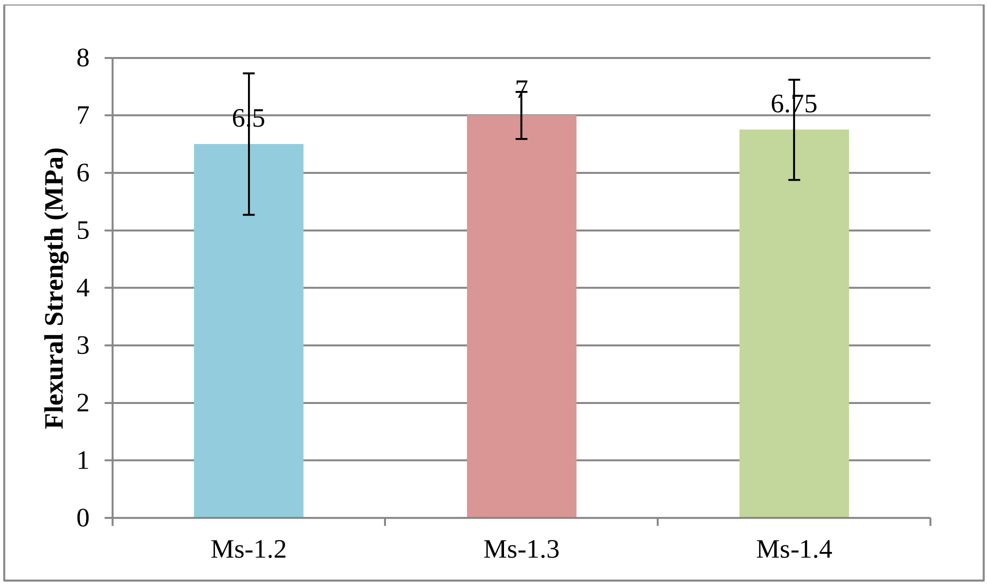


**Figure 6.7** Flexural strength of geopolymer mortars with different Ms ratio

As shown in Figure 6.7, Ms-1.3 showed the highest flexural strength with 7 MPa. Flexural strengths of Ms-1.2 and Ms-1.4 mixtures were determined as 6.5 MPa and 6.75 MPa, respectively. When the Ms ratio increased from 1.2 to 1.3, there was a 7.70% increase in flexural strength, and when the Ms ratio increased from 1.3 to 1.4, a decrease was observed at the level of 3.57%.

### 6.3.2 The effect of modulus of silica on compressive strength

The compessive strength of geopolymer mortars with different Ms ratios are presented in Figure 6.8.

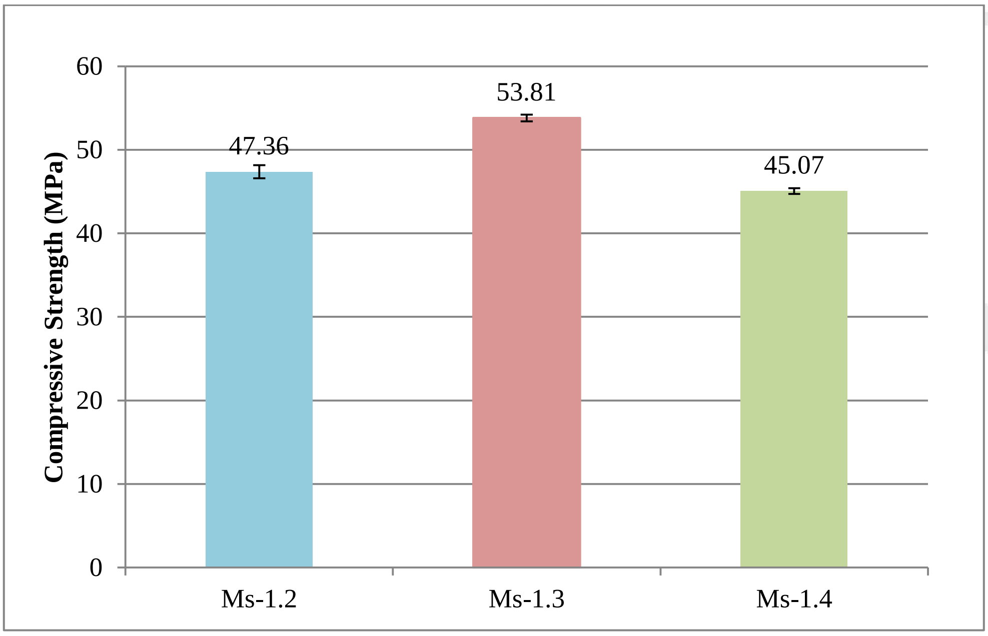


**Figure 6.8** Compressive strength of geopolymer mortars with different Ms ratio

As presented in Figure 6.8, Ms-1.3 showed the highest compressive strength with 53.81 MPa. Compressive strengths of Ms-1.2 and Ms-1.4 mixtures were determined as 47.36 MPa and 45.07 MPa, respectively. When the Ms ratio increased from 1.2 to 1.3, an increase in compressive strength was observed at the level of 13.61%, and when the Ms ratio increased from 1.3 to 1.4, a decrease was observed at the level of 16.24%. An increase in the activator concentration usually increases strength of geopolymer mortar, as it causes more silica and alumina bonds to dissolve. But after a certain value, a decrease in compressive strength is observed. This condition is mainly caused by excessive hydroxide ions, which cause precipitation of the alumino-silicate gel (Somna et al., 2011).

While there was no statistically significant change in the flexural strength of geopolymer mortars with changes in the Ms ratio ($p>0.05$), there was a statistically significant change in the compressive strength of geopolymer mortars ($p<0.05$). Ms-1.3 mixture showed the highest flexural and compressive strength. The optimum Ms ratio was selected as 1.3 for the continuation of the experimental studies.

## 6.4 Determination of Optimum Water-Binder Ratio

The amounts of materials belonging to the mortars used within the scope of optimization of water/binder ratio are given in Table 6.4. In order to examine the effect of water-binder ratio on geopolymer mortar, $Na_2O$ concentration, Ms ratio and curing conditions were kept constant. Water from sodium silicate was taken into account for the water-binder ratio of the mixture. A statistical paired t-test was applied to each individual compressive and flexural strength level obtained from different water-binder ratio at a 0.05 level of significance.

**Table 6.4** Geopolymer mortar mixtures used in water-binder ratio optimization

| ID | Ms | $Na_2O$ (%) | Fly Ash (g) | Granulated Blast Furnace Slag (g) | Brick Powder (g) | Sand (g) | Activator (g) | Water (g) | Cure Regime |
|---|---|---|---|---|---|---|---|---|---|
| w/b-0.42 | 1.3 | 10 | 319.15 | 98.2 | 73.65 | 1350 | 302.9 | 22.5 | 3 days at 50°C |
| w/b-0.44* | 1.3 | 10 | 319.15 | 98.2 | 73.65 | 1350 | 302.9 | 32.3 | 3 days at 50°C |
| w/b-0.46 | 1.3 | 10 | 319.15 | 98.2 | 73.65 | 1350 | 302.9 | 42.1 | 3 days at 50°C |
| w/b-0.48 | 1.3 | 10 | 319.15 | 98.2 | 73.65 | 1350 | 302.9 | 51.9 | 3 days at 50°C |

*w/b-0.44: the mixture contains with water/binder ratio of 0.44.

### 6.4.1 The effect of water-binder ratio on flow diameter

The flow diameter of the geopolymer mortar mixtures obtained as a result of the flow table test are shown in Figure 6.9. In terms of workability, the targeted flow diameter of mortar mixtures is 18±3 cm.

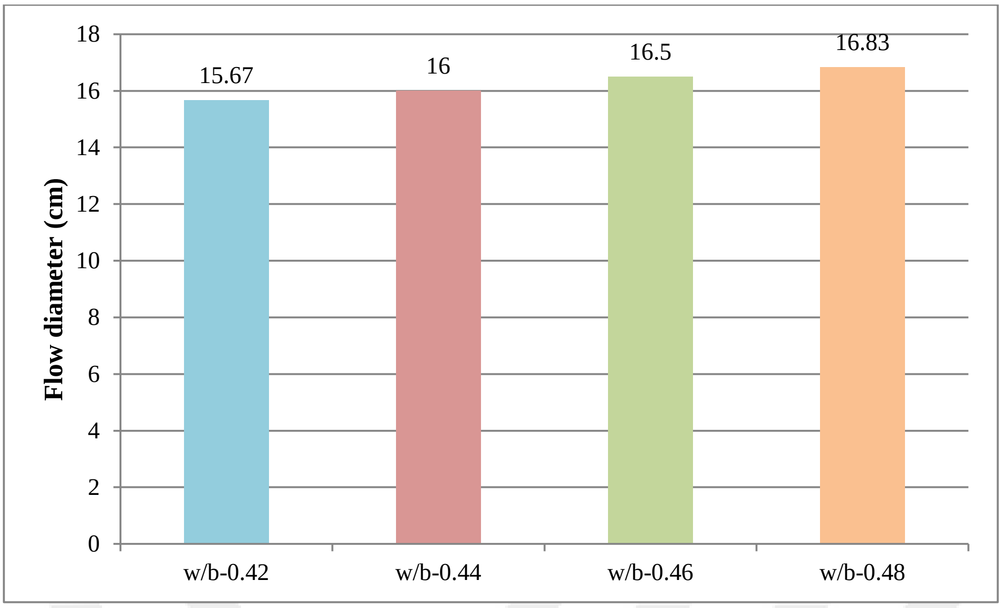


**Figure 6.9** Flow diameter of geopolymer mortars with different water-binder ratio

As presented in Figure 6.9, when the water-binder ratio decreased, the flow diameter of the geopolymer mortar mixtures decreased. It was observed that all mortar mixtures are in the targeted range in terms of workability.

### 6.4.2 The effect of water-binder ratio on flexural strength

The flexural strength of geopolymer mortars with different water-binder ratios are presented in Figure 6.10.

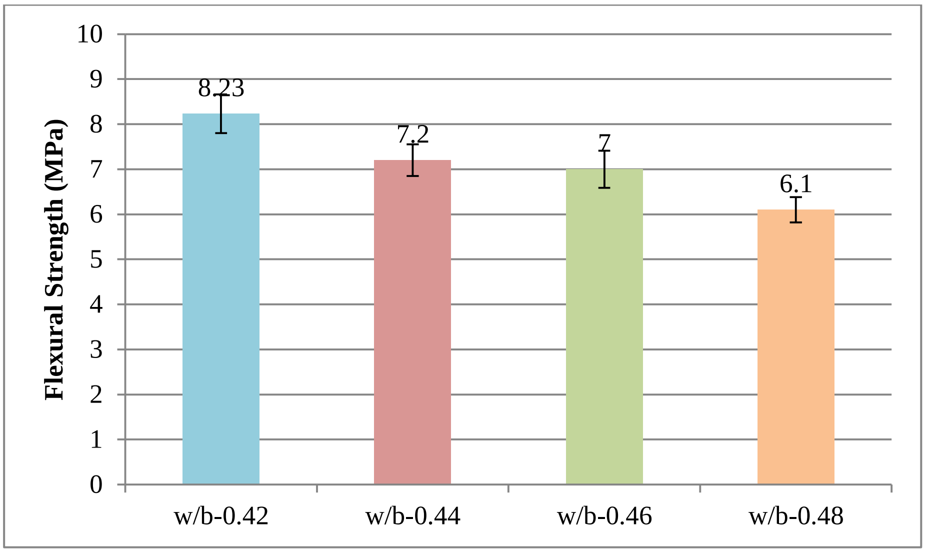


**Figure 6.10** Flexural strength of geopolymer mortars with different water-binder ratio

Unsurprisingly, the flexural strength of the samples decreased as the water-binder ratio increased. There was statistically significant difference between flexural strength of geopolymer mortars with different water-binder ratio ($p<0.05$). The w/b-0.42 mixture gave the highest flexural strength with 8.23 MPa. The flexural strengths of w/b-0.44, w/b-0.46 and w/b-0.48 mixtures were determined as 7.2 MPa, 7 MPa and 6.1 MPa, respectively. When the water-binder ratio increased from 0.42 to 0.44, a decrease in flexural strength was observed at the level of 12.52%, while when the water-binder ratio increased from 0.44 to 0.46 and from 0.46 to 0.48, a decrease was observed at the levels of 2.77% and 12.85%, respectively.

### 6.4.3 The effect of water-binder ratio on compressive strength

The compressive strength of geopolymer mortars with different water-binder ratios are presented in Figure 6.11.

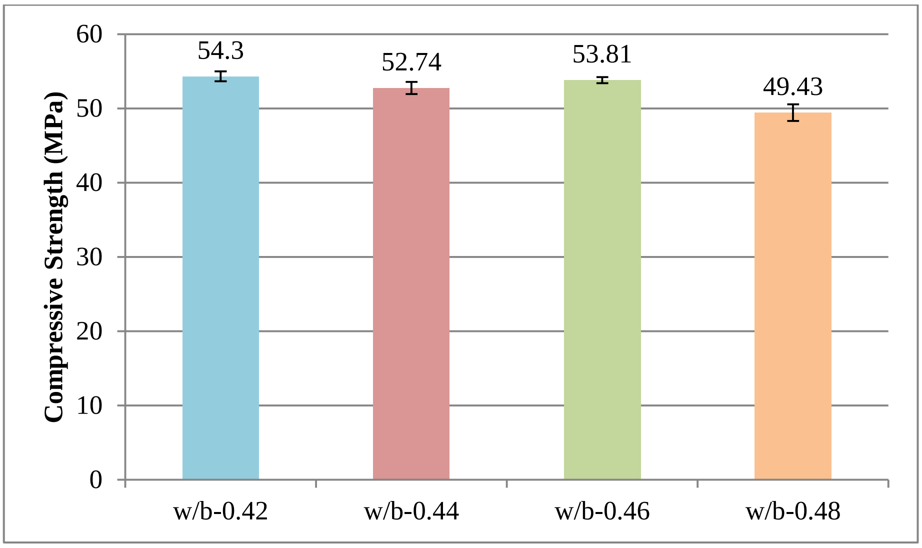


**Figure 6.11** Compresive strength of geopolymer mortars with different water-binder ratio

As presented in Figure 6.11, the w/b-0.42 mixture gave the highest compressive strength with 54.3 MPa. The compressive strengths of w/b-0.44, w/b-0.46 and w/b-0.48 mixtures were determined as 52.74 MPa, 53.81 MPa and 49.43 MPa, respectively. There was no statistically significant difference between compressive strength of geopolymer mortars with different water-binder ratio ($p>0.05$). Negligible differences were observed between the compressive strengths of w/b-0.42, w/b-0.44 and w/b-0.46. When the water-binder ratio increased from 0.46 to 0.48, a decrease in compressive strength was observed at the level of 8.14%. All mortar mixtures were found to be suitable in terms of workability.

Although there was no statistically significant differences in the compressive strength with the change in the water-binder ratio of the geopolymer mortar mixtures ($p>0.05$), there was a statistically significant differences in the compressive strength with the change in the water-binder ratio of the geopolymer mortar mixtures ($p<0.05$). The highest flexural and compressive strength was shown by a mixture of w/b-0.42. The optimum water-binder ratio was selected as 0.42 for the continuation of the experimental studies.

## 6.5 Determination of Optimum of Cure Regime

The amounts of materials belonging to the mortars used within the scope of optimization of cure regime are given in Table 6.5. In order to examine the effect of cure regime on geopolymer mortar, $Na_2O$ concentration, water-binder ratio and Ms ratio were kept constant. Water from sodium silicate was taken into account for the water-binder ratio of the mixture.

**Table 6.5** Geopolymer mortar mixtures used in cure regime optimization

| ID | Ms | $Na_2O$ (%) | Fly Ash (g) | Granulated Blast Furnace Slag (g) | Brick Powder (g) | Sand (g) | Activator (g) | Water (g) | Cure Regime |
|---|---|---|---|---|---|---|---|---|---|
| 1D-40C | 1.30 | 10 | 319.15 | 98.2 | 73.65 | 1350 | 309.2 | 22.5 | 1 days at 40°C |
| 1D-50C | 1.30 | 10 | 319.15 | 98.2 | 73.65 | 1350 | 309.2 | 22.5 | 1 days at 50°C |
| 1D-60C | 1.30 | 10 | 319.15 | 98.2 | 73.65 | 1350 | 309.2 | 22.5 | 1 days at 60°C |
| 3D-40C* | 1.30 | 10 | 319.15 | 98.2 | 73.65 | 1350 | 309.2 | 22.5 | 3 days at 40°C |
| 3D-50C | 1.30 | 10 | 319.15 | 98.2 | 73.65 | 1350 | 309.2 | 22.5 | 3 days at 50°C |
| 3D-60C | 1.30 | 10 | 319.15 | 98.2 | 73.65 | 1350 | 309.2 | 22.5 | 3 days at 60°C |
| 7D-40C | 1.30 | 10 | 319.15 | 98.2 | 73.65 | 1350 | 309.2 | 22.5 | 7 days at 40°C |
| 7D-50C | 1.30 | 10 | 319.15 | 98.2 | 73.65 | 1350 | 309.2 | 22.5 | 7 days at 50°C |
| 7D-60C | 1.30 | 10 | 319.15 | 98.2 | 73.65 | 1350 | 309.2 | 22.5 | 7 days at 60°C |

*3D-40C: mortar mixture cured at 40°C for 3 days.

### 6.5.1 The effect of cure regime on flexural strength

The flexural strength of geopolymer mortars cured at different temperatures and durations are presented in Figure 6.12.

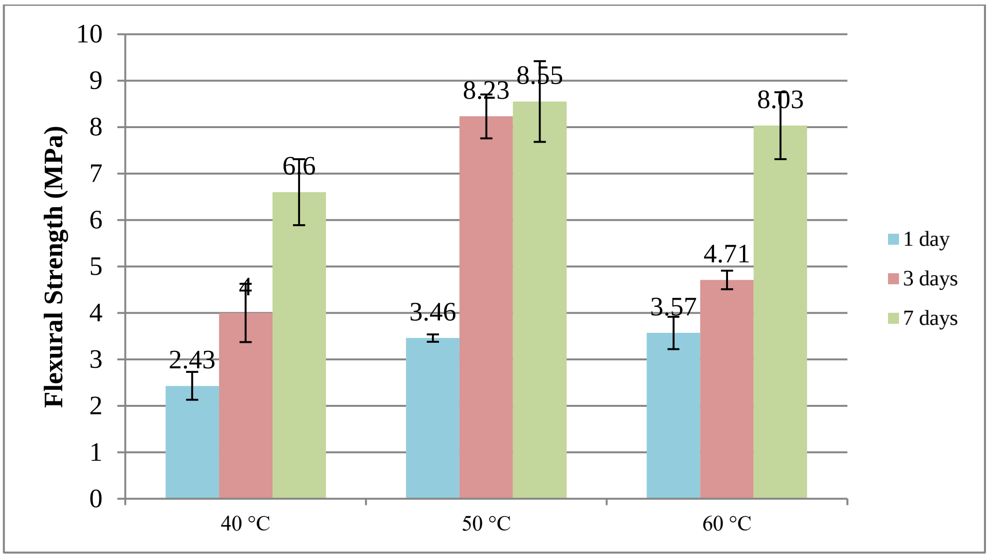


**Figure 6.12** Flexural strength of geopolymer mortars subjected to different curing conditions

As shown in Figure 6.12, the flexural strength increased as the curing time increased for all samples. The 7D-50C mixture gave the highest flexural strength with 8.55 MPa. The 3D-50C mixture showed the second highest flexural strength with 8.23 MPa. On the other hand, 1D-40C showed the lowest flexural strength of the mixture with 2.43 MPa. The 3D-50C sample reached 96.25% of the flexural strength of the 7D-50C sample with 8.23 MPa at the end of the 3-day curing. For the samples cured for 1 day, flexural strength increased as the curing temperature increased. For the samples cured for 3 and 7 days, when the temperature increased from 40°C to 50°C, an increase in flexural strengths was observed at the level of 105.75% and 42.5%, respectively, when the temperature increased from 50°C to 60°C, a decrease was observed at the level of 42.77% and 6.08%, respectively.

### 6.5.2 The effect of cure regime on compressive strength

The compressive strength of geopolymer mortars cured at different temperatures and durations are presented in Figure 6.13.

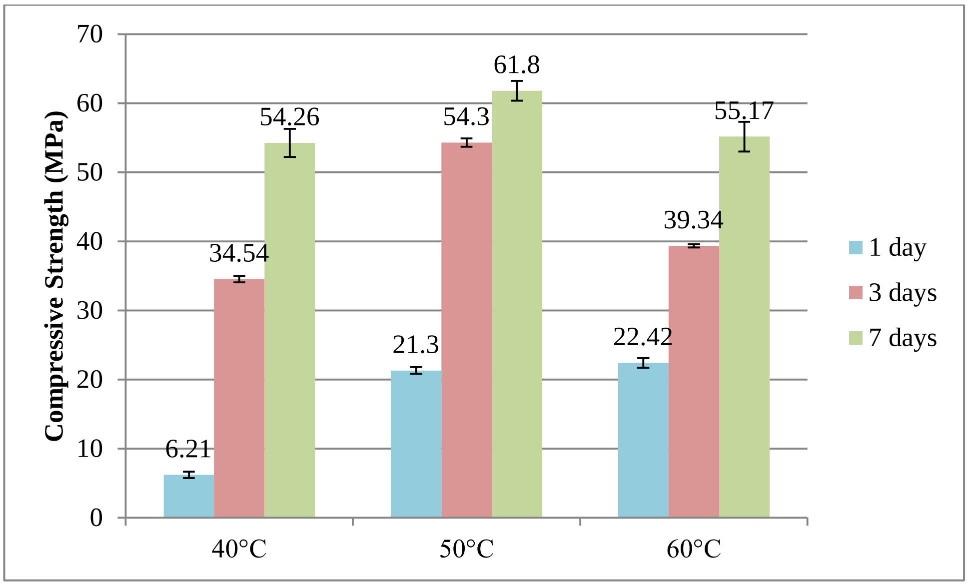


**Figure 6.13** Compressive strength of geopolymer mortars subjected to different curing conditions

As shown in Figure 6.13, the compressive strength increased as the curing time increased for all samples. The 7D-50C mixture gave the highest compressive strength with 61.8 MPa. The 3D-50C mixture showed the second highest compressive strength with 54.3 MPa. On the other hand, 1D-40C showed the lowest compressive strength of the mixture with 6.21 MPa. The 3D-50C sample reached 96.25% of the compressive strength of the 7D-50C sample with 54.3 MPa at the end of the 3-day curing. For the samples cured for 1 day, compressive strength increased as the curing temperature increased. For the samples cured for 3 and 7 days, when the temperature increased from 40°C to 50°C, an increase in compressive strength was observed at the level of 57.2% and 13.89%, respectively, when the temperature increased from 50°C to 60°C, a decrease was observed at the level of 27.55% and 10.72%, respectively.

The results showed that the flexural and compressive strength increases as the curing temperature increases. Thermal curing causes the polycondensation process, which produces early high compressive strength, to dissolve silica and alumina-based raw materials more quickly (Khater, 2012). However, the contribution of the cure applied above a certain temperature to strength decreases. High temperature curing processes lead to reactivity that causes rapid setting (Bing-hui et al., 2014). According to Singh et al., (2015), exceeding a certain curing temperature and/or duration cause causes dehydration and shrinkage, which leads to the contraction of the gel structure without forming a semi-crystalline network, causing the gel structure to deteriorate (Singh et al., 2015). Mixtures 3D-50C, 7D-50 C and 7D-60 C showing the highest flexural and compressive strength were selected for the investigation of energy consumption.

### 6.5.3 Determination optimum curing regime in terms of energy consumption

The compressive strength, flexural strength and the amount of electrical energy spent by geopolymer mortars are presented in Table 6.6.

**Table 6.6** Energy consumption of mixtures

| Compressive strength (MPa) | Flexural strength (MPa) | Cure Regime | Energy consumption (kWh) | Energy consumption /Compressive strength (kWh/MPa) | Energy consumption /Flexural strength (kWh/MPa) |
|---|---|---|---|---|---|
| 54.30 | 8.23 | 3 days at 50°C | 7.344 | 0.135 | 0.892 |
| 61.80 | 8.55 | 7 days at 50°C | 17.136 | 0.277 | 2.004 |
| 55.17 | 8.03 | 7 days at 60°C | 24.360 | 0.441 | 3.033 |

As expected, the amount of energy consumed increased as the curing time and/or curing temperature increased. Under these conditions, the optimum curing condition for the geopolymer mortar was selected as 3 days at 50°C.

## 6.6 The Effect of the Water Curing on the Strength Properties of Geopolymer Mortar

Geopolymer mortar samples, whose binder materials, Ms ratio, water-binder ratio and curing conditions were optimized, were cured at 50°C for 3 days and then left to water cure for 7, 14, 21 and 28 days. The control sample “C”, which was not left to water cure, was named as “S7”, which was cured in water for 7 days, “S14”, which was cured in water for 14 days, ”S21”, which was cured in water for 21 days, and the geopolymer mortar sample, which was cured in water for 28 days, was named as “S28”. The effect of water curing on the flexural and compressive strengths of geopolymer mortars is presented in Figures 6.14 and

Figure 6.15, respectively. A statistical paired t-test was applied to each individual compressive and flexural strength level obtained from the effect of water curing at a 0.05 level of significance.

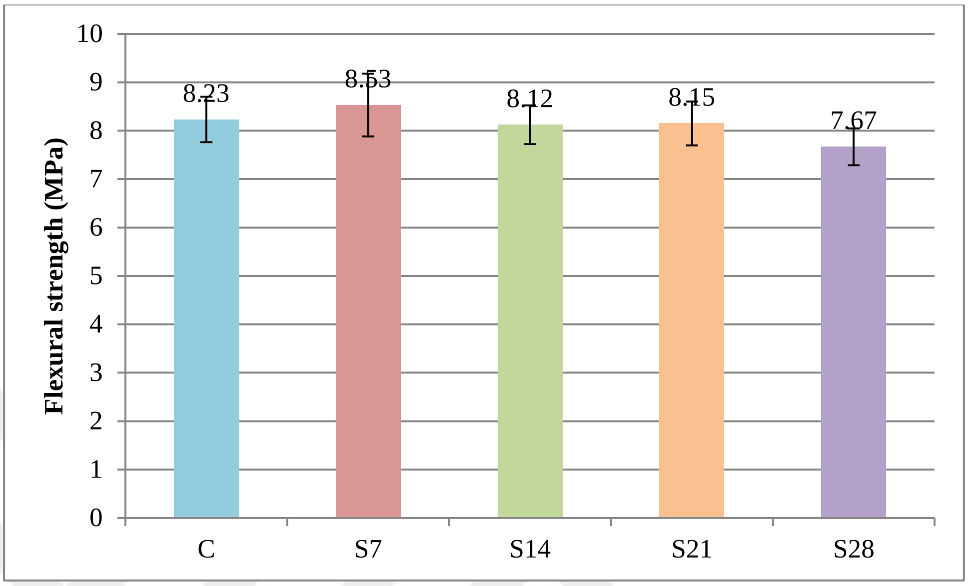


**Figure 6.14** Flexural strength of geopolymer mortars cured in water at different durations

As shown in Figure 6.14, it was found that water curing did not have a significant effect on the flexural strength of geopolymer mortars. There was no statistically significant difference between flexural strength of geopolymer mortars that cured in water ($p>0.05$). While the flexural strength of the sample cured in water for 7 days increased by 3.64% compared to the control sample, a decrease in strength was observed as the curing time increased. The S7 mixture showed the highest flexural strength with 8.53 MPa, while the S28 mixture showed the lowest flexural strength with 7.67 MPa.

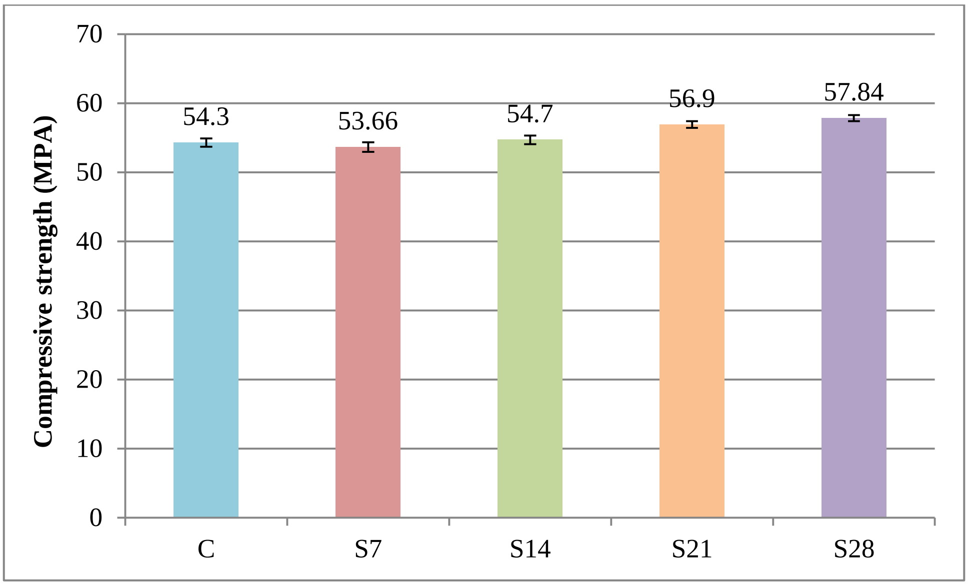


**Figure 6.15** Flexural strength of geopolymer mortars cured in water at different durations

As shown in Figure 6.15, it was determined that water curing has a positive effect on the compressive strength of geopolymer mortars. There was no statistically significant difference between compressive strength of geopolymer mortars that cured in water ($p>0.05$). As the water cure time of the samples increased, an increase in their compressive strength. It was observed that the S28 mixture showed the highest compressive strength with 57.84 MPa, an increase in compressive strength of 6.12% compared to the control sample.

## 6.7 The Effect of the Addition of Non-Encapsulated Bacteria on Setting Time and Strength Properties of Geopolymer Mortar

Bacteria suspension with different concentrations were added to the geopolymer mortar, whose binder materials, Ms ratio, water-binding ratio and curing conditions were optimized, instead of water. The control sample containing no bacteria was named ”C“, the ”B8“ containing bacteria at a concentration of $10^8$ cfu/ml, the ”B9“ containing bacteria at a concentration of $10^9$ cfu/ml and the geopolymer mortar sample containing bacteria at a concentration of $10^{10}$ cfu/ml were named ”B10". The effect of the addition of non-encapsulated bacteria on setting time of geopolymer mortars is given in Table 6.7. The effect of the addition of non-encapsulated bacteria on the flexural and compressive strengths of geopolymer mortars is presented in Figures 6.16 and Figure 6.17, respectively. A statistical paired t-test was applied to each individual compressive and flexural strength level obtained from addition of non-encapsulated bacteria different at a 0.05 level of significance.

**Table 6.7** Setting time of geopolymer mixtures

| Mix ID | Initial Setting Time (min) | Final Setting Time (min) | Setting Time (min) |
|---|---|---|---|
| C | 75 | 140 | 65 |
| B8 | 200 | 295 | 95 |
| B9 | 210 | 310 | 100 |

As shown in Table 6.7, the initial and final setting times of the bacteria-free C mixture are 75 min and 140 min. Inial setting time of samples containing bacteria at $10^8$ and $10^9$ cfu/ml concentrations is 200-210 min, while final setting time is 295-310 min. In various studies, it was stated that bacteria and/or their nutrients delay or prolong the setting time. Luo and Qian (2016) stated that the addition of bacterial healing agent has an setting retardant effect on cement mortar. While the initial and final setting times of the control samples were 136 min and 216 min, respectively, it was stated that the initial setting time for the cement paste containing the healing agent was 68 min and the final setting was 338 min. The addition of *D.nitroreducenes* resulted in a 40-minute delay in both initial and final setting times (Erşan et al., 2015). Polat et al. were determined that when bacteria are added to geopolymer mortars prepared at different NaOH concentrations, the setting time is extended. For samples cured under a room condition, it was observed that the setting times of control geopolymer mortars were 435-490 min, while the setting times of geopolymer mortars containing bacteria were in the range of 525-580 min (Polat et al., 2020).

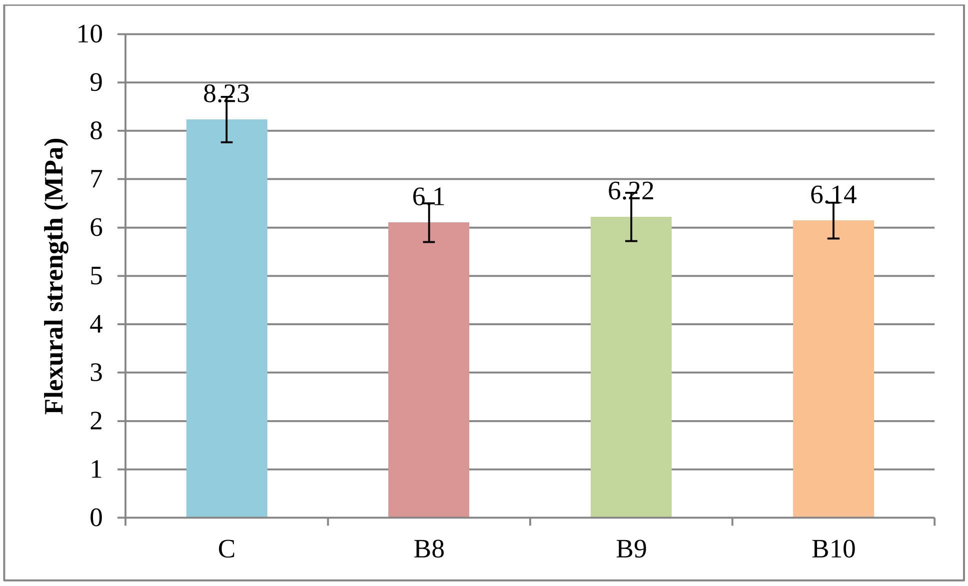


**Figure 6.16** Flexural strength of geopolymer mortars containing non-encapsulated bacteria with different concentrations

As shown in Figure 6.16, it was determined that the addition of non-encapsulated bacteria has a negative effect on the flexural strength of the geopolymer mortar. There was statistically significant difference between flexural strength of geopolymer mortars with addition of non-encapsulated bacteria ($p<0.05$). The flexural strength of the B8, B9 and B10 mixtures decreased by 25.88%, 24.42% and 25.39% compared to the control sample, respectively.

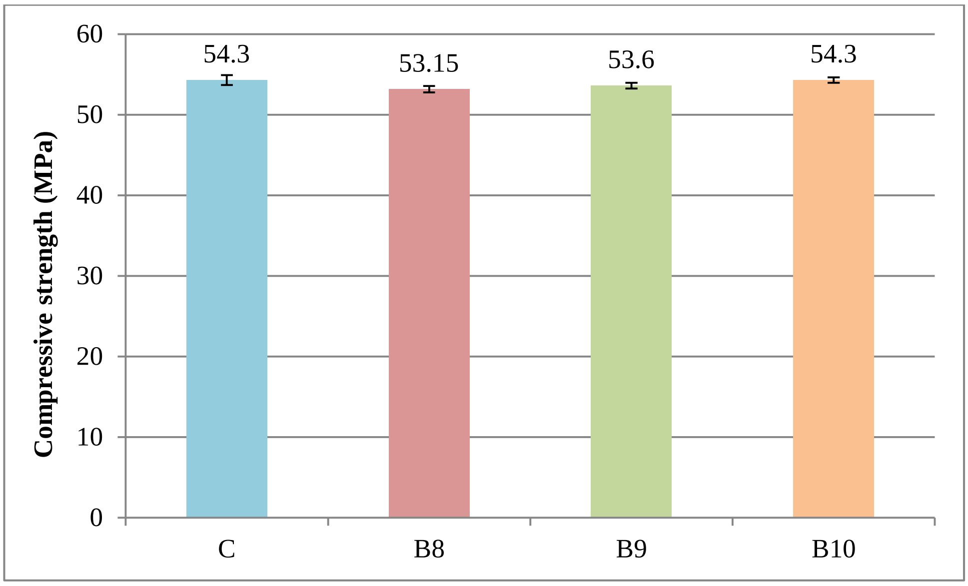


**Figure 6.17** Compressive strength of geopolymer mortars containing bacteria with different concentrations

As shown in Figure 6.17, it was determined that the addition of non-encapsulated bacteria does not have a significant effect on the compressive strength of the geopolymer mortar. There was no statistically significant difference between compressive strength of geopolymer mortars with addition of non-encapsulated bacteria ($p>0.05$). The compressive strengths of the B8 and B9 mixtures decreased by 2.11% and 1.28% compared to the control sample, respectively. B10 specimen reached the compressive strength of the control sample with 54.3 MPa. It was observed that there was a negligible increase in compressive strength with an increase in the concentration of bacteria.

In an another study, a increase was not observed in compressive strength despite the fact that the addition of bacteria completely healed the cracks in a metakaolin-based geopolymer mortar. It was confirmed with SEM images that the bacterial-derived $CaCO_3$ precipitate has a weaker structure and bond compared to the stable calcite structure (Polat and Uysal, 2021). Amiri and Undur did not observe an increase in compressive strength with the addition of microorganisms to cement mortar. They related this result to the fact that the $CaCO_3$ ratio in the mortar remained low (Amiri and Undur, 2019). The loss of vitality of endospore cells in a highly alkaline environment of endospore cells over time causes the formation of a gap in the mortar (Erşan et al., 2015). Although the compressive strength does not increase, the decrease in flexural strength was related with the relatively weaker $CaCO_3$-matrix bond and the more severe effect of the resulting pore structures on the flexural strength.

## 6.8 Ultrasonic Pulse Velocity Test Result and Effective Healing Levels of Geopolymer Mortars Containing Non-Encapsulated Bacteria

Bacteria suspension with different concentrations were added instead of water to the geopolymer mortar, whose binder materials, Ms ratio, water-binding ratio and curing conditions were optimized. At the end of the curing period, the cracked samples were subjected to UPV test. The control sample containing no bacteria was named ”C“, the ”NF8“ containing non-encapsulated bacteria at a concentration of $10^8$ cfu/ml, the ”NF9“ containing non-encapsulated bacteria at a concentration of $10^9$ cfu/ml and the geopolymer mortar sample containing non-encapsulated bacteria at a concentration of $10^{10}$ cfu/ml were named ”NF10". The UPV results and effective healing percentages of geopolymer mortars containing non-encapsulated bacteria are presented in Figures 6.18 and Figure 6.19, respectively.

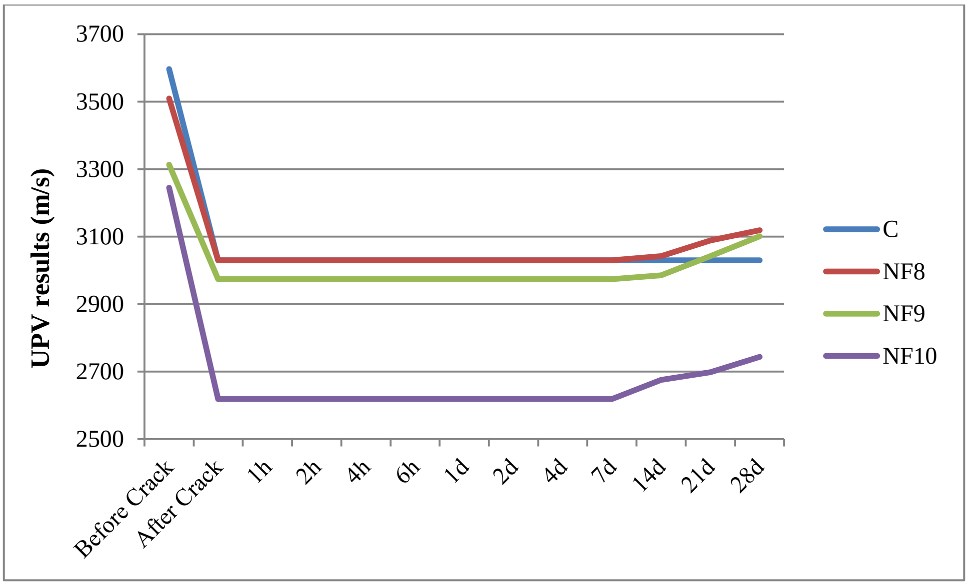


**Figure 6.18** UPV result of geopolymer mortars containing non-encapsulated bacteria

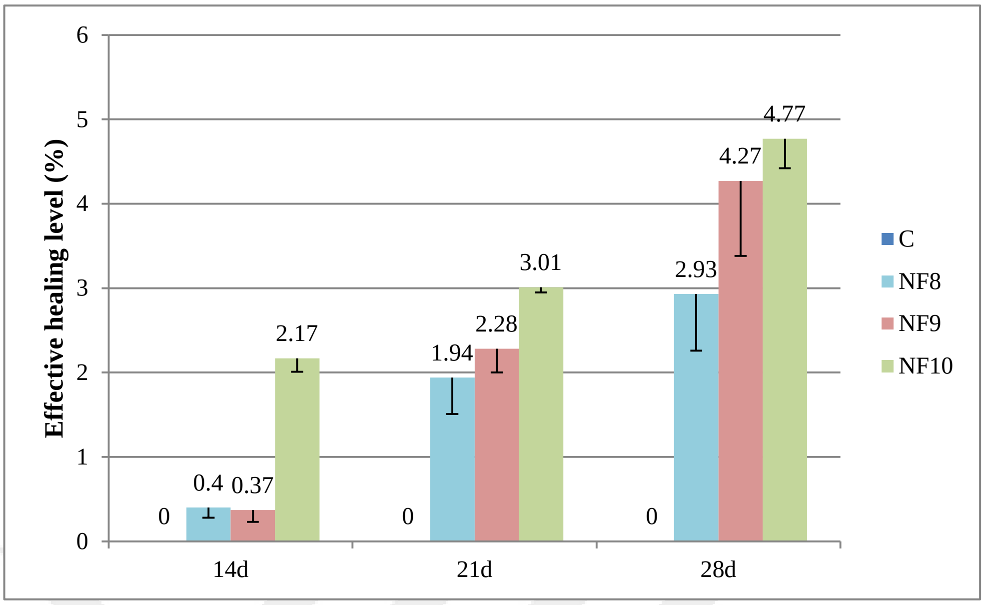


**Figure 6.19** Effective healing level of geopolymer mortars containing non-encapsulated bacteria

As shown in Figure 6.18, there was no healing in the bacterial-free control sample. While no healing was observed at the end of 7 days in all samples containing bacteria, healing was detected starting from 14 days. As can be seen in Figure 6.19, the effective healing level of the NF8 sample at 14 days was 0.4%, and at 21 and 28 days, healing was observed at 1.94% and 12.93%, respectively. On the other hand, the effective healing levels of NF9 samples at 14, 21 and 28 days were determined as 0.37%, 2.28% and 4.27%. On the other hand, the NF10 mixture showed an healing of 2.17% at 14 days, 3.01% at 21 days and 4.77% at the end of 28 days. The NF10 sample showed the most effective healing at the end of 28 days.

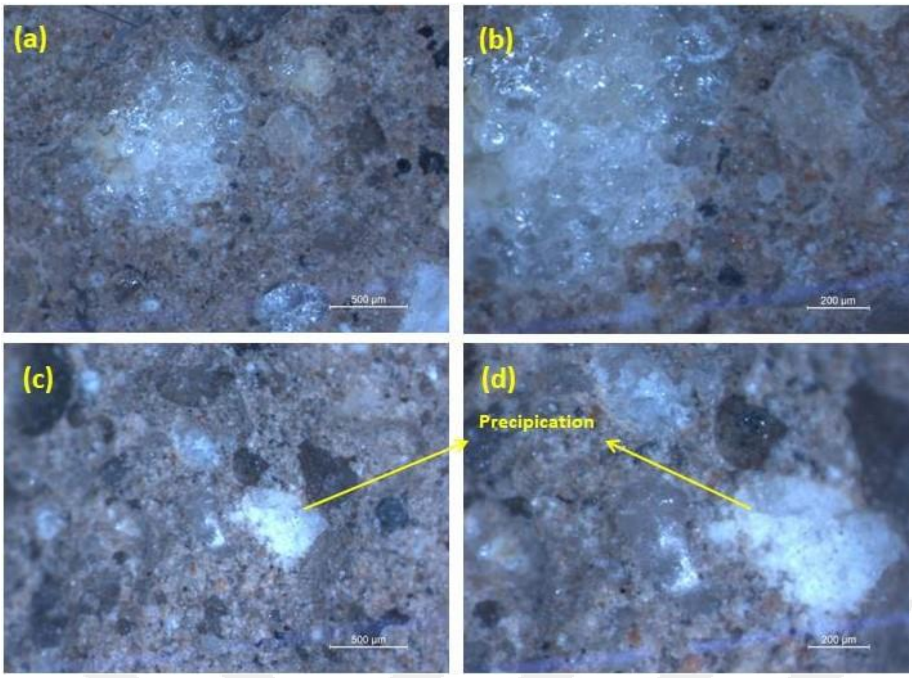


**Figure 6.20** Stereomicroscopic images of (a), (b) mixture “C” and; (c), (d) mixture “NF9”

As presented in Figure 6.20, no precipitation was observed on stereomicroscope images ((a), (b)) of the bacteria-free mixture “C”, which did not detect healing due to continuing geopolymerization. The transparent structure seen in the images of the C sample has been observed in all other mixtures. It has been thought that it may be the precipitation of aluminosilicate gel caused by excessive hydroxide ions that cause the precipitation of aluminosilicate gel (Somna et al., 2011). In the “NF9” mixture ((c), (d)) containing non-encapsulated bacteria at a concentration of $10^9$ cfu/ml, white precipitates were detected at the crack area.

## 6.9 Ultrasonic Pulse Velocity Test Result and Effective Healing Levels of Geopolymer Mortars Containing Encapsulated Bacteria

Encapsulated bacteria with different concentrations in the amount of 2% by weight of binder were added to the geopolymer mortar, whose binder materials, Ms ratio, water-binder ratio and curing conditions were optimized. At the end of the curing period, the cracked samples were subjected to UPV test. The control sample containing no bacteria was named ”C“, the ”E8“ containing encapsulated bacteria at a concentration of $10^8$ cfu/ml, the ”E9“ containing encapsulated bacteria at a concentration of $10^9$ cfu/ml and the geopolymer mortar sample containing encapsulated bacteria at a concentration of $10^{10}$ cfu/ml were named ”E10". The UPV results and effective healing percentages of geopolymer mortars containing encapsulated bacteria are presented in Figure 6.21 and Figure 6.22, respectively.

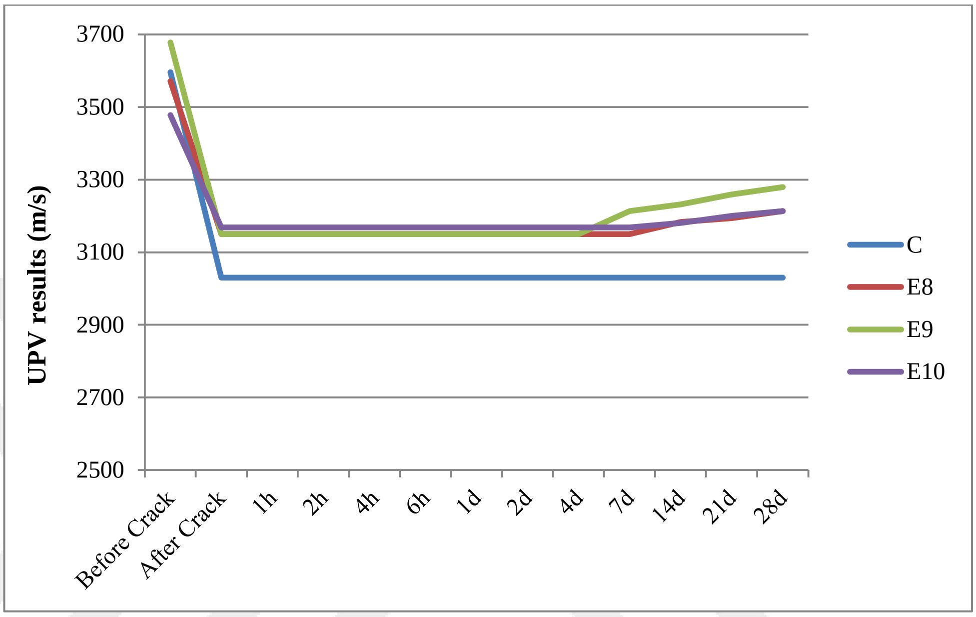


**Figure 6.21** UPV result of geopolymer mortars containing encapsulated bacteria

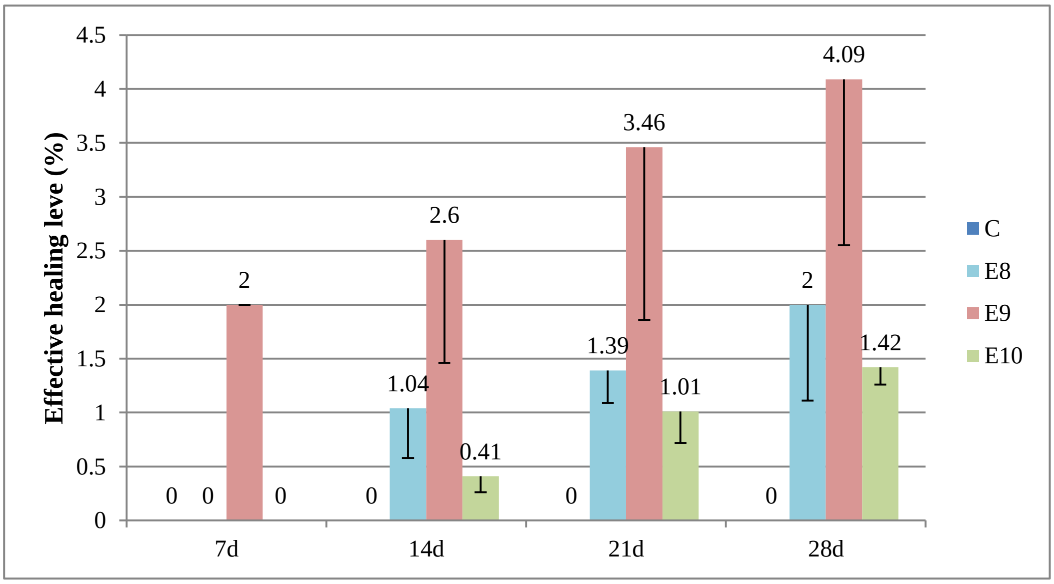


**Figure 6.22** Effective healing level of geopolymer mortars containing encapsulated bacteria

As shown in Figure 6.21, it was determined that all samples containing encapsulated bacteria showed healing. The healing was observed in the E9 mixture from 7 days, while healing was observed in the E8 and E10 mixtures from 14 days. As can be seen in Figure 6.22, the effective healing level of the E8 sample at 14 days was 1.04%, and at 21 and 28 days, effective healing was observed at 1.39% and 2%, respectively. On the other hand, the effective healing levels of E9 samples at 7,14, 21 and 28 days were determined as 2%, 2.6%, 3.46% and 4.09%. The E9 sample showed the most effective healing at the end of 28 days. On the other hand, the E10 mixture showed a effective healing of 0.41% at 14 days, 1.01% at 21 days and 1.42% at the end of 28 days.

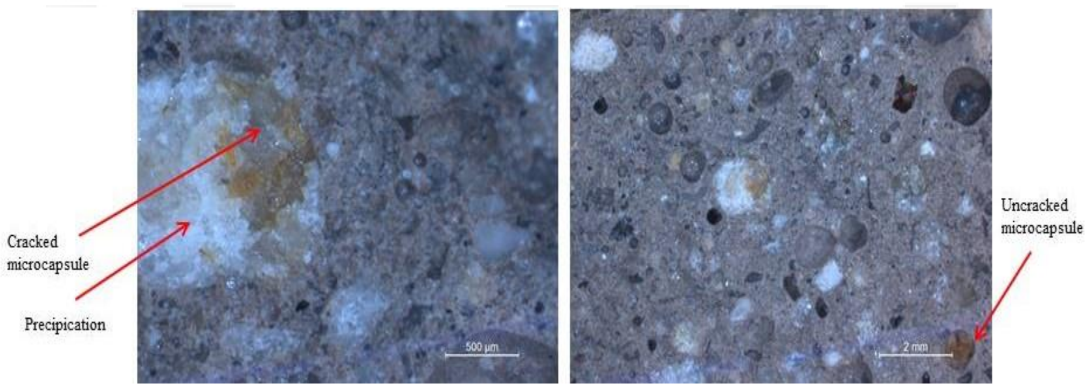


**Figure 6.23** Stereomicroscopic images of mixture “E9”

As shown in Figure 6.23, the stereomicroscope images of the “E9” mixture containing encapsulated bacteria at a concentration of $10^9$ cfu/ml, broken microcapsules and white precipitates were detected in the crack area, while unbroken microcapsules were observed. Effective healing level of geopolymer mortar samples containing encapsulated bacteria remained low compared to samples containing non-encapsulated bacteria was related with unbroken microcapsules that prevent the release of the healing agent after crack formation.

The highest effective healing levels were shown by a mixture of E9. The optimum bacteria concentration was selected as $10^9$ cfu/ml for the continuation of the experimental studies.

## 6.10 Ultrasonic Pulse Velocity Test Result and Effective Healing Levels of Geopolymer Mortars Containing Encapsulated Bacteria Immobilized by Magnetic Nanoparticles

Encapsulated immobilized bacteria at $10^9$ cfu/ml concentration with different amount of magnetic nanoparticles in the amount of 2% by weight of binder were added to the geopolymer mortar, whose binder materials, Ms ratio, water-binder ratio and curing conditions were optimized. At the end of the curing period, the cracked samples were subjected to UPV test. The control sample containing no bacteria was named ”C“, the ”MNP-0.5“ containing nanoparticles at 0.5% of amount of bacteria, the ”MNP-1“ containing nanoparticles at 1% of amount of bacteria and the geopolymer mortar sample containing nanoparticles at 1.5% of amount of bacteria were named ”MNP-1.5". The UPV results and effective healing percentages of geopolymer mortars containing encapsulated bacteria which immobilized by magnetic nanoparticles are presented in Figure 6.24 and Figure 6.25, respectively.

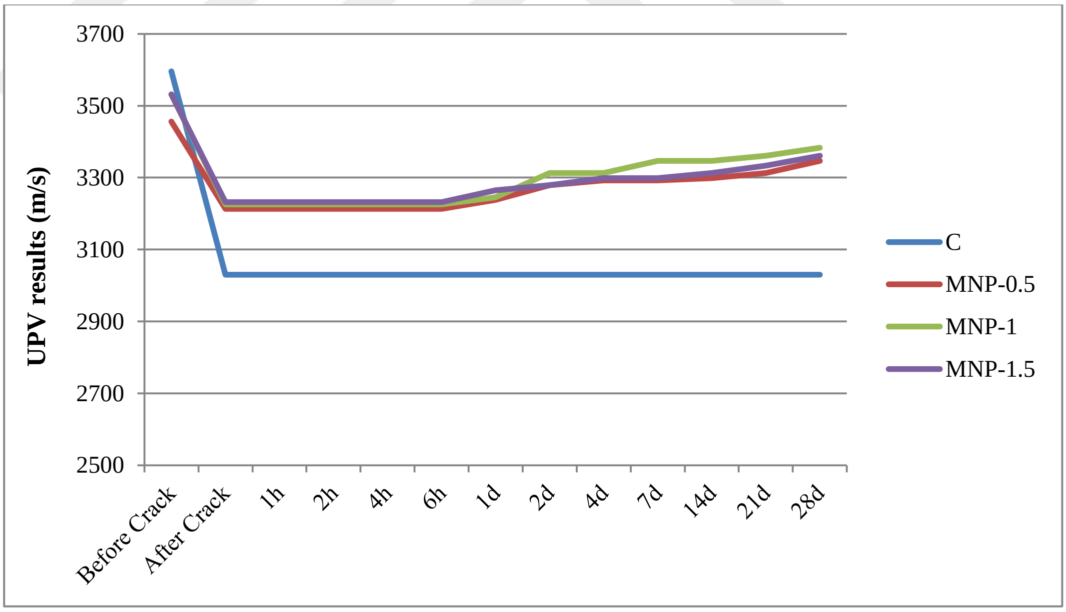


**Figure 6.24** UPV results of geopolymer mortars containing encapsulated bacteria immobilized by magnetic nanoparticles

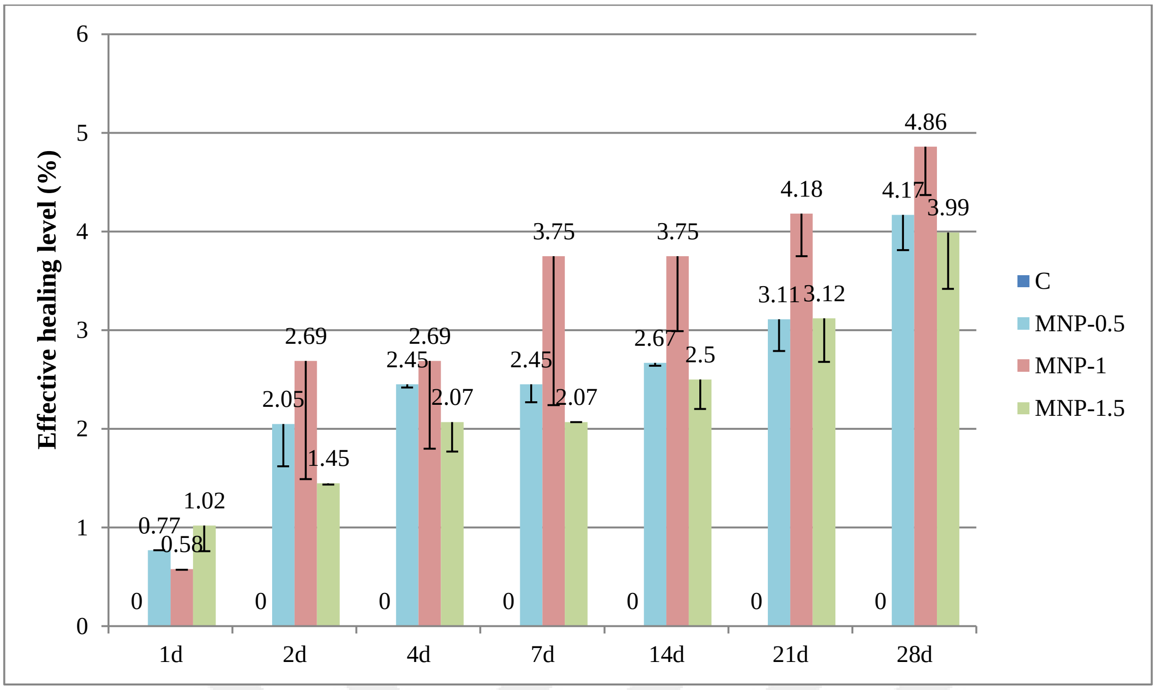


**Figure 6.25** Effective healing level of geopolymer mortars containing encapsulated bacteria immobilized by magnetic nanoparticles

As shown in Figure 6.24, it was determined that all samples containing bacteria with magnetic nanoparticles showed healing. The healing was observed in the mixtures from 1 day. As can be seen in Figure 6.25, the effective healing level of the MNP-0.5 sample at 1 day was 0.77%, and at 2, 4, 7, 14, 21 and 28 days, healing was observed at 2.05%, 2.45%, 2.45%, 2.67%, 3.11% and 4.17%, respectively. On the other hand, the effective healing levels of MNP-1 samples at 1, 2, 4, 7,14, 21 and 28 days were determined as 0.58%, 2.69%, 2.69%, 3.75%, 3.75%, 4.18% and 4.86%, respectively. The MNP-1 sample showed the most effective healing at the end of 28 days. While MNP-1.5 showed 1.02% of effective healing at 1 day, effective healing levels of sample were observed as 1.45%, 2.07%, 2.07%, 2.5%, 3.12% and 3.99% at 2, 4, 7, 14, 21 and 28 days, respectively.

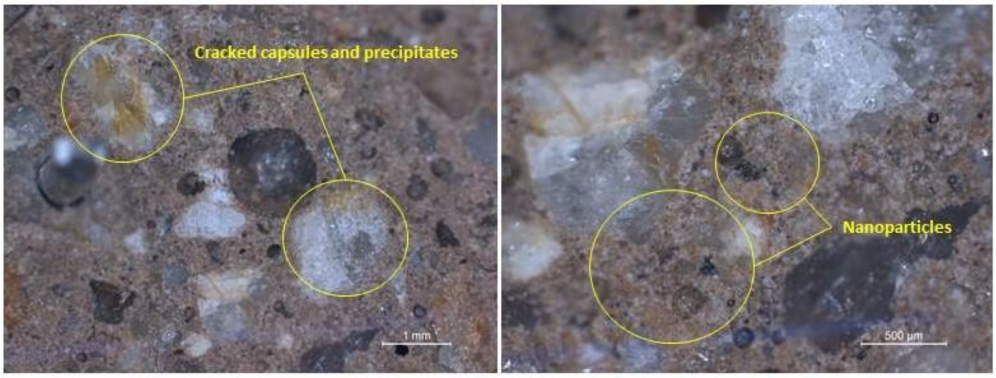


**Figure 6.26** Stereomicroscopic images of mixture “MNP-0.5”

As shown in Figure 6.26, the stereomicroscope images of the “MNP-0.5”, cracked microcapsules and white precipitates were detected in the crack area, while unbroken microcapsules were observed. It was observed that there are black colored nanoparticles dispersed in or around the white precipitates.

## 6.11 Ultrasonic Pulse Velocity Test Result and Effective Healing Levels of Geopolymer Mortars Containing Encapsulated Bacteria Immobilized by Nanoparticles Obtained by Green Synthesis Method

Encapsulated immobilized bacteria at $10^9$ cfu/ml concentration with different amount of nanoparticles obtained by green synthesis method in the amount of 2% by weight of binder were added to the geopolymer mortar, whose binder materials, Ms ratio, water-binder ratio and curing conditions were optimized. At the end of the curing period, the cracked samples were subjected to UPV test. The control sample containing no bacteria was named ”C“, the ”GNP-0.5“ containing nanoparticles at 0.5% of amount of bacteria, the ”GNP-1“ containing nanoparticles at 1% of amount of bacteria and the geopolymer mortar sample containing nanoparticles at 1.5% of amount of bacteria were named ”GNP-1.5". The UPV results and effective healing percentages of geopolymer mortars containing encapsulated bacteria which immobilized by nanoparticles obtained by green synthesis method are presented in Figure 6.27 and Figure 6.28, respectively.

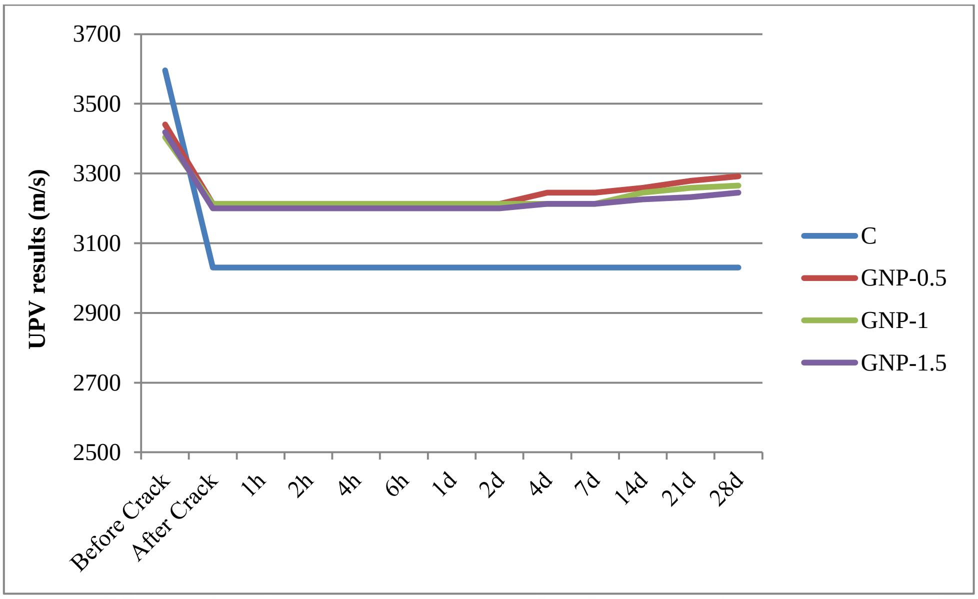


**Figure 6.27** UPV results of geopolymer mortars containing encapsulated bacteria immobilized by nanoparticles obtained by green synthesis method

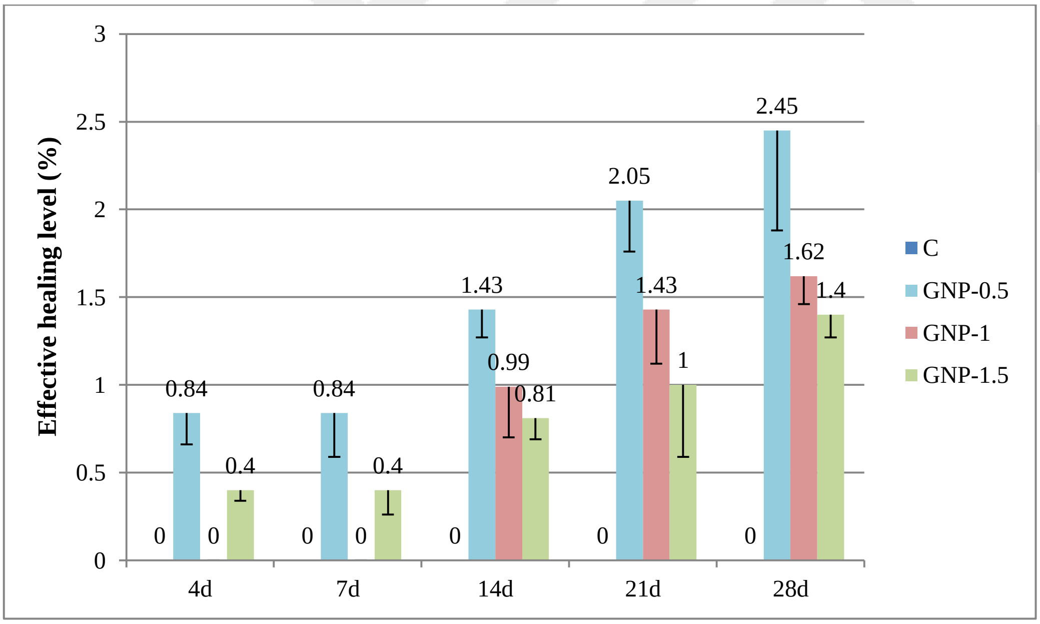


**Figure 6.28** Effective healing levels of geopolymer mortars containing encapsulated bacteria immobilized by nanoparticles obtained by green synthesis method

As shown in Figure 6.27, it was determined that all samples containing bacteria with nanoparticles obtained by green synthesis method showed healing. The healing was observed in the GNP-0.5 and GNP-1.5 from 4 days, while healing was observed in the GNP-1 from 14 days. As can be seen in Figure 6.28, the effective healing level of the GNP-0.5 sample at 4 day was 0.84%, and at 7, 14, 21 and 28 days, effective healing was observed at 0.84%, 1.43%, 2.05% and 2.45%, respectively. The GNP-0.5 sample showed the most effective healing at the end of 28 days. On the other hand, the effective healing levels of GNP-1 samples at 14, 21 and 28 days were determined as 0.99%, 1.43% and 1.62%, respectively. While GNP-1.5 showed 0.4% of effective healing at 4 days, effective healing levels of sample were observed as 0.4%, 0.81%, 1% and 1.4% at 7, 14, 21 and 28 days, respectively. As the amount of nanoparticles increased from 0.5% to 1.5%, a decrease in effective healing levels of geopolymer mortars was observed.

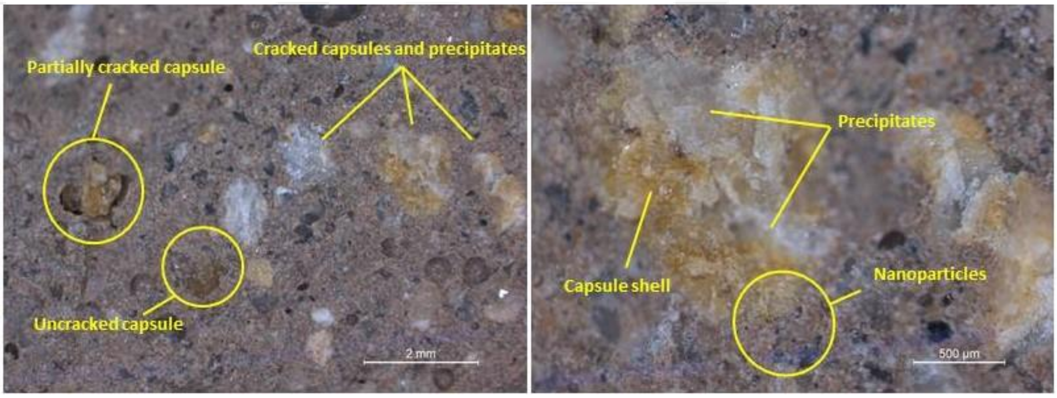


**Figure 6.29** Stereomicroscopic images of mixture “GNP-0.5”

As shown in Figure 6.29, the stereomicroscope images of the “GNP-0.5”, uncracked, partially cracked and cracked microcapsules and white precipitates were detected in the crack area, while in the stereomicroscope images of the “MNP-0.5”, uncracked microcapsules were not observed. It was observed that there are black colored nanoparticles dispersed in or around the white precipitates. Effective healing level of GNP-0.5 remained low compared to MNP-0.5 was related with unbroken microcapsules that prevent the release of the healing agent after crack formation.

### 6.11.1 Comparison of effective healing level of self-healing geopolymer mortars

The effective healing level of self-healing geopolymer mortars mixtures at the end of 28 days is given in Figure 6.30.

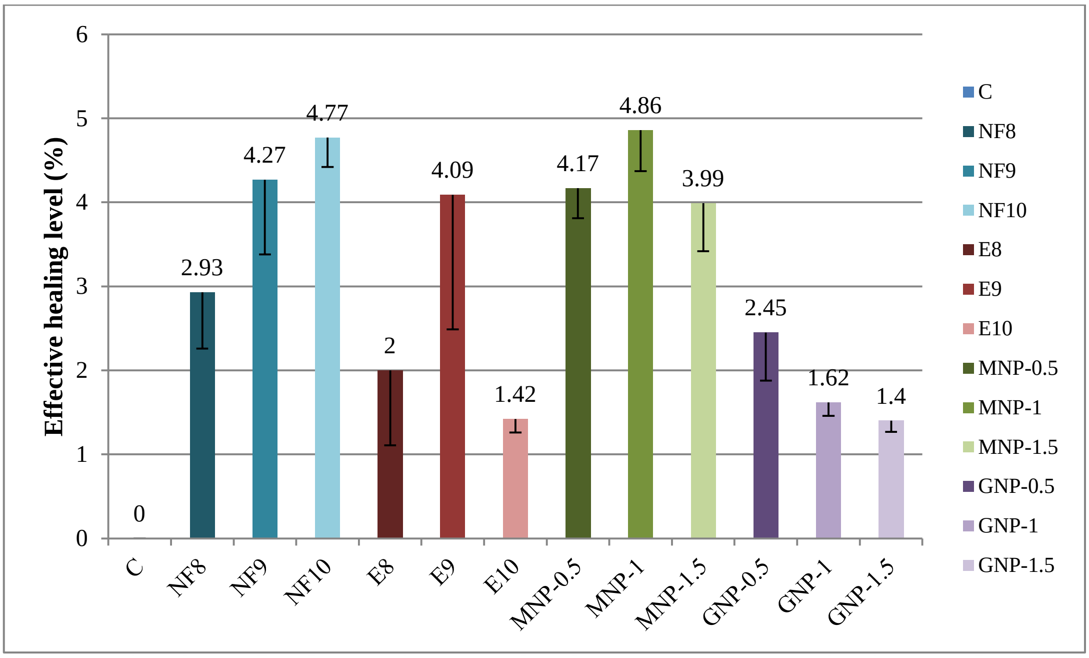


**Figure 6.30** Effective healing level of self-healing geopolymer mortars

The bacteria-free C sample showed no healing at the end of 28 days. For effective self-healing detection, all samples subjected to UPV test were kept in room condition for 28 days during test measurements at the end of a cure at 50°C for 3 days. The fact that the C sample does not show healing can be attributed to the geopolymer mortar does not form products due to continuing geopolymerization at an ambient temperature below the required curing temperature. In geopolymer mortars containing non-encapsulated bacteria series, With the increase of bacterial concentration from $10^8$ cfu/ml to $10^{10}$ cfu/ml, the increase in effective healing levels can be attributed to an increase in the amount of bacterial-derived precipitates with an increase in the number of bacteria. E9 samples containing encapsulated bacteria at a concentration of $10^9$ cfu/ml, showed the highest effective healing with 4.09%. The lower effective healing levels of encapsulated bacterial samples (E8, E9 and E10) compared to non-encapsulated bacterial samples (NF8, NF9 and NF10) may be associated with unbroken microcapsules prevent product (precipitate) formation by leakage of the healing agent after crack formation and microstructural improvement of geopolymer mortars due to calcite formation of non-encapsulated bacteria. In samples containing bacteria immobilized with magnetic nanoparticles and nanoparticles obtained by the green synthesis method, MNP-0.1 and GNP-0.5 samples showed the highest effective healing with 4.86% and 2.45%, respectively. There was statistically significant difference between effective healing level of geopolymer mortars containing magnetic nanoparticles and encapsulated bacteria ($p<0.05$). It was determined that while the presence of magnetic nanoparticle positively affects the healing level, especially at early ages, and the presence of nanoparticle obtained by the green synthesis method showed no positive effect for the healing level of geopolymer mortars.

# 7 CONCLUSION AND RECOMMENDATIONS

Within the scope of the thesis study, the design and characterization of geopolymer mortar and the self-healing behavior of geopolymer mortar were investigated. According to the materials used and the experiments applied, the following results were obtained:

- Among the geopolymer mortars prepared in various combinations of binder materials, it was found that the mixture with 65% fly ash, 20% granulated blast furnace slag and 15% brick dust (65FA+20BFS+15BP) in the binder gives the highest strengths. The flexural strength of this geopolymer mortar mixture at the end of the curing period of 3 days at 50°C was determined as 7 MPa and the compressive strength was determined as 53.81 MPa.

- The mixture with a Ms ratio of 1.3 (Ms-1.3) showed a flexural strength of 7 MPa and a compressive strength of 53.81 MPa at the end of the 3-day 50°C cure. When the Ms ratio increased from 1.2 to 1.3, there was a 7.70% flexural in compressive strength, and when the Ms ratio increased from 1.3 to 1.4, a decrease was observed at the level of 3.57%. When the Ms ratio increased from 1.2 to 1.3, an increase in compressive strength was observed at the level of 13.61%, and when the Ms ratio increased from 1.3 to 1.4, a decrease was observed at the level of 16.24%.

- The mixture with a water-binder ratio of 0.42 (w/b-0.42) showed a flexural strength of 8.23 MPa and a compressive strength of 54.3 MPa at the end of the 3-day 50°C cure. When the water-binder ratio increased from 0.42 to 0.44, a decrease in flexural strength was observed at the level of 12.52%, while when the water-binder ratio increased from 0.44 to 0.46 and from 0.46 to 0.48, a decrease was observed at the levels of 2.77% and 12.85%, respectively. When the water-binder ratio increased from 0.46 to 0.48, a decrease in compressive strength was observed at the level of 8.14%. All mortar mixtures were found to be suitable in terms of workability.

- Since the strength properties and energy consumption were taken into account, the sample cured at 50°C for 3 days (3D-50C) was found to have optimal values. The flexural strength of the mixture was determined as 8.23 MPa and the compressive strength was determined as 54.3 MPa. The energy consumption is 0.135 kWh/MPa for compressive strength and 0.892 kWh for flexural strength. The optimum curing time was 3 days and the curing temperature was 50°C.

- It was determined that water curing does not have a significant effect on the strength of geopolymer mortar. It was observed that the addition of non-encapsulated bacteria has a negative effect on the flexural strength of the geopolymer mortar. It was observed that setting time of geopolymer mortars increase with non-encapsulated bacteria addition.

- The mixture with a non-encapsulated bacteria at $10^{10}$ cfu/ml concentration (NF10) showed %34.77 healing. The NF9 sample showed the most effective healing at the end of 28 days.

- The mixture with an encapsulated bacteria at $10^{9}$ cfu/ml concentration (E9) showed %4.09 healing. The E9 sample showed the most effective healing at the end of 28 days.

- The mixture (MNP-1) with a magnetic nanoparticles up to 0.5% of amount of bacteria ($10^{9}$ cfu/ml) showed %4.86 healing. The MNP-1 sample showed the most effective healing at the end of 28 days.

- Mixture with a magnetic nanoparticles (MNP-0.5, MNP-1 and MNP-1.5) were effective for early ages healing. Healing of all mixture with a magnetic nanoparticles were measured for 1 day after crack formation.

- The mixture (GNP-0.5) with a nanoparticles obtained by green synthesis method up to 0.5% of amount of bacteria ($10^{9}$ cfu/ml) showed %2.45 healing. The GNP-0.5 sample showed the most effective healing at the end of 28 days.

- It was observed that among the self healing geopolymer mortars, bacterial immobilization with magnetic nanoparticles was determined as the most effective method for giving the geopolymer mortar a self-healing property.

The following topics can be explored in further researches;

- Investigation of the detection of self-healing under thermal cure after cracking of bacteria-free geopolymer mortar.

- Investigation of the effect of the non-encapsulated bacteria immobilized with nanoparticles on effective healing.

- Investigation of the effect of geopolymer mortar on strength properties in empty capsules.

- Investigation of the effect of different mediums on effective healing of geopolymer mortar.

# REFERENCES

**Achal, V., Mukherjee, A., & Sudhakara Reddy, M.** (2011). Microbial Concrete way to enhance the durability of building structures. *Cell*, *2*, 2.

**Allahverdi, A., & Najafi Kani, E.** (2009). Construction wastes as raw materials for geopolymer binders. *International Journal of Civil Engineering*, *7*(3), 154-160.

**Amrina, E., & Vilsi, A. L.** (2015). Key performance indicators for sustainable manufacturing evaluation in cement industry. *Procedia Cirp*, *26*, 19-23.

**Andalib, R., Abd Majid, M. Z., Hussin, M. W., Ponraj, M., Keyvanfar, A., Mirza, J., & Lee, H. S.** (2016). Optimum concentration of Bacillus megaterium for strengthening structural concrete. Construction and Building Materials, 118, 180-193.

**Andrew, R. M.** (2019). Global CO2 emissions from cement production, 1928–2018. Earth System Science Data, 11(4), 1675-1710.

**Aydin, S.** (2010). *Alkalilerle aktive edilmiş yüksek fırın cürufu bağlayıcılı lifli kompozit geliştirilmesi* (Doctoral dissertation, DEÜ Fen Bilimleri Enstitüsü).

**Bang, S. S., Galinat, J. K., & Ramakrishnan, V.** (2001). Calcite precipitation induced by polyurethane-immobilized Bacillus pasteurii. *Enzyme and microbial technology*, *28*(4-5), 404-409.

**Barrasa, R. C., López, V. B., Montoliu, C. M. P., Ibáñez, V. C., Pedrajas, J., & Santarén, J.** (2014). Addressing durability of asphalt concrete by self-healing mechanism. *Procedia-Social and Behavioral Sciences*, *162*, 188-197.

**Bashir, J., Kathwari, I., Tiwary, A., & Singh, K.** (2016). Bio concrete-the self-healing concrete. *Indian Journal of Science and Technology*, *9*(47), 1-5.

**Bederina M, Makhloufi Z and Bouziani T** (2011). Effect of limestone fillers the physic-mechanical properties of limestone concrete. Physics Procedia 21: 28–34

**Bing-hui, M., Zhu, H., Xue-min, C., Yan, H., Si-yu, G.** (2014). Effect of curing temperature on geopolymerization of metakaolin-based geopolymers. Appl. Clay Sci. 99, 144-148.

**Bondar, D., Lynsdale, C. J., Milestone, N. B., Hassani, N., & Ramezanianpour, A. A.** (2011). Effect of type, form, and dosage of activators on strength of alkali-activated natural pozzolans. *Cement and Concrete Composites*, *33*(2), 251-260.

**Boquet, E., Boronat, A., & Ramos-Cormenzana, A.** (1973). Production of calcite (calcium carbonate) crystals by soil bacteria is a general phenomenon. *Nature*, *246*(5434), 527-529.

**Cailleux, E., & Pollet, V.** (2009, June). Investigations on the development of self-healing properties in protective coatings for concrete and repair mortars. In *Proceedings of the 2nd international conference on self-healing materials, Chicago, IL, USA* (Vol. 28, p. 1).

**Carolyn, D.** (1990, July). Alteration of matix permeability, pore and crack structure by the time release of internal chemicals. In *Proceedings of the ACS/NIST Conference on Advances in Cementitious Material, American Ceramic Society, co-sponsored by National Institute of Standards and Technology, Gaithersburg, Maryland* (Vol. 768).

**Chalal, N., Siddique, R., & Rajor, A.** (2012). Influence of bacteria on the compressive strength, water absorption and rapid chloride permeability of fly ash concrete. *Construction and Building Materials*, *28*(1), 351-356.

**Chassevent, L.** (1937). Hydraulicity of slags. *Compt Rend*, *205*, 670-672.

**Chindaprasirt, P., Chareerat, T., & Sirivivatnanon, V.** (2007). Workability and strength of coarse high calcium fly ash geopolymer. *Cement and concrete composites*, *29*(3), 224-229.

**Cho, Y. K., Yoo, S. W., Jung, S. H., Lee, K. M., & Kwon, S. J.** (2017). Effect of Na2O content, SiO2/Na2O molar ratio, and curing conditions on the compressive strength of FA-based geopolymer. *Construction and Building Materials*, *145*, 253-260.

**Cui, J., Li, X., Pei, Z., & Pei, Y.** (2019). A long-term stable and environmental friendly self-healing coating with polyaniline/sodium alginate microcapsule structure for corrosion protection of water-delivery pipelines. *Chemical Engineering Journal*, *358*, 379-388.

**Davidovits, J.** (1979). Synthesis of new high temperature geo-polymers for reinforced plastics/composites. *Spe Pactec*, *79*, 151-154.

**Davidovits, J.** (1991). Geopolymers: inorganic polymeric new materials. *Journal of Thermal Analysis and calorimetry*, *37*(8), 1633-1656.

**Davidovits, J.** (1999, June). Chemistry of geopolymeric systems, terminology. In *Geopolymer* (Vol. 99, No. 292, pp. 9-39). sn.

**Davidovits, J.** (2002, October). years of successes and failures in geopolymer applications. Market trends and potential breakthroughs. In *Geopolymer 2002 conference* (Vol. 28, p. 29). Saint-Quentin, France; Melbourne, Australia: Geopolymer Institute.

**Davidovits, J.** (2008). Geopolymer. *Chemistry and Applications. Institute Geopolymere, Saint-Quentin, France*.

**Davidovits, J. and Sawyer, J.L.,** (1985), Early high-strength mineral polymer, US Patent 4,509,985, 1985, filed February 22, 1984. The first commercial geopolymer cement was coined Pyrament 2000™ designed for repair and patching operations.

**Deb, P. S., Nath, P., & Sarker, P. K.** (2014). The effects of ground granulated blast-furnace slag blending with fly ash and activator content on the workability and strength properties of geopolymer concrete cured at ambient temperature. *Materials & Design (1980-2015)*, *62*, 32-39.

**Diercks, C. S., & Yaghi, O. M.** (2017). The atom, the molecule, and the covalent organic framework. *Science*, *355*(6328), eaal1585.

**Dry, C. M.** (2000). Three designs for the internal release of sealants, adhesives, and waterproofing chemicals into concrete to reduce permeability. *Cement and Concrete Research*, *30*(12), 1969-1977..

**Du, F., Warsinger, D. M., Urmi, T. I., Thiel, G. P., Kumar, A., & Lienhard V, J. H.** (2018). Sodium hydroxide production from seawater desalination brine: process design and energy efficiency. *Environmental science & technology*, *52*(10), 5949-5958.

**Duxson, P. S. W. M., Mallicoat, S. W., Lukey, G. C., Kriven, W. M., & Van Deventer, J. S.** (2007a). The effect of alkali and Si/Al ratio on the development of mechanical properties of metakaolin-based geopolymers. *Colloids and Surfaces A: Physicochemical and Engineering Aspects*, *292*(1), 8-20.

**Duxson, P., Fernández-Jiménez, A., Provis, J. L., Lukey, G. C., Palomo, A., & van Deventer, J. S.** (2007b). Geopolymer technology: the current state of the art. *Journal of materials science*, *42*(9), 2917-2933.

**Duxson, P., Provis, J. L., Lukey, G. C., & Van Deventer, J. S.** (2007c). The role of inorganic polymer technology in the development of 'green concrete'. *cement and concrete research*, *37*(12), 1590-1597.

**Ebead, U., Lau, D., Lollini, F., Nanni, A., Suraneni, P., & Yu, T.** (2022). A review of recent advances in the science and technology of seawater-mixed concrete. *Cement and concrete research*, *152*, 106666.

**Edvardsen, C.** (1999). Water permeability and autogenous healing of cracks in concrete. In *Innovation in concrete structures: Design and construction* (pp. 473-487). Thomas Telford Publishing.

**Ekinci, E., Türkmen, İ., & Birhanli, E.** (2022). Mechanical and durability characteristics of GGBS-based self-healing geopolymer mortar produced using by an endospore-forming bacterium. *Journal of Building Engineering*, *57*, 104944.

**Erşan, Y. Ç., Da Silva, F. B., Boon, N., Verstraete, W., & De Belie, N.** (2015). Screening of bacteria and concrete compatible protection materials. Construction and building materials, 88, 196-203.

**Erşan, Y. Ç., De Belie, N., & Boon, N.** (2015). Microbially induced CaCO3 precipitation through denitrification: an optimization study in minimal nutrient environment. Biochemical Engineering Journal, 101, 108-118.

**Erşan, Y. Ç., Hernandez-Sanabria, E., Boon, N., & De Belie, N.** (2016). Enhanced crack closure performance of microbial mortar through nitrate reduction. *Cement and concrete composites*, *70*, 159-170.

**Feret, R.** (1939). Slags for the manufacture of cement. *Rev. Mater. Constr. Tr. Publications*, 1-145.

**Fernández-Jiménez, A., & Palomo, A.** (2003). Characterisation of fly ashes. Potential reactivity as alkaline cements☆. *Fuel*, *82*(18), 2259-2265.

**Fernández-Jiménez, A., & Palomo, A.** (2005). Composition and microstructure of alkali activated fly ash binder: Effect of the activator. *Cement and concrete research*, *35*(10), 1984-1992.

**Fernández-Jiménez, A., Palomo, A.** (2005a). "Composition and microstructure of alkali activated fly ash binder: Effect of the activator", Cement and Concrete Research, 35(10), 1984-92.

**Fernández-Jiménez, A., Palomo, A., & Alonso, M. M.** (2005b). Alkali activation of fly ashes: mechanisms of reaction. In *Congress of Non-Traditional Cement and Concrete II* (pp. 1-12).

**Fernández-Jiménez, A., Palomo, A., Pastor, J. Y., & Martin, A.** (2008). New cementitious materials based on alkali-activated fly ash: performance at high temperatures. *Journal of the American Ceramic Society*, *91*(10), 3308-3314.

**Fernández-Jiménez, A., Palomo, A., Sobrados, I., & Sanz, J.** (2006). The role played by the reactive alumina content in the alkaline activation of fly ashes. *Microporous and Mesoporous materials*, *91*(1-3), 111-119.

**Forss, B.** (1983). Experiences from the use of F-cement—a binder based on alkali-activated blastfurnace slag. *Alkalis in Concrete, Danish Concrete Association, Copenhagen, Denmark*, 101-104.

**Garces, J. I. T., Dollente, I. J., Beltran, A. B., Tan, R. R., & Promentilla, M. A. B.** (2021). Life cycle assessment of self-healing geopolymer concrete. *Cleaner Engineering and Technology*, *4*, 100147.

**García-González, J., Rodríguez-Robles, D., Wang, J., De Belie, N., Morán-del Pozo, J. M., Guerra-Romero, M. I., & Juan-Valdés, A.** (2017). Quality improvement of mixed and ceramic recycled aggregates by biodeposition of calcium carbonate. *Construction and Building Materials*, *154*, 1015-1023.

**García-Lodeiro, I., Palomo, A. Y., & Fernández-Jiménez, A.** (2007). Alkali–aggregate reaction in activated fly ash systems. *Cement and Concrete Research, 37*(2), 175-183.

**Garside, M.** (2020). Global cement production 1995–2019. *Statista, dostupno na: https://www.statista.com/statistics/267364/world-cement-production-bycountry/(Pristupljeno: 17. siječnja 2020.)*.

**Gartner, E.** (2004). Industrially interesting approaches to "low-CO2" cements. *Cement and Concrete research*, *34*(9), 1489-1498.

**Ghodke, P., & Mote, S.** (2018). The self-healing concrete–a review. *International Journal of Advances in Engineering & Technology*, *11*(1), 29-34.

**Glanville, W. H.** (1931). The permeability of portland cement concrete, Building Research Establishment, Tech.

**Glukhovsky, V.** (1959). Soil silicates. Gostroiizdat Publish. *Kiev, Ukraine (in Russian), 301*.

**Glukhovsky, V. D.** (1965). Soil silicates: Their properties, technology and manufacturing and fields of application. *Doct. Tech. Sc. Degree Thesis, Civil Engineering Institute, Kiev, Ukraine*.

**Glukhovsky, V. D.** (1994, October). Ancient, modern and future concretes. In *Proceedings of the First International Conference on Alkaline Cements and Concretes* (pp. 1-9). Kiev, Ukraine.

**Gourley, J. T.** (2003, October). Geopolymers; opportunities for environmentally friendly construction materials. In *Materials 2003 Conference: Adaptive*

*Materials for a Modern Society, Sydney, Institute of Materials Engineering Australia*.

**Gurunathan, S., Kalishwaralal, K., Vaidyanathan, R., Venkataraman, D., Pandian, S. R. K., Muniyandi, J., ... & Eom, S. H.** (2009). Biosynthesis, purification and characterization of silver nanoparticles using Escherichia coli. Colloids and Surfaces B: Biointerfaces, 74(1), 328-335.

**Hardjito, D., Wallah, S. E., Sumajouw, D. M., & Rangan, B. V.** (2004). On the development of fly ash-based geopolymer concrete. *Materials Journal*, *101*(6), 467-472.

**Hearn, N.** (1998). Self-sealing, autogenous healing and continued hydration: What is the difference?. *Materials and structures*, *31*(8), 563-567.

**Hemsley, A. R., & Griffiths, P. C.** (2000). Architecture in the microcosm: biocolloids, self-assembly and pattern formation. *Philosophical Transactions of the Royal Society of London. Series A: Mathematical, Physical and Engineering Sciences*, *358*(1766), 547-564.

**Hoag, G. E., Collins, J. B., Holcomb, J. L., Hoag, J. R., Nadagouda, M. N., & Varma, R. S**. (2009). Degradation of bromothymol blue by 'greener'nano-scale zero-valent iron synthesized using tea polyphenols. Journal of Materials Chemistry, 19(45), 8671-8677.

**Homma, D., Mihashi, H., & Nishiwaki, T.** (2009). Self-healing capability of fibre reinforced cementitious composites. *Journal of Advanced Concrete Technology*, *7*(2), 217-228.

**Huang, L., Weng, X., Chen, Z., Megharaj, M., & Naidu, R.** (2014). Green synthesis of iron nanoparticles by various tea extracts: comparative study of the reactivity. Spectrochimica Acta Part A: Molecular and Biomolecular Spectroscopy, 130, 295-301.

**Huseien, G. F., Shah, K. W., & Sam, A. R. M.** (2019). Sustainability of nanomaterials based self-healing concrete: An all-inclusive insight. *Journal of Building Engineering*, *23*, 155-171.

**Hyde, G. W., & Smith, W. J.** (1889). Results of experiments made to determine the permeability of cements and cement mortars. *Journal of the Franklin Institute*, *128*(3), 199-207.

**Jacobsen, S., & Sellevold, E. J.** (1996). Self healing of high strength concrete after deterioration by freeze/thaw. *Cement and Concrete Research*, *26*(1), 55-62.

**Jadhav, U. U., Lahoti, M., Chen, Z., Qiu, J., Cao, B., & Yang, E. H.** (2018). Viability of bacterial spores and crack healing in bacteria-containing geopolymer. *Construction and Building Materials*, *169*, 716-723.

**Jonkers, H. M.** (2007). Self healing concrete: a biological approach. In *Self healing materials* (pp. 195-204). Springer, Dordrecht.

**Jonkers, H. M., Thijssen, A., Muyzer, G., Copuroglu, O., & Schlangen, E.** (2010). Application of bacteria as self-healing agent for the development of sustainable concrete. *Ecological engineering*, *36*(2), 230-235.

**Joseph, C., Jefferson, A. D., & Cantoni, M. B.** (2007, April). Issues relating to the autonomic healing of cementitious materials. In *First international conference on self-healing materials* (pp. 1-8).

**Justnes, H., & Martius-Hammer.** (2016) T. A. SUSTAINABILITY–A DRIVER FOR CONCRETE INNOVATION.

**Kan, L. L., Lv, J. W., Duan, B. B., & Wu, M.** (2019). Self-healing of Engineered Geopolymer Composites prepared by fly ash and metakaolin. *Cement and Concrete Research*, *125*, 105895.

**Kaya, M., Uysal, M., Yilmaz, K., Karahan, O., & Atis, C. D.** (2020). Mechanical properties of class C and F fly ash geopolymer mortars.

**Khale, D., & Chaudhary, R.** (2007). Mechanism of geopolymerization and factors influencing its development: a review. *Journal of materials science*, *42*(3), 729-746.

**Khater, H.M.** (2012). Effect of calcium on geopolymerization of aluminosilicate wastes. J. Mater. Civ. Eng. 24(1), 92-101.

**Khattab, I. M., Shekha, H., & Abdi, M. A.** (2019). Study on Self-healing Concrete types–A review. *Sustainable Structures and Materials, An International Journal*, *2*(1), 76-87.

**Khushnood, R. A., ud din, S., Shaheen, N., Ahmad, S., & Zarrar, F.** (2019). Bio-inspired self-healing cementitious mortar using Bacillus subtilis immobilized on nano-/micro-additives. *Journal of Intelligent Material Systems and Structures*, *30*(1), 3-15.

**Kourkoutas Y, Bekatorou A, Banat IM, Marchant R, Koutinas AA** (2004). Immobilization technologies and support materials suitable in alcohol beverages production: a review. Food Microbiol 21:377–397. https://doi.org/10.1016/j.fm.2003.10.005

**Kovalchuk, G., Fernández-Jiménez, A., & Palomo, A.** (2007). Alkali-activated fly ash: effect of thermal curing conditions on mechanical and microstructural development–Part II. *Fuel*, *86*(3), 315-322.

**Kuehl, H.** (1908). *U.S. Patent No. 900,939*. Washington, DC: U.S. Patent and Trademark Office.

**Kumar, S., Kumar, R., & Mehrotra, S. P.** (2010). Influence of granulated blast furnace slag on the reaction, structure and properties of fly ash based geopolymer. *Journal of materials science*, *45*(3), 607-615

**Kutti, T.** (1982). Investigation of mechanical properties and structure of alkali activated blast-furnace slag mortars.

**Lee, W. K. W., & Van Deventer, J. S. J.** (2004). The interface between natural siliceous aggregates and geopolymers. *Cement and Concrete Research*, *34*(2), 195-206.

**Li V.C., Yang E.H.** (2007). Self-healing in concrete materials, in self-healing material: an alternative approach to centuries of materials sciences.

**Luo, J., Chen, X., Crump, J., Zhou, H., Davies, D. G., Zhou, G., ... & Jin, C.** (2018). Interactions of fungi with concrete: Significant importance for bio-based self-healing concrete. *Construction and building materials*, *164*, 275-285.

**Luo, M., & Qian, C.** (2016). Influences of bacteria-based self-healing agents on cementitious materials hydration kinetics and compressive strength. Construction and Building Materials, 121, 659-663.

**McDonald, M., & Thompson, J. L.** (2006). Sodium silicate a binder for the 21st century. *National silicates and PQ Corporation of Industrial Chemicals Division*.

**Mehta, P. K., & Monteiro, P. J.** (2014). *Concrete: microstructure, properties, and materials*. McGraw-Hill Education.

**Mihashi, H., Kaneko, Y., Nishiwaki, T., & Otsuka, K.** (2000). Fundamental study on development of intelligent concrete characterized by self-healing capability for strength. *Transactions of the Japan Concrete Institute*, *22*, 441-450.

**Miller, S. A., Horvath, A., and Monteiro, P. J. M.** (2016). Readily implementable techniques can cut annual CO2 emissions from the production of concrete by over 20%, *Environmental Research Letters*, *11*(7), 074029 https://doi.org/10.1088/1748-9326/11/7/074029

**Naik, R. R., Stringer, S. J., Agarwal, G., Jones, S. E., & Stone, M. O.** (2002). Biomimetic synthesis and patterning of silver nanoparticles. Nature materials, 1(3), 169-172.

**Neville, A.** (2002). Autogenous healing—a concrete miracle?. *Concrete international*, *24*(11), 76-82.

**Nishiwaki, T.** (1997). Fundamental study on development of intelligent concrete with self-healing capability. *Master's Thesis*.

**Orsted, H. L., Keast, D. H., Forest-Lalande, L., Kuhnke, J. L., & O'Sullivan-Drombolis, D.** (2018). Foundations of Best Practice for Skin and Wound Management. *Skin: Anatomy, Physiology and Wound Healing. Wounds Canada*, 1-26.

**Pacheco-Torgal, F., Castro-Gomes, J., & Jalali, S.** (2008). Alkali-activated binders: A review. Part 2. About materials and binders manufacture. *Construction and building materials*, *22*(7), 1315-1322.

**Pacheco-Torgal, F., Labrincha, J., Leonelli, C., Palomo, A., & Chindaprasit, P. (Eds.).** (2014). *Handbook of alkali-activated cements, mortars and concretes*. Elsevier.

**Pacheco-Torgal, F., Moura, D., Ding, Y., & Jalali, S.** (2011). Composition, strength and workability of alkali-activated metakaolin based mortars. *Construction and Building Materials*, *25*(9), 3732-3745.

**Palomo, A., Fernández-Jimenez, A., & Kovalchuck, G.** (2005). Some key factors affecting the alkali activation of fly ash. In *2nd International Symposium of Non-Traditional Cement and Concrete*.

**Palomo, A., Grutzeck, M. W., & Blanco, M. T.** (1999). Alkali-activated fly ashes: A cement for the future. *Cement and concrete research*, *29*(8), 1323-1329.

**Pan, Z. Y., Li, G., Hong, C. Y., Kuang, H. L., Yu, Y., Feng, F. X., ... & Du, H.** (2015). Modified recycled concrete aggregates for asphalt mixture using microbial calcite precipitation. *RSC Advances*, *5*(44), 34854-34863.

**Patankar, S. V., Jamkar, S. S., & Ghugal, Y. M.** (2013). Effect of water-to-geopolymer binder ratio on the production of fly ash based geopolymer concrete. *Int. J. Adv. Technol. Civ. Eng*, *2*(1), 79-83.

**Polat, B. Y., & Uysal, M.** (2021). Bacterial crack healing in metakaolin based geopolymer mortars. *Journal of Building Engineering*, *39*, 102291.

**POLAT, B. Y., UYSAL, M., & Korkmaz, V.** (2020). A research for bacterial self-healing in metakaolin based geopolymer mortars. Sigma Journal of Engineering and Natural Sciences, 38(3), 1401-1414.

**Ponraj, M., Talaiekhozani, A., Zin, R. M., Ismail, M., Abd Majid, M. Z., Keyvanfar, A., & Kamyab, H.** Bioconcrete Strength, Durability, Permeability, Recycling and Effects on Human Health: A.

**Provis, J. L., & Van Deventer, J. S. (Eds.).** (2013). *Alkali activated materials: state-of-the-art report, RILEM TC 224-AAM* (Vol. 13). Springer Science & Business Media.

**Pungrasmi, W., Intarasoontron, J., Jongvivatsakul, P., & Likitlersuang, S.** (2019). Evaluation of microencapsulation techniques for MICP bacterial spores applied in self-healing concrete. *Scientific reports*, *9*(1), 1-10.

**Purdon, A. O.** (1940). The action of alkalis on blast-furnace slag. *Journal of the Society of Chemical Industry*, *59*(9), 191-202.

**Ramachandran, S. K., Ramakrishnan, V., & Bang, S. S.** (2001). Remediation of concrete using micro-organisms. *ACI Materials Journal-American Concrete Institute*, *98*(1), 3-9.

**Rangan, B. V.** (2008). Fly ash-based geopolymer concrete.

**Reig, L., Tashima, M. M., Borrachero, M. V., Monzó, J., Cheeseman, C. R., & Payá, J.** (2013). Properties and microstructure of alkali-activated red clay brick waste. *Construction and Building Materials*, *43*, 98-106.

**Rovnaník, P., Řezník, B., & Rovnaníková, P.** (2016). Blended alkali-activated fly ash/brick powder materials. *Procedia Engineering*, *151*, 108-113.

**Roy, D. M.** (1999). Alkali-activated cements opportunities and challenges. *Cement and concrete research*, *29*(2), 249-254.

**Sarda, D., Choonia, H. S., Sarode, D. D., & Lele, S. S.** (2009). Biocalcification by Bacillus pasteurii urease: a novel application. *Journal of Industrial Microbiology and Biotechnology*, *36*(8), 1111-1115.

**Scott JR, Barnett TC** (2006) Surface proteins of gram-positive bacteria and how they get there. Annu Rev Microbiol 60:397–423. https://doi.org/10.1146/annurev.micro.60.080805.142256

**Seifan, M., Ebrahiminezhad, A., Ghasemi, Y., & Berenjian, A.** (2019). Microbial calcium carbonate precipitation with high affinity to fill the concrete pore space: nanobiotechnological approach. Bioprocess and biosystems engineering, 42, 37-46.

**Seifan, M., Samani, A. K., & Berenjian, A.** (2016). Bioconcrete: next generation of self-healing concrete. *Applied microbiology and biotechnology*, *100*(6), 2591-2602.

**Seifan, M., Sarmah, A. K., Ebrahiminezhad, A., Ghasemi, Y., Samani, A. K., & Berenjian, A.** (2018). Bio-reinforced self-healing concrete using magnetic iron oxide nanoparticles. Applied microbiology and biotechnology, 102, 2167-2178.

**Seifan, M., Sarmah, A. K., Samani, A. K., Ebrahiminezhad, A., Ghasemi, Y., & Berenjian, A.** (2018). Mechanical properties of bio self-healing concrete containing immobilized bacteria with iron oxide nanoparticles. *Applied microbiology and biotechnology*, *102*(10), 4489-4498.

**Shaheen, N., Khushnood, R. A., Khaliq, W., Murtaza, H., Iqbal, R., & Khan, M. H.** (2019). Synthesis and characterization of bio-immobilized nano/micro inert and reactive additives for feasibility investigation in self-healing concrete. *Construction and Building Materials*, *226*, 492-506.

**Shahid, S., Aslam, M. A., Ali, S., Zameer, M., & Faisal, M.** (2020). Self-healing of cracks in concrete using Bacillus strains encapsulated in sodium alginate beads. *ChemistrySelect*, *5*(1), 312-323.

**Shahwan, T., Sirriah, S. A., Nairat, M., Boyacı, E., Eroğlu, A. E., Scott, T. B., & Hallam, K. R.** (2011). Green synthesis of iron nanoparticles and their application as a Fenton-like catalyst for the degradation of aqueous cationic and anionic dyes. Chemical Engineering Journal, 172(1), 258-266.

**Shankar, S. S., Rai, A., Ankamwar, B., Singh, A., Ahmad, A., & Sastry, M.** (2004). Biological synthesis of triangular gold nanoprisms. Nature materials, 3(7), 482-488.

**Shi, C., Jiménez, A. F., & Palomo, A.** (2011). New cements for the 21st century: The pursuit of an alternative to Portland cement. *Cement and concrete research*, *41*(7), 750-763.

**Shinde, B. H., & Kadam, D. K. N.** (2015). Properties of fly ash based geopolymer mortar. *International Journal of Engineering Research And*, *4*(7), 203-206.

**Siddique, R., & Chahal, N. K.** (2011). Effect of ureolytic bacteria on concrete properties. *Construction and building materials*, *25*(10), 3791-3801.

**Singh, B., Ishwarya, G., Gupta, M., Bhattacharyya, S.K.** (2015). Geopolymer concrete: A review of some recent developments. Constr. Build. Mater. 85, 78-90.

**Škvára, F., Doležal, J., Svoboda, P., Kopecký, L., Pawlasová, S., Lucuk, M., ... & Šulc, R.** (2006). Concrete based on fly ash geopolymers. *IBAUSIL, Weimar*.

**Somna, K., Jaturapitakkul, C., Kajitvichyanukul, P., Chindaprasirt, P.** (2011). NaOH activated ground fly ash geopolymer cured at ambient temperature. Fuel. 90(6), 2118-2124.

**Soundharya, S., & Nirmal, K.** (2014). Strength improvement studies on self-healing characteristics of bacterial concrete. *International Journal of Engineering Science Invention Research and Development*, 162-164.

**Souradeep, G., & Kua, H. W.** (2016). Encapsulation technology and techniques in self-healing concrete. *Journal of Materials in Civil Engineering*, *28*(12), 04016165.

**Sumajouw, D. M. J., Hardjito, D., Wallah, S. E., & Rangan, B. V.** (2004, May). Geopolymer concrete for a sustainable future. In *Presented: Green Processing Conference, Fremantle, WA* (pp. 10-12).

**Şinik, O.** (2019). *Geopolimer betonlarda dayanıklılık özelliklerinin araştırılması* (Master's thesis).

**Talaiekhozani, A., & Abd Majid, M. Z.** (2014). A review of self-healing concrete research development. *Journal of Environmental Treatment Techniques, 2*(1), 1-11.

**Tuyan, M.** (2017). *Doğal ve Atık Malzemelerle Geopolimer Harç ve Beton Geliştirilmesi.*( Doctoral Thesis, Ege University)

**Tuyan, M., Andiç-Çakir, Ö., & Ramyar, K.** (2018). Effect of alkali activator concentration and curing condition on strength and microstructure of waste clay brick powder-based geopolymer. *Composites Part B: Engineering*, *135*, 242-252.

**Van Breugel, K.** (2007, April). Is there a market for self-healing cement-based materials. In *Proceedings of the first international conference on self-healing materials* (pp. 1-9).

**Verma, M., & Dev, N.** (2022). Effect of ground granulated blast furnace slag and fly ash ratio and the curing conditions on the mechanical properties of geopolymer concrete. *Structural concrete*, *23*(4), 2015-2029.

**Vijay, K., Murmu, M., & Deo, S. V.** (2017). Bacteria based self healing concrete–A review. *Construction and Building Materials*, *152*, 1008-1014.

**Wang, J. Y., Soens, H., Verstraete, W., & De Belie, N.** (2014). Self-healing concrete by use of microencapsulated bacterial spores. *Cement and concrete research*, *56*, 139-152.

**Wang, J., Mignon, A., Snoeck, D., Wiktor, V., Van Vliergerghe, S., Boon, N., & De Belie, N.** (2015). Application of modified-alginate encapsulated carbonate producing bacteria in concrete: A promising strategy for crack self-healing. *Frontiers in microbiology*, *6*, 1088.

**Wang, K., Shah, S. P., & Mishulovich, A.** (2004). Effects of curing temperature and NaOH addition on hydration and strength development of clinker-free CKD-fly ash binders. *Cement and Concrete Research*, *34*(2), 299-309.

**Warscheid, T., & Braams, J.** (2000). Biodeterioration of stone: a review. *International Biodeterioration & Biodegradation*, *46*(4), 343-368.

**Wiktor V and Jonkers HM** (2011). Quantification of crackhealing in novel bacteria-based self-healing concrete. Cement and Concrete Composites 33: 763–770.

**Wong, L. S.** (2015). Microbial cementation of ureolytic bacteria from the genus Bacillus: a review of the bacterial application on cement-based materials for cleaner production. *Journal of Cleaner Production*, *93*, 5-17.

**Wu, M., Johannesson, B., & Geiker, M.** (2012). A review: Self-healing in cementitious materials and engineered cementitious composite as a self-healing material. *Construction and Building Materials*, *28*(1), 571-583.

**Xiang, J., Liu, L., Cui, X., He, Y., Zheng, G., & Shi, C.** (2018). Effect of limestone on rheological, shrinkage and mechanical properties of alkali–Activated slag/fly ash grouting materials. *Construction and Building Materials*, *191*, 1285-1292.

**Xie, T., & Ozbakkaloglu, T.** (2015). Behavior of low-calcium fly and bottom ash-based geopolymer concrete cured at ambient temperature. *Ceramics International*, *41*(4), 5945-5958.

**Xu, H., & Van Deventer, J. S. J.** (2000). The geopolymerisation of alumino-silicate minerals. *International journal of mineral processing*, *59*(3), 247-266.

**Yaşar, H.** (1992). *Plastikler dünyası*. TMMOB.

**Zawrah, M. F., Gado, R. A., Feltin, N., Ducourtieux, S., & Devoille, L.** (2016). Recycling and utilization assessment of waste fired clay bricks (Grog) with granulated blast-furnace slag for geopolymer production. *Process Safety and Environmental Protection*, *103*, 237-251.

**Zeybek, O.** (2009). *Uçucu kül esaslı geopolimer tuğla üretimi* (Master's thesis, Anadolu Üniversitesi).

**Zhang, L. V., Suleiman, A. R., Allaf, M. M., Marani, A., Tuyan, M., & Nehdi, M. L.** (2022). Crack self-healing in alkali-activated slag composites incorporating immobilized bacteria. *Construction and Building Materials*, *326*, 126842.

**Zhang, W., Zheng, Q., Ashour, A., & Han, B.** (2020). Self-healing cement concrete composites for resilient infrastructures: A review. *Composites Part B: Engineering*, *189*, 107892.

**Zolfagharifard, E.** " Wise Crack: Self-Healing Concrete", https://www.theengineer.co.uk/content/in-depth/wise-crack-self-healing-concrete/ (2011) (Last Access on November, 2022)

**Zuda, L., Rovnaník, P., Bayer, P., & Černý, R.** (2008). Effect of high temperatures on the properties of alkali activated aluminosilicate with electrical porcelain filler. *International Journal of Thermophysics*, *29*(2), 693-705.

## ACKNOWLEDGEMENTS

Firstly, to my supervisor Prof. Dr. Özge ANDİÇ ÇAKIR, I would like to express my sincerest gratitude to my consultant, whose especially valuable opinions, made it easy to provide the necessary materials and data during this study, and who did not spare his close attention.

I also offer my thanks to my friends, who constantly helped and guided me in my work.

I would like to thank my beloved family, who have not withheld their love and support from me all my life.

**Kerem ŞENÇAMLAR**

**İzmir, 2023**

# RESUME

Kerem ŞENÇAMLAR graduated primary, secondary and high school education in Izmir. He completed his bachelor education from Izmir University of Economics in 2019. He started his master's degree education at Ege University, Department of Civil Engineering, Department of Building Materials in the spring semester of 2019-2020.